2019

ANALYSIS OF THE PILE LOAD TESTS AT THE US 68/KY 80 BRIDGE OVER KENTUCKY LAKE

Edward Lawson
University of Kentucky, ed_lawson@live.com
Digital Object Identifier: https://doi.org/10.13023/etd.2019.248

STUDENT AGREEMENT:

I represent that my thesis or dissertation and abstract are my original work. Proper attribution has been given to all outside sources. I understand that I am solely responsible for obtaining any needed copyright permissions. I have obtained needed written permission statement(s) from the owner(s) of each third-party copyrighted matter to be included in my work, allowing electronic distribution (if such use is not permitted by the fair use doctrine) which will be submitted to UKnowledge as Additional File.

I hereby grant to The University of Kentucky and its agents the irrevocable, non-exclusive, and royalty-free license to archive and make accessible my work in whole or in part in all forms of media, now or hereafter known. I agree that the document mentioned above may be made available immediately for worldwide access unless an embargo applies.

I retain all other ownership rights to the copyright of my work. I also retain the right to use in future works (such as articles or books) all or part of my work. I understand that I am free to register the copyright to my work.

REVIEW, APPROVAL AND ACCEPTANCE

The document mentioned above has been reviewed and accepted by the student's advisor, on behalf of the advisory committee, and by the Director of Graduate Studies (DGS), on behalf of the program; we verify that this is the final, approved version of the student's thesis including all changes required by the advisory committee. The undersigned agree to abide by the statements above.

Edward Lawson, Student

Dr. L. Sebastian Bryson, Major Professor

Dr. Timothy Taylor, Director of Graduate Studies

ANALYSIS OF THE PILE LOAD TESTS AT THE US 68/KY 80 BRIDGE OVER KENTUCKY LAKE

THESIS

A thesis submitted in partial fulfillment of the
Requirements for the degree of Master of Science in Civil Engineering
in the College of Engineering
at the University of Kentucky

By

Edward Lawson

Lexington, KY

Director: Dr. L. Sebastian Bryson, Associate Professor of Civil Engineering

Lexington, KY

2018

ABSTRACT OF THESIS

ANALYSIS OF THE PILE LOAD TESTS AT THE US 68/KY 80 BRIDGE OVER KENTUCKY LAKE

Large diameter piles are widely used as foundations to support buildings, bridges, and other structures. As a result, it is critical for the field to have an optimized approach for quality control and efficiency purposes to measure the suggested number of load tests and the required measured capacities driven piles. In this thesis, an analysis of a load test program designed for proposed bridge replacements at Kentucky Lake is performed. It includes a detailed site exploration study with in-situ and laboratory testing. The pile load test program included monitoring of a steel H-pile and steel open ended pipe pile during driving and static loading. The pile load test program included static and dynamic testing at both pile testing locations. Predictions of both pile capacities were estimated using commonly applied failure criterion, and a load transfer analysis was carried out on the dynamic and static test data for both piles. The dynamic tests were then compared to the measured data from the static test to examine the accuracy. This thesis concludes by constructing t-z and q-z curves and comparing the load transfer analyses of the static and dynamic tests.

KEYWORDS: Bearing Capacity, Large Diameter Piles, Load Transfer, T-Z Curves.

Edward Lawson

November 15, 2018

ANALYSIS OF THE PILE LOAD TESTS AT THE US 68/KY 80 BRIDGE OVER KENTUCKY LAKE

By

Edward Lawson

Dr. L. Sebastian Bryson
Director of Thesis

Dr. Timothy Taylor
Director of Graduate Studies

November 15, 2018

ACKNOWLEDGMENTS

I would first like to acknowledge my advisor Dr. L. Sebastian Bryson. Dr. Bryson has been more than simply my research advisor. He has been a mentor in both the classroom and life. He is the most inspiring teacher and is responsible for sparking an interest in learning that I would never have achieved without his guidance. I cannot express the depth of my appreciation for my two years spent researching on Dr. Bryson's research team and will be forever grateful.

I would also like to thank my professors at the University of Kentucky, who allowed me to expand my knowledge and ability to learn in the classroom: Dr. Michael Kalinski, Dr. Michael Kalinski, Dr. Kyle Perry, Dr. Gabriel Dadi, and Dr. Mahboub. Dr. Kalinski provided me with my first soil mechanics textbook and told me to return it to him once I received my degree. I will be very proud to return his textbook to him after graduation. His constant support and encouragement have been very impactful.

Most importantly, I want to thank my family and close friends for their support in this journey. My parents, grandparents, and teachers along this journey. My parents could not have been more supportive throughout my life, and luckily, knew much better than I did about my potential life choice. Their guidance has been essential and will continue to lead me in future endeavors.

TABLE OF CONTENTS

LIST OF TABLES

LIST OF FIGURES

CHAPTER 1

1 INTRODUCTION

1.1 Background

The improvement in engineering technology and construction equipment has forced the design of bridge foundations to evolve to account for issues of extreme loading such as scour, ice, boat collisions, seismic events, and liquefaction. The improvements have led to an increase in the use of large diameter piles because of their substantial strength and durability. Large diameter H-piles and steel pipe piles are popular choices for structural supports in bridge designs because they can provide significant axial and lateral resistance in relatively poor soil conditions.

Pile capacity failure occurs when either the structural or load-carrying capacity gives way. The structural capacity of a pile is a function of the material properties of the pile, while the load-carrying capacity is a function of the soil-pile interaction. Pile analysis assumes that the bearing capacity failure of the pile will occur (shear failure along the shaft, followed by punching shear failure under the tip) before the pile buckles. As a result of this assumption, the load carrying capacity is the limiting failure criteria in most driven pile designs.

In large diameter pile design, considering the degree of plugging and existing internal friction is imperative. Plugging behavior can vary in different geomaterials. If the soil does not plug during driving, the soil inside a pipe pile or between H-pile flanges slips and produces internal shaft resistance. Slippage results in the limited toe resistance being the controlling variable in the capacity equation and the end bearing resistances being inaccurate. If the pile develops a plug and the soil moves with the pile, the test may yield higher estimates than the actual capacity.

The resistance of a pile typically changes over time. The capacity may increase from compaction or decrease from relaxation. Consequently, the dynamic analysis should be done at the end of the first drive and again after the restrike to accurately quantify time-dependent changes in the capacity. The load required for toe mobilization of large diameter steel piles may not be practical to achieve. The current correlation between large diameter piles, and small diameter test piles is not proportional. The use of different pile types,

geometries, and soil mixtures creates uncertainty in the dynamic model of the soil-pile interface because of the variations that can occur to the active forces.

The methods for predicting the load-settlement behavior of deep foundations are based on the load transfer model, where the foundation is modeled as a beam supported by non-linear springs. The t-z curve analysis defines the load transfer relationship along the shaft of the foundation, and q-z curve analysis defines the relationship at the toe where t is the mobilized unit shaft resistance, q is the mobilized unit toe resistance, and z is the vertical movement of a point on the pile. The construction of t-z curves identifies the soil-pile interaction with depth, as well as quantifies the stresses brought forth with each load increment.

The rapid evolution in engineering technology and the continuous expansion of offshore projects will increase the demand for large diameter piles. There is an agreement in the literature that the pile diameter influences the capacity and load transfer behavior of test piles. However, there is currently no consensus about the suitability of applying criteria designed for small diameter piles to large diameter piles or no available t-z curve database developed for large diameter piles. This study provides capacity and load transfer analyses of a steel H-Pile and steel closed-ended Pipe Pile in mixed soils.

1.2 Objectives

The objectives of the load test program analysis are as follows:

1) Determine how accurately dynamic methods predict the ultimate capacities of the large diameter Pipe Pile and large diameter H-Pile.

❖ This investigation will quantify the accuracy of the dynamic capacity analysis in this case study and determine if the theories and assumptions at the core of dynamic analysis formulated from research considering small diameter piles and idealized soil conditions are applicable to large diameter piles driven in mixed soils. The results may provide insight into the limitations of dynamic testing as well as how the degree of plugging and existing internal friction affects capacity predictions of large diameter piles.

- Assess the dynamic reports generated by CAPWAP and GRLWEAP.

- Predict the static and dynamic capacities of the piles using load-settlement data and multiple applicable failure criteria.
- Identify which failure criteria are the most appropriate for each set of data.
- Estimate the ultimate capacity using the bearing capacity equations.
- Quantify the effects that the lateral earth (at rest) coefficient (K_o)and soil-pile friction angle (δ) have on the ultimate bearing capacity through parametric analyses of the bearing capacity equations.
- Compare the static capacity to the capacities predicted by GRLWEAP, CAPWAP, and the bearing capacity equations
- Observe how close the dynamic capacities were to the static capacities and explore the probable factors that may have caused the dissimilarities.

2) Determine how accurately dynamic methods predict the load transfer behavior of the large diameter Pipe Pile and large diameter H-Pile.

❖ This investigation will evaluate the accuracy of the dynamic load transfer analyses completed by the CAPWAP software and determine if the assumed idealized general conditions in the wave equation can produce load transfer data that accounts for the variations that can occur to the active forces at the soil-pile interface due to different pile geometries and soil types. The results may provide insight about the soil-pile interaction of in silty gravel and lean clays. The results may also provide insight into the capabilities and limitations of dynamic testing.

- Determine the unit end bearing and unit side friction resistances from the static load-settlement data.
- Calculate the ultimate load along the entire length of the test piles.
- Calculate the mobilized tip resistance of the test piles using calculated load transfer data.
- Identify if pile mobilization occurred during testing.
- Calculate the elastic shortening.

- Construct t-z curves to represent the load transfer relationship along the shaft of the piles, and q-z curves to represent the soil-pile relationship at the pile toes
- Compare the static and dynamic load transfer data for both piles.
- Observe how close the static t-z curves compare to theoretical curves derived from idealized soil conditions (perfectly elastic, or undrained clay) considering small diameter piles.
- Discuss the probable causes for differences in the static and dynamic load transfer analyses

1.3 Relevance of Research

A complete load test program with both dynamic and static testing is the standard procedure to the determine the capacity and settlement parameters for large diameter piles in Load and Resistance Factor Design (LRFD). However, static load testing is expensive and takes time. Static tests are generally not performed until the construction phase for most large projects and are rarely ever performed on small projects. There is an agreement in the literature that the pile diameter influences the capacity and load transfer behavior of test piles. The rapid evolution in engineering technology and the continuous expansion of offshore projects will increase the demand for large diameter piles and the importance of large diameter pile research. The focus of this paper is to conduct a load transfer analysis on the data from the large diameter piles and compare how accurate the more cost-efficient dynamic methods are for predicting the capacity and load transfer behavior of large diameter piles.

1.4 Contents of Thesis

The contents of this thesis are as follows:

❖ Chapter 2 presents the analyses of the dynamic and static capacities from the load-settlement data of a pile load test program designed for a bridge replacement at Kentucky Lake. This chapter provides descriptions of the project site, development of the soil parameters, in-situ testing, lab testing, drivability analysis, pile instrumentation, and load test procedures. The paper concludes by calculating the bearing capacity for

both tests using different failure criteria and comparing the results of the dynamic and static methods.

The contents of the analysis portion of chapter 2 are as follows:

- Capacity predictions using all applicable failure criteria for static and dynamic tests.
- Capacity predictions using the bearing capacity equations.
- Parametric study of bearing capacity equation capacity predictions.
- Discussion of results
- Conclusion

❖ Chapter 3 presents the load transfer analyses of the load-settlement data from the load test program designed for a bridge replacement at Kentucky. This chapter provides descriptions of the project site, soil profiles, GRLWEAP drivability results, pile instrumentation, and load test procedures. The chapter concludes with the calculation of the load transfer data and the construction of t-z, and q-z curves along with a discussion of the results.

The contents of the analysis portion of chapter 3 are as follows:

- Load transfer curves
- Unit side friction and unit end bearing results for static and dynamic testing
- Ultimate load determinations for static load-settlement data.
- T-z curves derived from static load-settlement data
- T-z curves plotted with theoretical curves
- Q-z curves derived from static load-settlement data
- Discussion of results
- Conclusion

- ❖ Chapter 4 compares the capacity and load transfer calculation from Chapter 2 and Chapter 3. This chapter provides summaries of the project site details, development of the soil parameters, soil profiles, pile instrumentations, and test methods. A driveability study, pile instrumentation description, and load test methodology are also explained in this chapter. The chapter concludes with the presentation of the capacity predictions and the load transfer data for the load tests of both piles.

The contents of the information presented in chapter 4 are as follows:

- Bearing capacity predictions from the load test program for static and dynamic tests
- Unit side friction and unit end bearing calculations for static and dynamic test

- ❖ Appendix A presents the soil data used to generate the soil parameters. This encompasses grain size distribution tables, specific gravity data, CPT soundings, bore logs, and the results from shear strength test (UU & CU).
- ❖ Appendix B presents the maps used for site descriptions. This encompasses boring locations, test locations, strain gage placements, and topographic maps.
- ❖ Appendix C presents the dynamic testing results. This encompasses CAPWAP reports, Driven Analyses, and GRLWEAP results.
- ❖ Appendix D presents the static testing results. This encompasses the load-settlement data, and the failure criteria plots used to predict the capacity
- ❖ Appendix E contains the t-z curves at various elevations

CHAPTER 2

2 Load Test Program with Large Diameter Bridge Piles

2.1 Introduction

Deep foundational system designs rely on load test programs to provide reliable geotechnical data for soils and reinforcement materials. Load test programs are the most accurate method of predicting capacity and settlement parameters for piles. Many factors can affect the accuracy of pile capacity estimations. Some of these factors include load testing method, hammer selection, pile geometry, and failure criteria used in the analysis. Design decisions should consider the influence of diameter, pile wall thickness, the degree of soil plugging, and scalability because they can affect the driving resistance of the pile and govern equipment demands. Load test programs with static testing measure the capacity and settlement directly.

Dynamic load tests are economical testing procedures that improve construction control and pile installation. Dynamic tests use signal matching software to generate capacity predictions and model hammer-soil-pile systems from strain and acceleration measurements. The theories and assumptions used in dynamic analyses were formulated assuming idealized general conditions in the wave equation. As a result, the theories and assumptions at the core of dynamic analysis were derived from research based on small diameter piles, homogenous soils, and ideal installation techniques. The use of different pile types, geometries, and soil mixtures creates uncertainty in dynamic results because of the active force variations that can occur at the soil-pile interface when the soil/pile behavior does not fit an idealized soil/pile interaction model.

In large diameter piles, considering the degree of plugging and existing internal friction is imperative. Plugging behavior can vary in different geomaterials. If the soil does not plug during driving, the soil inside a pipe pile or between H-pile flanges slips and produces internal shaft resistance. Slippage results in the limited toe resistance being the controlling variable in the capacity equation and the end bearing resistances being inaccurate. If the pile develops a plug and the soil moves with the pile, the test may yield higher estimates than the actual capacity. The resistance of a pile typically changes over time. The capacity may increase from compaction or decrease from relaxation. Consequently, dynamic

analyses should be done at the end of the first drive and again after the restrike to accurately quantify time-dependent changes in the capacity.

The load required movement for toe mobilization of large diameter steel piles may not be practical to achieve. The correlation between high capacity, large diameter piles, and small diameter test piles is not proportional using current dynamic modeling methods. In high profile pile foundation designs, static tests subsequently commence after dynamic tests conclude to provide reference data used for back calculations and corrections. The existing literature indicated that the uncertainties associated with dynamic capacity predictions for large diameter piles are likely to result in overly conservative designs or structural failures if not supplemented by static load tests.

This paper presents the analysis of pile load test data from a bridge replacement project in western Kentucky. First, a description of the site and soil conditions are provided. Next, the dynamic and static load test methodologies are defined. The paper concludes by calculating the bearing capacity of the results for both tests using different failure criteria and comparing the results of the dynamic and static tests.

2.2 Literature Review

Failure criteria determine the maximum load a pile can support without failure from an applied load. Often in the literature, piles used to verify design criteria considered small-diameter driven piles. There is currently no consensus about the suitability of applying criteria designed for small diameter piles to large diameter piles.

2.2.1 Davvison Failure Criterion

The Davvison method (1972) assumes elastic pile compression. The Davvison Offset Limit was developed based on comparisons between the results of wave equation analyses of driven steel piles and load transfer research. The Davvison Offset Limit is the most commonly accepted failure criterion for driven piles. The criterion is applied by drawing a parallel line to the elastic compression line (Δ) offset by a specified amount of displacement. The geometry of the pile controls the amount of displacement. The point of intersection between the offset line and the load-settlement curve represents the ultimate capacity. The elastic compression line (Δ) is plotted by applying Equation 1 where P is the

axial load, L is the pile length, A is the pile cross-sectional area, and E is the elastic modulus of the pile material.

$$\Delta = PL / AE \quad (1)$$

The elastic compression line makes an approximately 20-degree angle with the load axis. The recommended offset (x) in the Davvison method (1972) is based on the pile diameter and calculated is determined using Equation 2, where x is the offset, B is the pile diameter in millimeters, A is the pile cross-sectional area, and E is the elastic modulus of the pile material.

$$x = \Delta + (4.0 + 0.008B) \quad (2)$$

For large diameter piles (B > 60.6 cm), Equation 3 is often used. The offset calculations presented in this study where determined using Equation 3.

$$x = \Delta + (B / 30) \quad (3)$$

The Davvison method (1972) provides conservative estimations and has the advantage of drawing the limit line on the load-settlement plot before testing has begun. The Davvison method (1972) provides conservative estimations and has the advantage of drawing the limit line on the load-settlement plot before testing has begun. Figure 1 provides an example of a plot of the Davvison method (1972).

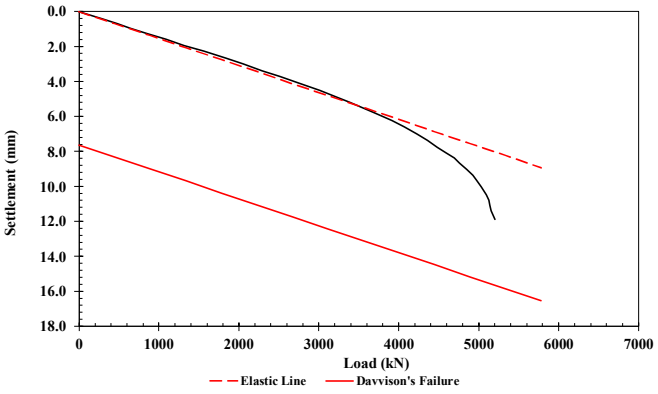

Figure 1. Davvison Failure Criterion

2.2.2 Butler and Hoy Failure Criterion

The Butler and Hoy method (1977) identifies the ultimate capacity as the point in which the tangents to the elastic and plastic portions of the load-settlement curve intersect. The Butler and Hoy method (1977) defines the failure load as the maximum slope of the load movement curve or the load where the load-displacement curve exceeds 0.12 mm/kN. The limiting capacity is the tangent line on the maximum slope of the load-settlement curve. The load location is generally located slightly above the load value that plastic behavior becomes observed. This location is known as the point of plunging failure. Figure 2 is a graphical representation of the Butler and Hoy method (1977).

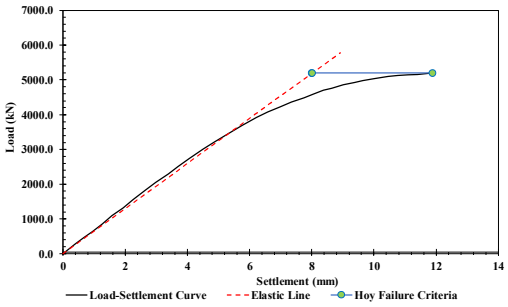

Figure 2. Butler and Hoy Failure Criterion

2.2.3 De Beer Failure Criterion

The De Beer method (1967) identifies the failure capacity as the intersection of the elastic and plastic portions of the load-settlement curves on a log-log scale. The interpreted failure load is where the two straight lines intersect on double logarithmic scale. This point is shown in Figure 3. The effectiveness of this method depends on the lognormal distribution of load-settlement data.

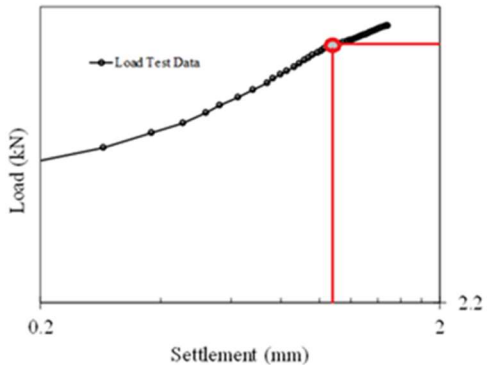

Figure 3. De Beer Failure Criterion

2.2.4 Hanson (80%) Failure Criterion

The Hanson (80%) method (1963) is an extrapolation method for defining capacity failure. This method is most commonly applied when load tests do not get carried out till failure or the applied load approached the failure load so closely that the other failure criteria produce unreliable data. The Hanson (80%) method (1963) states failure occurs when the gives four times the movement of the pile head as obtained for 80 % of the load. The Hanson (80%) method (1963) states the capacity can be determined by graphing the square root of each movement value divided by its load value and plotted against the movement. Figure 4 is a graphical representation of the Hanson (80%) method (1963).

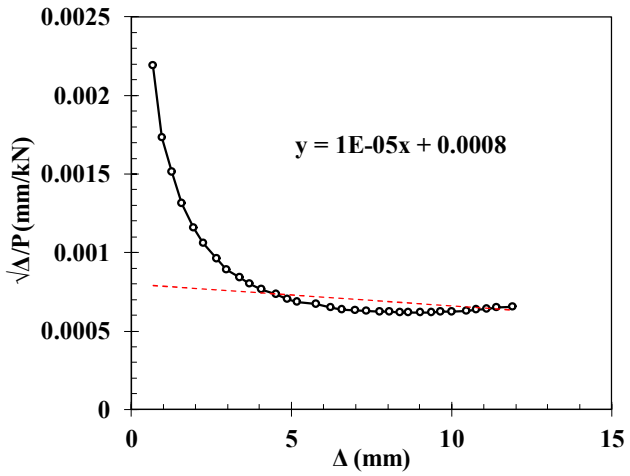

Figure 4. Hanson Failure Criterion

Once the data is plotted, a line can be fitted to the data, and the constants can be determined. The slope of the best fit line = C_1, and y-intercept = C_2. The ultimate capacity and settlement can then be calculated using Equation 4 and Equation 5, respectively.

$$Q_u = \frac{1}{2\sqrt{C_1 * C_2}} \tag{4}$$

$$\Delta_u = \frac{C_1}{C_2} \tag{5}$$

The Hanson (80%) method (1963) is most commonly applied to situations where the load-settlement data is skewed and the data is unreliable at loads near failure. This method was empirically generated by Hanson considering bored shafts, so it is necessary to check if the calculated 0.8 Qu intersects the best fit line. It often does not with drilled piles, however when the failure load is so high that toe mobilization is difficult.

Equation 6 is the equation used to plot the Hanson (80%) method (1963).

$$Q = \frac{\sqrt{\Delta}}{\Delta\ C_1+C_2} \tag{6}$$

2.2.5 Hanson (90%) Failure Criterion

The Hanson (90%) method (1963) defines failure load as the load that gives twice the movement of the pile head as obtained for 90% of that load. The stress at failure is equal to two times the strain a 10% smaller stress. The International Building Codes incorporated the Hanson (90%) method (1963) in 2000 as an extrapolation method for defining capacity failure. The Hanson (90%) method (1963) is a slightly more conservative linear approximation estimation than the Hansen 80% failure criterion (failure stress occurs when the strain is equal to four times the strain at a 20% smaller stress). Dotson (2013) purposed a direct solution to approximate the Hanson (90%) method (1963) using a system of equations. Dotson (2013) used Equation 7 to represent the load and deflection at 90% of the ultimate capacity.

$$\frac{9}{10}Q_u - \frac{\sqrt{\frac{\Delta}{2}}}{\frac{\Delta}{2}\ C_1+C_2} = 0 \tag{7}$$

After solving by substitution and re-arranging the equation, the approximate solution is expressed by Equation 8.

$$Q_u = \frac{2\sqrt{3}}{7\sqrt{C_1*C_2}} \tag{8}$$

The deflection corresponding to the 90% failure load is given by Equation 9.

$$\Delta_u = \frac{3C_1}{4C_2} \tag{9}$$

2.2.6 Bearing Capacity Equations

The API (1993) method is a semi-empirical approach of calculating the pile skin friction, based on the total stresses induced in the soil and calculated using the soil's undrained shear strength (c_u). This method works well for cohesive or clay soils. It has been used for many years and has proven to provide reasonable design capacities for displacement and non-displacement piles. This method depends on the alpha factor (α), which is indirectly

related to the soil's undrained shear strength (c_u). The element was back-calculated from several pile load tests.

2.2.7 Skin Friction and End Bearing Resistance in Cohesive Soils

Driving piles into cohesive soils create a reduction in the effective stress because it increases the pore water pressure. Drilling large diameter piles into clays can potentially lead to strain softening. This happens when large strains in the clay build up as the pile driven and a significant reduction in skin friction occurs. The adhesion factor α was developed empirically to address these concerns with clay.

The API (1993) adhesion factor α can be calculated using Equation 10 where σ'_v is the effective vertical stress calculated at the midpoint of each segment, and c_u is the undrained shear strength of the segments.

$$\psi = \frac{c_u}{\sigma'_v} \tag{10}$$

$$\alpha = 0.5\psi^{-.5}, \qquad \psi \leq 1.0, \qquad \alpha \leq 1.0$$

$$\alpha = 0.5\psi^{-.25}, \qquad \psi > 1.0, \qquad \alpha \leq 1.0$$

The API (1993) method to determine the ultimate unit skin friction for driven piles in clay is provided by Equation 11:

$$\tau_{ult} = \alpha * c_u \tag{11}$$

The API (1993) method to determine the ultimate unit end-bearing resistance for clay in units of force per area is calculated using Equation 12:

$$q_p = 9c_u \tag{12}$$

2.2.8 Skin Friction and End Bearing Resistance in Non-Cohesive Soils

Driving a pile has different effects on the soil surrounding it depending on the relative density of the soil. In loose soils, the soil is compacted, forming a depression in the ground around the pile. In dense soils, any further compaction is small, and the soil is displaced upward causing ground heave. In loose soils, driving is preferable to boring since compaction increases the end-bearing capacity.

The API (1993) method to determine the unit skin friction for driven piles in cohesionless soil can be calculated using Equation 13 where K_o is the lateral earth (at rest) coefficient and (δ) is soil-pile friction angle.

$$q_s = K_o * \sigma'_v * \tan\delta \quad (13)$$

The API (1993) method to determine the ultimate end-bearing resistance in cohesionless soils is given by Equation 14.

$$q_p = \sigma'_v * N_q \quad (14)$$

The bearing capacity factor (N_q) in cohesionless soils is grived by Equation 15 where Φ' is the effective friction angle.

$$N_q = \tan^2(45+\frac{\pi}{2}) * e^{\pi \tan\Phi'} \quad (15)$$

The bearing capacity factor (N_q) can also be estimated based on the density soil and anticipated soil-pile friction angle (δ) using API (1993) recommendations for cohesionless soils. The API (1993) bearing capacity factor (Nq) recommendations for cohesionless soils is listed in Table 1.

Table 1. API (1993) Recommendations for Cohesionless Soils

Soil Density	**Soil-Pile Friction Angle (δ)**	**Bearing (N_q) Capacity Factor**
Very Loose - Loose to Medium	15	8
Loose Medium- Dense	20	12
Medium Dense	25	20
Dense -Very Dense	30	40
Very Dense	35	50

2.3 Project Description of Kentucky Lake Bridge

The proposed Lagoon Bridge was part of the Kentucky Lake Bridge Advance Contract (CID 131305) in Marshall and Trigg Counties, Kentucky. The Kentucky Transportation

Cabinet (KYTC) has proposed a bridge replacement for an existing crossing at Kentucky Lake. The crossing follows the existing US 68/KY 80 highway corridor. The bridge is a multi-span structure that is served by causeways on the east and west banks of Kentucky Lake that extend into the lake and serve as approaches. The project site was located within the perimeter of the red square depicted in Figure 5.

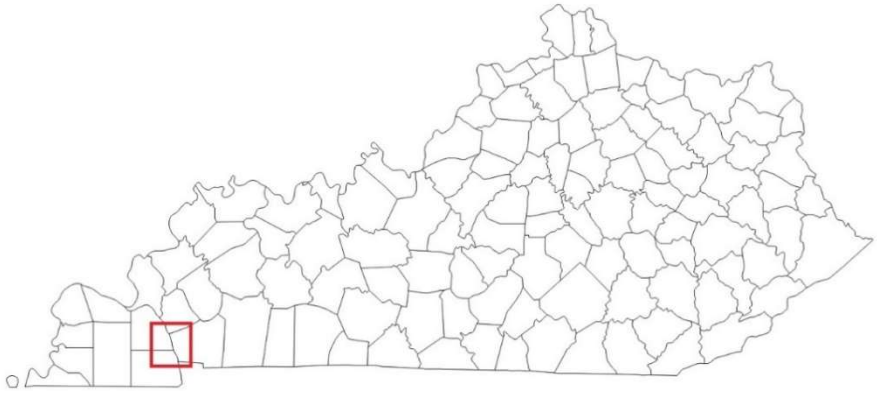

Figure 5. Project Location

The purposed bridge replacement is approximately 30.48 m north of the centerline of the existing bridge. The new structure is designed to have a length of 176.80 m and a width of 19.6 m. The causeways to the east and west of the bridge extend into the lake and will serve as approaches. The steel girder bridge will be supported on integral end bents and two interior piers. The interior piers are in turn supported on three columns that are connected to a single beam support. The plan view of the purposed bridge replacement is pictured in Figure 6.

Figure 6. Proposed Bridge Replacement

2.4 Site Conditions

The geology of the site is influenced by the Mississippi Embayment to the west and is composed primarily of a cherty Mississippian-age residuum within the Ft. Payne Formation. This formation is described as a residual chert interbedded with residual clay. Existing grades currently slope from south to north over much of the site from the existing highway embankment to the existing lagoon. At the west end of the site, near L-1, grades slope from southwest to northeast toward the lagoon. Grades at the site range from approximately 7H:1V near the lagoon to as steep as 3H:1V near the west end of the site. The summer pool elevation is 109.42 m, and the winter pool elevation is 107.90 m.

The effective strength parameters of the granular soils for Test Pile Location L-1 were estimated using the SPT N-value data from test borings using published AASHTO correlations. Data from SPT testing supplemented with data from CPT soundings was also used to estimate the unit weight parameters of the fine-grained soils at the site. Corrected N-values were used to estimate the compression and recompression indices.

The bulk and split tube samples collected during SPT testing, boring logs, and CPT soundings provided the data and intact samples for testing in the upper lean clay soils at L-2. The results of consolidated-undrained (CU) and unconsolidated undrained (UU) triaxial shear tests were used to estimate the effective and total soil shear strength parameters. The compression/recompression indices and over-consolidation ratios (OCR) were estimated from CPT data.

2.5 In Situ Testing Program

The borings were extended to depths of 13.89 m or 49 m. The bedded chert was extremely difficult to penetrate using the rotary drill equipment. A split-barrel sampler was used to collect a sample at depths 12.83 m to 25.3 m below existing grades. An observation well was installed at B5 with a screen depth of 10.97 m.

Bulk samples were collected at 0 to 7.31m depth in boring B4, 2.34 m to 9.87 m in depth in boring B2, 9.87m to 7.31 m in boring B2, and 7.31 m to 11.5 m in boring B2. Due to the introduction of drilling fluid to facilitate casing advancement in all borings, groundwater levels were not obtained while drilling, or after the completion of drilling in these borings. Considering the low permeability of some of the soils encountered in the borings, a

relatively long period may be necessary for a groundwater level to develop and stabilize in a borehole in these materials. When the observation well B5 was checked, the elevation of the water was 103.97 m. Groundwater level fluctuations in the soils surrounding the lagoon bridge site occur due to seasonal variations in the amount of rainfall, runoff, and the varying pool levels of the immediately adjacent lagoon and Kentucky Lake. Based on this, long-term groundwater monitoring was determined to be unnecessary.

The soil profiles at the pile test locations were developed based on the subsurface conditions encountered in nearby test borings logged during the field exploration phase of the project. The in-situ testing program consisted of five penetration test borings. The five test borings were advanced at the locations shown in Figure 7.

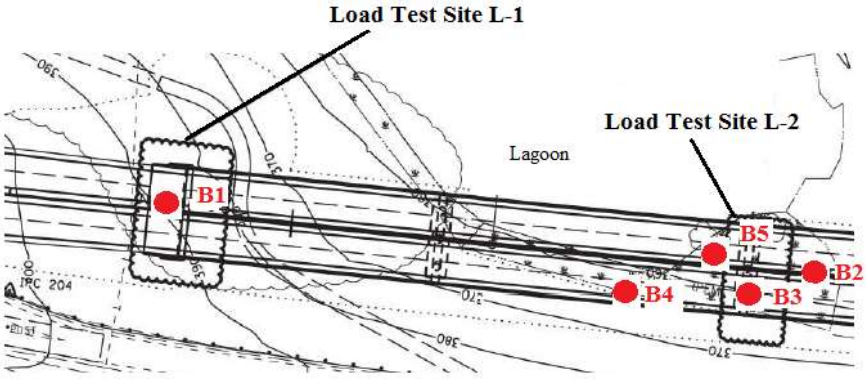

Figure 7. Boring Locations

Test boring B1 encountered cohesive hard silt (ML) from ground surface to a depth of 2.1 m. Between depths of 2.1 m to 8.5 m test boring B1 encountered cohesionless dense gravel with silt (GM). Between depths of 8.5 m to 10.05 m test boring B1 encountered cohesive hard silt (ML). From the depth of 10.05 m to the bottom of the boring (14 m), test boring B1 encountered cohesionless silty gravel with chert and bedded chert (GM-ML). The subsurface profile at the H-Pile (L-1) load test site is shown in Figure 8.

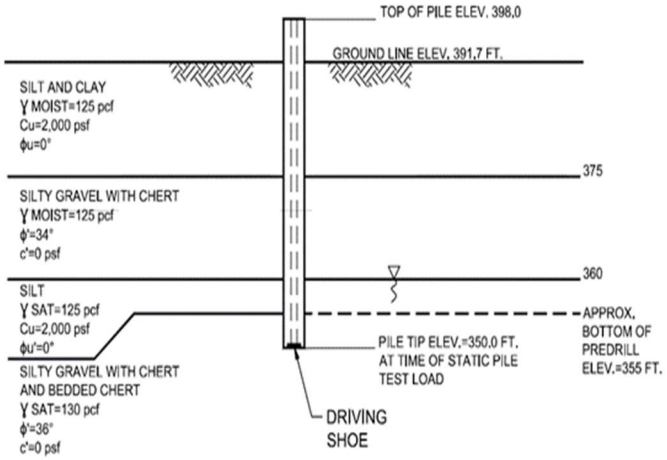

Figure 8. H-Pile Subsurface Profile

The test borings B2, B3, B4, and B5, encountered alluvial clay (CL) and silt soils (ML) with some chert pieces from the muddy ground surface at a depth of 11.2 m. Within this depth test, boring B2 encountered a layer of loose gravel with silt (GC) from a depth of 2.7 m to 4.2 m. Between the depths of 4.2 m to 20.4 m test borings B2, B3, and B4 encountered silty gravel with chert (GP-GM). From the depth of 20.4 m to 24.56 m at the bottom of the boring test, borings B3 and B4 encountered silty gravel with chert and chert layers (GC-GM). The subsurface profile at the Pipe Pile (L-2) load test site is shown in Figure 9.

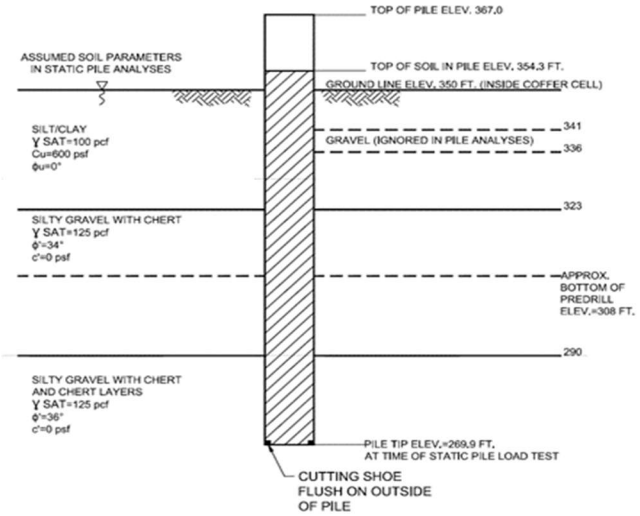

Figure 9. Pipe Pile Subsurface Profile

The moisture contents of all tested soils ranged from 16.6% to 28.2% (average = 23.44%), and the dry unit weights ranged from 1490 kN/m3 to 1794 kN/m3 (median = 1582 kN/

m3). Atterberg limits tests (per ASTM D4318) indicated the liquid limits (LL) ranging from 21 to 47 percent (average = 31%) , plastic limits (PL) ranging from 13 to 28 percent (average = 20.9%), and plasticity indices (PI) ranging from 3 to 26 (average = 10.7%) percent.

2.6 Laboratory Testing Program

The boring tests from the field study provided sound samples for geotechnical laboratory testing. The high-quality samples provided site-specific soil parameters under dynamic loading. The shear strength parameters of the granular soils were determined using the SPT N-values data from the test borings and were supplemented with CPT soundings data. In locations where the N-values were skewed, the estimated internal angle of friction ranged between 36 and 38 degrees. In specific locations when the SPT data appeared to be accurate, the shear strength parameters of the granular soils were estimated using AASHTO correlations.

The bulk and split tube samples collected during SPT testing, boring logs, and CPT soundings provided the data and intact samples for testing in the upper lean clay soils at L-2. The CPT data from B2 and results of the consolidated-undrained (CU) and unconsolidated undrained triaxial (UU) shear tests of the split tube samples collected in nearby boring locations were used to estimate the strength properties and unit weight parameters of the clay soils near L-2. Moisture content (MC) tests (ASTM D2216) performed on selected penetrations indicated that the upper layers of soil in the area were generally lean clays. The classification and properties of the upper lean clay layers encountered in this study are shown in Figure 10.

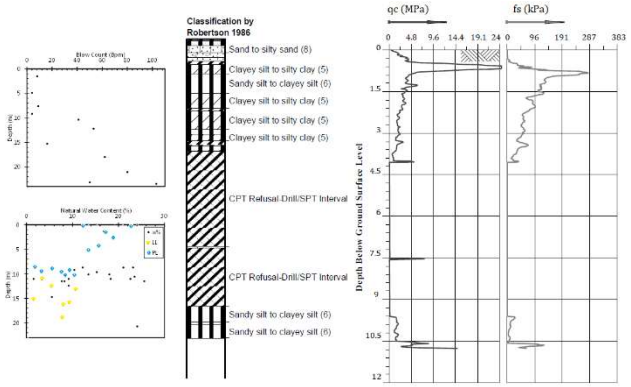

Figure 10. Classification and Properties of Encountered Clays.

2.7 Pile Driveability Analyses

Wave equation analyses indicated that the wall thickness of the pile needs to be a minimum of 2.54 cm to avoid overstressing the piles during driving. The analyses assume that a pile plug condition will begin at 15.24 m the pile cap for the pipe pile and at 4.6 m and 7.62 m below the pile cap for the H-pile, respectively. The GRLWEAP analyses indicated the proposed pile types could be driven to the anticipated bearing depths, assuming the allowable compressive and tensile stresses are 85% of the steel yield stress for the pipe piles and the H-Piles. The results showed that hammer blows in the final 4.6 to 6.1 m might exceed 150 blows per foot for the hammers selected, which will increase the installation time of the piles. The GRLWEAP results indicate that a hammer with a rated energy of 112.5 kN-m to 122 kN-m will be required to drive the unplugged pipe piles and a hammer with a rated energy of 206 kN-m to 217 kN-m. The results indicated a hammer with a rated energy of 37 kN-m to 66 kN-m will be required to drive unplugged H-piles and a hammer with a rated energy of 206 kN-m to 217 kN-m. The nominal resistance for the H-Pile and Pipe Pile were 2,668 kN and 10,675, respectively. The ultimate capacities estimated by the GRLWEAP software during the driveability study are shown in Figure 11.

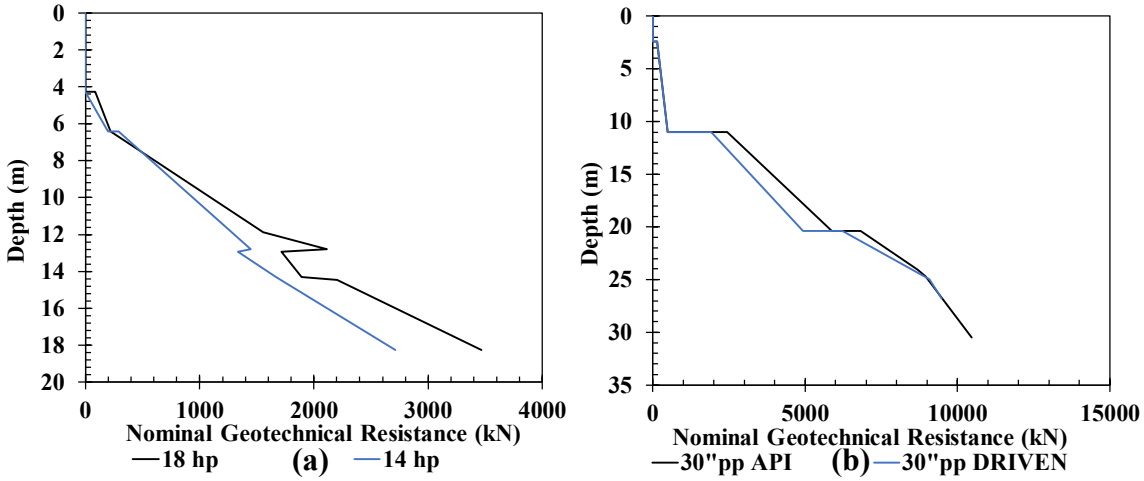

Figure 11. GRLWEAP Nominal Geotechnical Resistance (a) H-Pile (b) Pipe Pile

2.8 Pile Load Test Program

2.8.1 Test Piles Description

The pile load test program tested two test piles designated as L-1 and L-2. Test pile L-1 was an HP18x204, ASTM A572, Grade 50 steel H-Pile with a length of 18.3 m. Test pile L-2 was a 762 mm (O.D.) steel pipe pile with a wall thickness of 25.4 mm and had an

overall length of 32 m. The prescribed lengths assumed a water level elevation of 11.3 m plus an additional 6.1 m for instrumentation gages, leads/sleeves, and to provide sufficient stickup to perform pile testing. The analyses assumed all pipe piles would consist of ASTM A252 steel having a yield strength of at least 310 MPa, whereas the assumed yield strength is 344.7 MPa for the H-piles.

2.8.2 H-Pile Instrumentation

The H-Pile arrived in one 18.3 m piece (area = 387 cm^2). A pile driving point was placed at the tip of the H-pile by KYTC standard specifications. The shape of the recommended pile point is designed explicitly for sloping rock surfaces. It was used to help penetrate the encountered bedded chert zones and chert boulders in the foundation soil during pile installation. A schematic depicting the instrumentation of the H-Pile is presented in Figure 12.

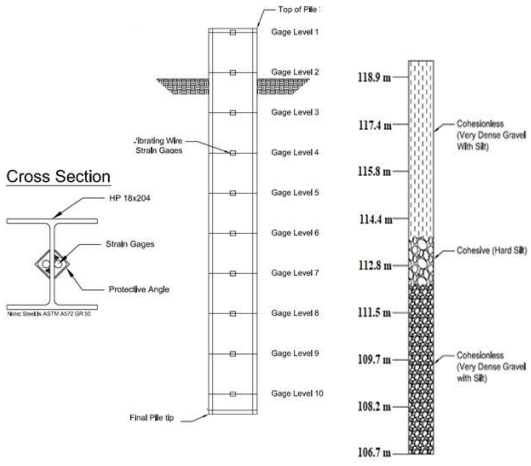

Figure 12. H-Pile Schematic

Strain gages were placed at ten different locations along the pile length. The strain gages were protected during driving with a welded steel angle over the gages and associated wires. The strain gage instrumentation is pictured in Figure 13.

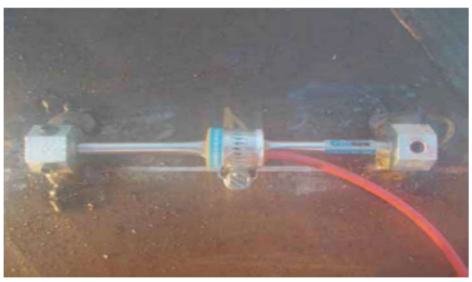

Figure 13. Strain Gage Instrumentation

The test pile was instrumented using vibrating wire strain gages at ten depth intervals along two vertical lines along the centerline of each side of the H-Pile web. The depths and elevations of the strain gages are listed in Table 2.

Table 2. Strange Gage Locations for H-Pile

Location	Description	Depth Below Pile Top (m)	Elevation (m)
Pile Top	Synchronous Lift System Four Top Displacement Transducers Two Displacement Transducers Digital Survey Manual Survey Measurement	0	121.3104
Ground Level	Two Strain Gages	0.1524	121.158
Gage Level 1	Two Strain Gages	1.6764	119.634
Gage Level 2	Two Strain Gages	1.92024	119.3902
Gage Level 3	Two Strain Gages	3.2004	118.11
Gage Level 4	Two Strain Gages	4.7244	116.586
Gage Level 5	Two Strain Gages	6.2484	115.062
Gage Level 6	Two Strain Gages	7.7724	113.538
Gage Level 7	Two Strain Gages	9.2964	112.014
Gage Level 8	Two Strain Gages	10.8204	110.49
Gage Level 9	Two Strain Gages	12.31392	108.966
Gage Level 10	Two Strain Gages, End of Tell-Tale Housing	13.8684	107.442
Pile Tip	-	14.6304	106.68

2.8.3 Pipe Pile Instrumentation

The pipe pile was manufactured in two sections. The bottom part of the test pile was 4.65 m in length, and the top part was 5.11 m feet in length. The two pile sections were joined together with a field welded splice on the project site during installation. The upper section of the test pile was then raised and set into place for the field splicing process. After the

two sections of the test pile were spliced together in the field, the cabling for the strain gages on the bottom section of the test pile was ran through the upper part of the test pile within the preinstalled protection angle. The cabling was then subsequently closed by splicing the top and bottom section of the protection angle together. The pile splicing instrumentation procedure is pictured in Figure 13 (a).

Once the splicing process was complete, a pile driving shoe was placed at the end of the pipe to improve driveability and durability. Driving shoes for the pipe piles are flush with the exterior surface of the pile and to fit inside of the pile. The driving shoe was used to help maintain the exterior skin friction on the pile and aid in the driving of the piles in the bedded chert and chert boulders. Figure 13 (b) depicts the driving shoe that was placed on the end of the pile to improve driveability.

(a) (b)

Figure 14. Pipe Pile Instrumentation: (a) Pile Splicing; (b) Driving Shoe

The test pile was instrumented using vibrating wire strain gages at ten depth intervals along four vertical lines located 90 degrees to one another along the exterior of the pipe pile. A schematic depicting the instrumentation of the Pipe Pile is presented in Figure 14.

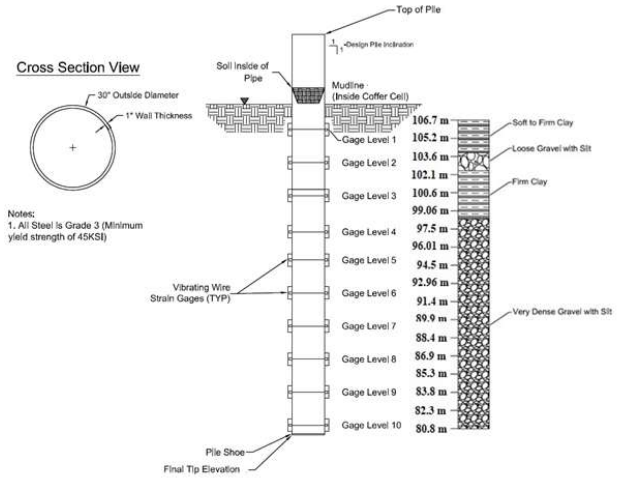

Figure 15. Pipe Pile Schematic

Strain gages were placed at ten different locations along the pile length. The depth and elevation of the strain gages are listed in Table 3

Table 3. Strange Gage Locations for Steel Pile

Location	Description	Depth Below Pile Top (m)	Elevation (m)
Pile Top	Synchronous Lift System Four Top Displacement Transducers Two Displacement Transducers Digital Survey Manual Survey Measurement	0	111.8616
Ground Surface	-	5.1816	106.68
Gage Level 1	Four Strain Gages	7.04088	104.82072
Gage Level 2	Four Strain Gages	9.47928	102.38232
Gage Level 3	Four Strain Gages	11.91768	99.94392
Gage Level 4	Four Strain Gages	14.56944	97.29216
Gage Level 5	Four Strain Gages	16.67256	95.18904
Gage Level 6	Four Strain Gages	19.11096	92.75064
Gage Level 7	Four Strain Gages	21.54936	90.31224
Gage Level 8	Four Strain Gages	23.98776	87.87384
Gage Level 9	Four Strain Gages	26.42616	85.46592
Gage Level 10	Four-Strain Gages, End of Tell-Tale Housing	28.86456	83.02752
Pile Tip	-	29.59608	82.26552

2.9 Pile Installation Methods and Dynamic Testing Procedure

2.9.1 H-Pile Installation Procedures

Before installing the test pile, a pre-probing program was implemented to determine if predrilling was required. This program determined that pre-drilling should be done due to the limited number of test borings at the site, and because of the presence of bedded chert. The predrilled hole extended to an elevation of 102.108 m. The pile was driven with an

ICE I-30v2 open-ended diesel hammer. After completion of the initial drive, a restrike was performed 72 hours later. Dynamic testing data was recorded using pile driving monitoring equipment manufactured by Pile Dynamics Inc. (Model PAX, strain and accelerometer calibrations attached) and analyzed with the CAPWAP software during the initial drive and subsequent restrike.

Upon completion of the 72-hour restrike, the pile was cut down to 14.60 m. The head of the pile was at an elevation of +121.31 m, and the final pile tip elevation was +106.68 m. The ground surface was at the height of +119.39 m, giving the pile an embedment length of 12.71 m within the soil.

2.9.2 Pipe Pile Installation Procedures

Before installing the test pile, predrilling was performed using a 60.96 cm diameter auger to Elevation 108.204 m. The decision to pre-drill made as a result of the presence of chert in the encountered soils during field exploration. Predrilling at the testing location was performed down to an elevation 108.204 m.

The test pile was driven using an ICE I-100v2 open-ended diesel hammer to a tip elevation of 84.7 m on the initial drive. Additional PDA restrikes were performed on August 19, 2013, and September 10, 2013. This corresponded to 72 hours after the completion of the redrive and four days after the completion of the static load test. Dynamic pile testing (PDA) was recorded during the initial drive, redrive, and subsequent restrikes.

After the completion of the 72-hour restrike on August 19, 2013, the test pile was cut-off to bring the pile top to the required load testing elevation. The final tip elevation was +25.07 m and the top of pile elevation at the time of testing was +34.10 m, giving the tested pile a length of 9.02 m. The ground surface was at an elevation of +32.52 m, giving the pile an embedment length of 7.44 m within the soil. The surface was at an altitude of +32.52 m, which led to a pile embedment length of 7.44 m within the ground.

2.10 Static Load Test Procedure

The load was applied using three 3558.56 kN hydraulic jacks equipped with a common manifold and single electric hydraulic pump. The hydraulic jacks had an effective area of 0.056 m^2 hydraulic jack (0.168 m^2 total). The load test frame was designed by Genesis Structures, a sub-consultant to Jim Smith Contracting. The hydraulic jacks acted against

an engineered reaction frame with a total of 8 reactions placed in-line with the cylinders. The static load applying equipment used in this study are pictured in Figure 16.

(a) (b)

Figure 16. Static Load Test Equipment: (a) Hydraulic Jacks; (b) Load Test Frame

The top of pile movement was measured using four displacement transducers mounted on a reference beam. Two telltales were installed along the exterior of the pile and terminated near the toe of the H-Pile. Backup pile head measurements and measurements of reaction pile movements were measured using survey methods. The instruments used to measure the top of pile movement are shown in Figure 17.

(a) (b)

Figure 17. Head Movement Measurement: (a) Pressure Transducers; (b) Reference Beam

The applied load was measured with an Enerpac ESS Synchronous Lift System that records the applied load and hydraulic jack elongation data in real time. The test load was applied

in increments of 5% of the maximum applied test load. During each load interval, the load was maintained for a time interval of 10 minutes, using the same time interval for all loading increments except at 50% and 100 % on the applied test load. At 50% of the applied test load, the load was maintained for 30 minutes, and at 100% of the applied test load, the load was maintained for 1 hour. The applied test load was removed in ten, approximately equal, decrements. The load at each decrement was maintained for 15 minutes. The same time interval was utilized for all unloading decrements. Readings continued to be taken for 30 minutes after complete unloading of the test pile. The pile stiffness multiplied the average strain at each gage level. The Enerpac ESS Synchronous Lift System used to measure the applied load, and hydraulic jack elongation data is depicted in Figure 18.

Figure 18. Enerpac ESS Synchronous Lift System

2.11 Dynamic Test Results

2.11.1 H-Pile Dynamic Testing Results

The subject pile was monitored with dynamic pile testing equipment during initial drive, all subsequent re-strikes, and extended drive. The CAPWAP software was used to generate load-settlement curves from the data collected during testing. Compression and tension pile driving stresses were below the acceptable limit of 279237 kPa. The acceptable limit of compression and tension driving stresses is defined as 90 percent of the applied load. The load-settlement curves produced by CAPWAP are plotted in Figure 19.

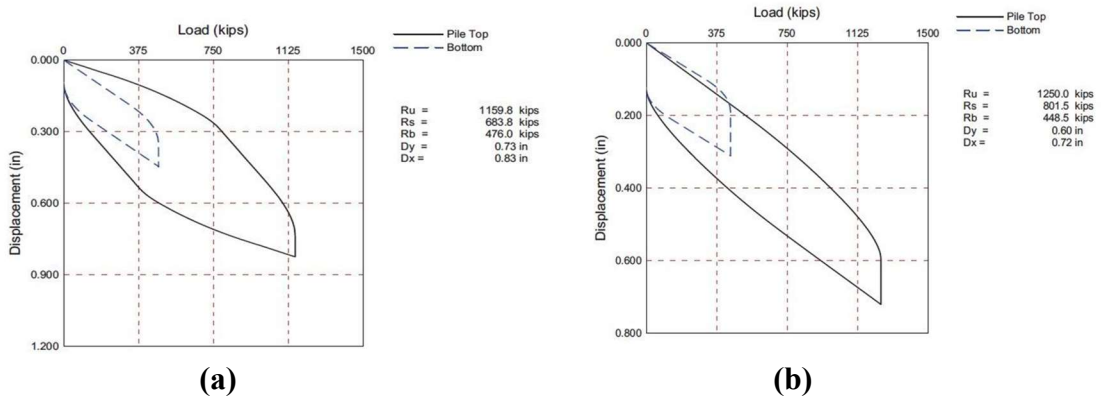

(a) **(b)**

Figure 19. H-Pile CAPWAP Load-Settlement Curves: (a) First Re-strike; (b) Second Re-strike

The ultimate capacities predictions CAPWAP produced were made using the case method. The ultimate capacities ranged from approximately 1,160 kips (5160kN) at the end of the initial drive to approximately 1,250 kips (5560 kN) during the 72-hour re-strike. The ultimate capacities determined by various commonly applied failure criteria using the load-settlement data produced by CAPWAP is shown in Figure 20.

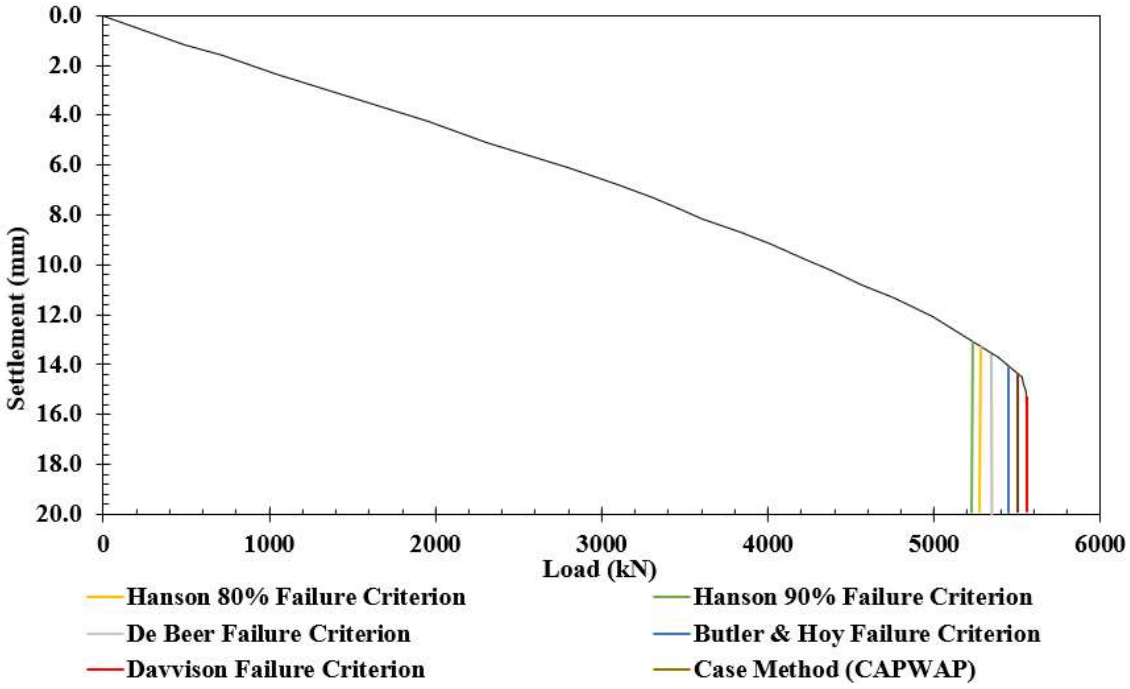

Figure 20. H-Pile Dynamic Testing Capacity Estimations

The 72-hour re-strike capacity showed an increase of approximately 90 kips (400 kN). However, the subsequent final re-strike (after the static load test) showed a slight decrease

in capacity with respect to the initial drive. This was most likely caused by the lower hammer energy utilized during the final re-strike not fully mobilizing the pile capacity. The ultimate capacities predicted during the initial drive, and final re-strike of the pipe pile dynamic test are listed in Table 4.

Table 4. H-Pile Dynamic Capacity Estimations

Initial Drive		**Final Drive**	
Failure Criterion	**Ultimate Capacity**	**Failure Criterion**	**Ultimate Capacity**
De Beer	3,638 kN	De Beer	5,361 kN
Case Method	5,160 kN	Case Method	5,560 kN
Butler & Hoy	5,198 kN	Butler & Hoy	5,557.5 kN
Hanson 80%	5,590 kN	Hanson 80%	5,270 kN
Hanson 90%	5,533 kN	Hanson 90%	5,216 kN
-	-	Davvison	5,782 kN

The GRLWEAP software estimated the unit side shear resistances in the dense to very dense gravel ranged from approximately 95.76 kPa to 191 kPa and generally increased with depth (Figure 21 (a)). Unit end bearings at the pile tip (plugged condition) ranged from approximately 636 to 911 kPa. However, the end bearings are likely much higher due to the pile likely only being partially plugged. The low hammer energy utilized during the final restrike did not mobilize the pile. This is graphically represented in Figure 21 (b).

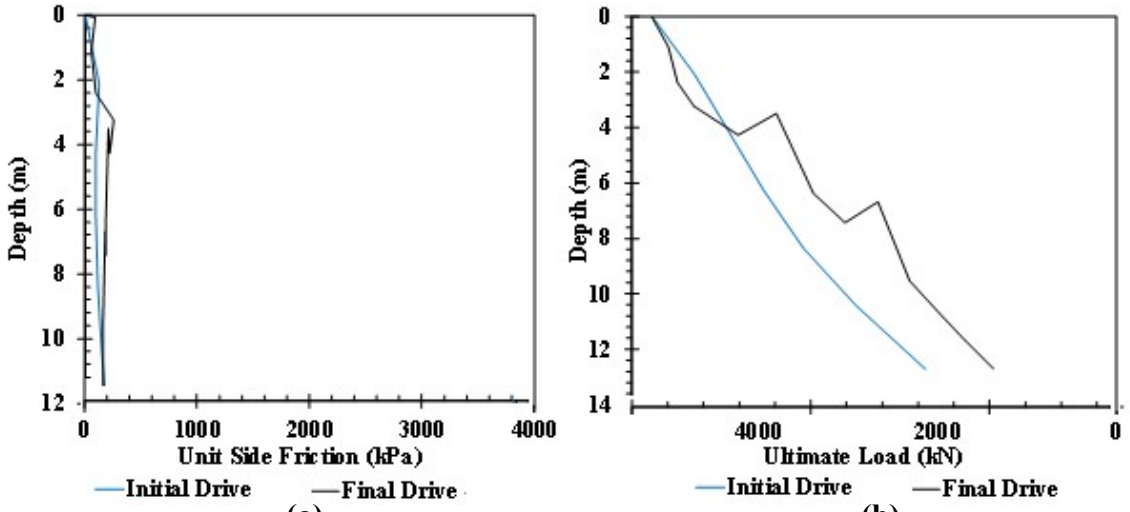

(a) (b)

Figure 21. H-Pile Dynamic Load Transfer: (a) Unit Side Friction; (b) Ultimate Load

2.11.2 Pipe Pile Dynamic Testing Results

The pile was monitored with dynamic pile testing equipment during initial drive, all subsequent re-strikes, and extended drive. Compression and tension pile driving stresses were below the acceptable limit of 279237 kPa. The match qualities (MQ) for the signal matching results were less than 4. Lower match qualities may be achievable; however, to achieve lower match qualities the ultimate capacity of the pile may be unrealistic given the soil conditions, transferred hammer energy, and the measured sets. The acceptable limit for compression and tension driving stresses is defined as 90 percent of Fy. The load-settlement curves produced by CAPWAP are plotted in Figure 22.

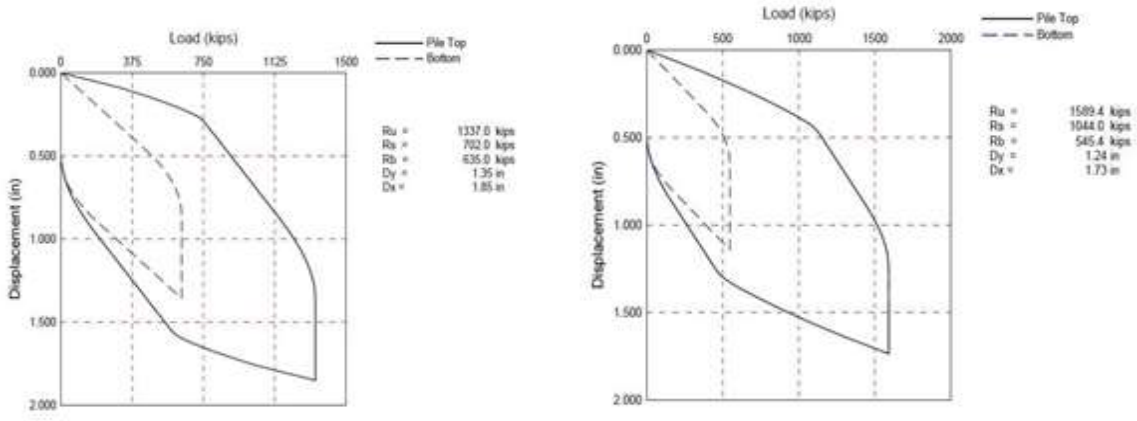

(a) (b)

Figure 22. Pipe Pile CAPWAP Load-Settlement Curves: (a) First Re-strike; (b) Second Re-strike

The ultimate capacities predicted by CAPWAP ranged from approximately 5947.27 kN at the end of the initial drive to approximately 10675.73 kN during the final re-strike. The re-strike capacities for the first (48 hour) and second (72 hour) re-strike showed an increase in capacity of approximately 1120.95 kN and 271.34 kN, respectively. The capacity predictions from the dynamic load test of the pipe pile are graphically represented in Figure 23.

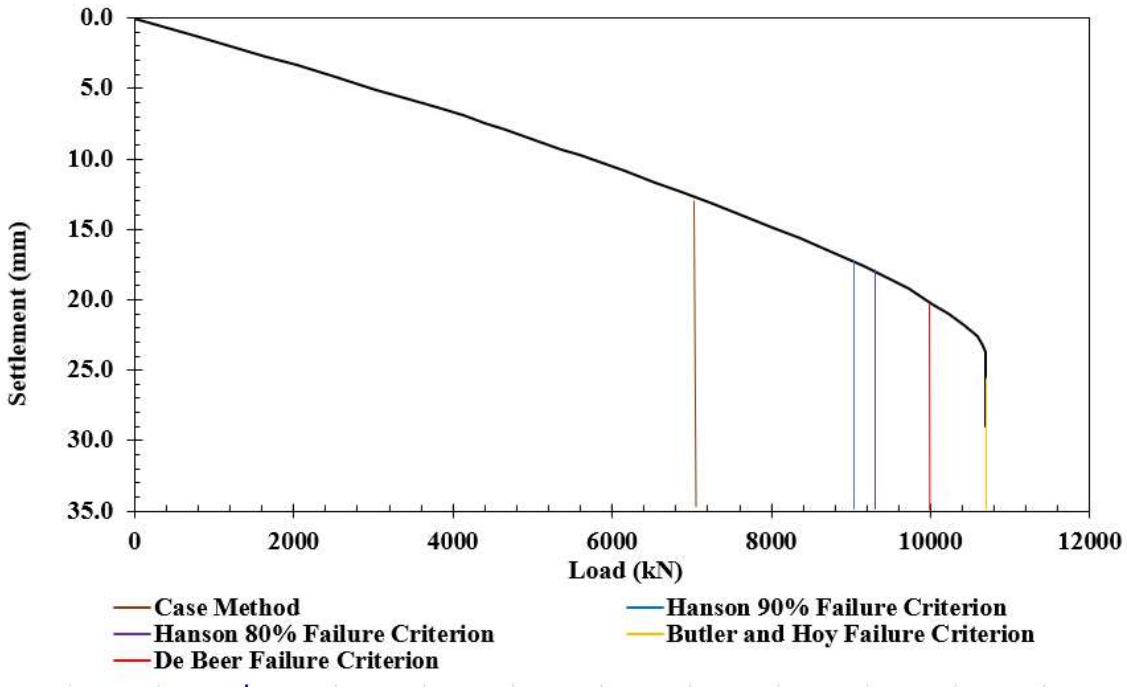

Figure 23. Pipe Pile Dynamic Testing Capacity Estimations

It should be noted the driving shoe located at the pile tip was not included as part of the pile model within the CAPWAP software. The signal matching results would only be marginally affected even if the pile shoe was included, given the size and depth of the driving shoe relative to the pile. The impedance changes in the bottom few inches would have been very small. The ultimate capacities predicted during the initial drive, and final re-strike of the pipe pile dynamic test are listed in Table 5.

Table 5. Pipe Pile Dynamic Capacity Estimations

Initial Drive		Final Drive	
Failure Criterion	**Ultimate Capacity**	**Failure Criterion**	**Ultimate Capacity**
De Beer	3,749 kN	De Beer	10,000 kN
Case Method	5,947 kN	Case Method	7,068 kN
Butler & Hoy	5,772 kN	Butler & Hoy	10,683 kN
-	-	Hanson 80%	9,128 kN
-	-	Hanson 90%	9,035 kN

The GRLWEAP software estimated the unit side shear resistances in the dense to very dense gravel ranged from approximately 47.8 kPa to 311 kPa and increased with depth. Figure 24 plots the shear resistance against depth. The end bearing resistance (using an end area based on a plugged condition) ranged from approximately 5314 kPa to 5793.5 kPa. However, unit end bearings are likely much higher due to the pile likely only being partially plugged.

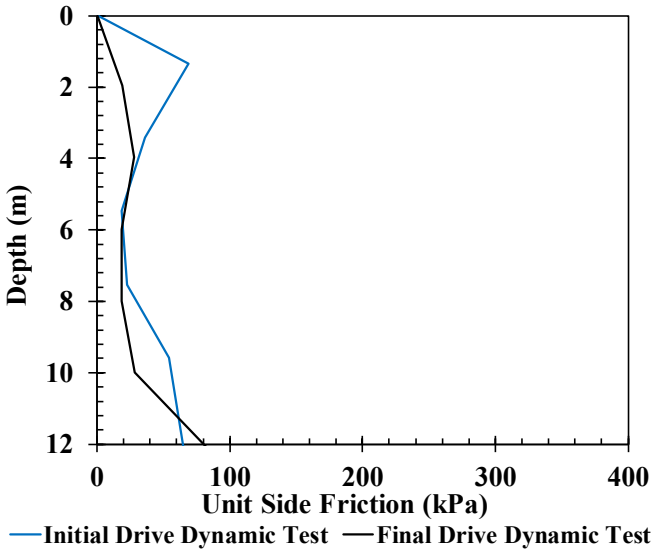

Figure 24. Pipe Pile Unit Side Friction

2.12 Static Load Test

2.12.1 H-Pile Static Load Testing Results

The Maximum Test Load (MTL) applied to the H-Pile was 5417.93 kN and exhibited a downward deflection of 0.7394 cm. The permanent displacement after unloading was 0.09144 cm. The load-settlement curve for the H-Pile static load test is presented in Figure 25.

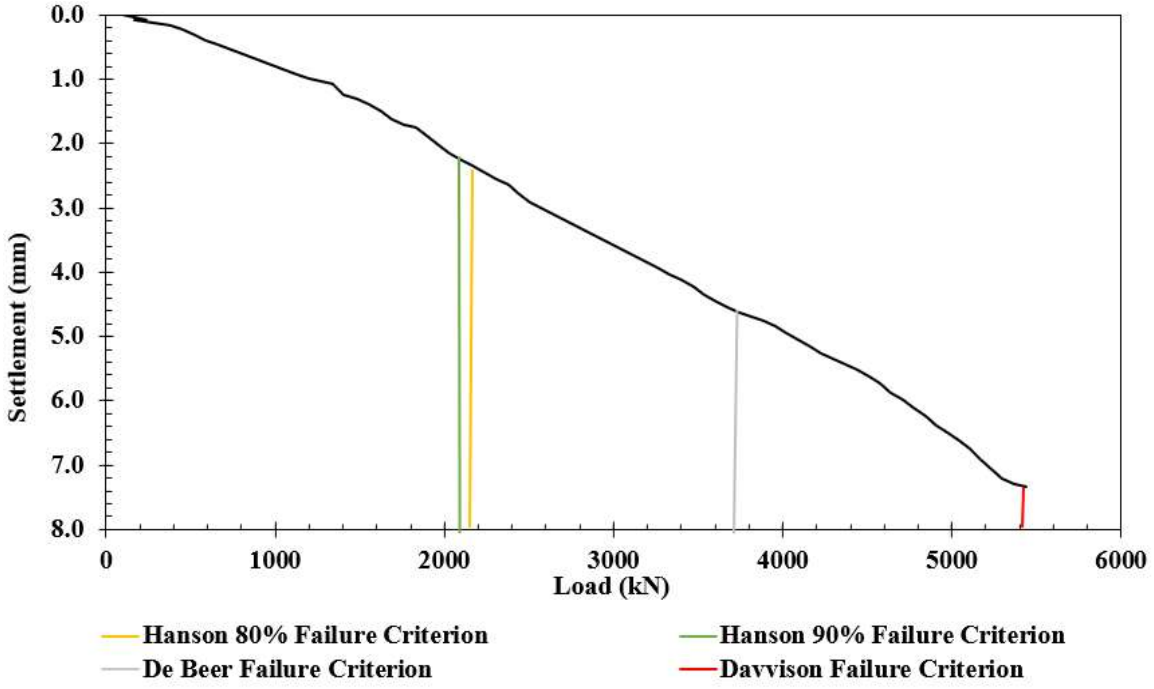

Figure 25. H-Pile Static Load-Settlement Curve

The H-Pile did not achieve geotechnical failure 100% of the design test load. Therefore, three additional load increments were added up to the maximum test load. The deflection measured at the pile head during the pile load test never exceeded the calculated elastic shortening of the test pile. Thus, the FHWA failure criteria for an HP18x204 pile was not achieved. Table 6 lists the ultimate capacity predictions from the H-Pile static load test.

Table 6. H- Pile Static Test Ultimate Capacities

Failure Criterion	Ultimate Capacity
Hanson 90%	2,130 kN
Hanson 80%	2,152 kN
De Beer	3,755 kN
Davvison	5,438 kN

2.12.2 Pipe Pile Static Load Testing Results

The Maximum Test Load (MTL) applied to the pile was 6418.78 kN and exhibited a downward deflection of 1.05156 cm. The permanent displacement after unloading was 0.127 cm. The load-settlement curve for the Pipe Pile static load test is presented in Figure 26.

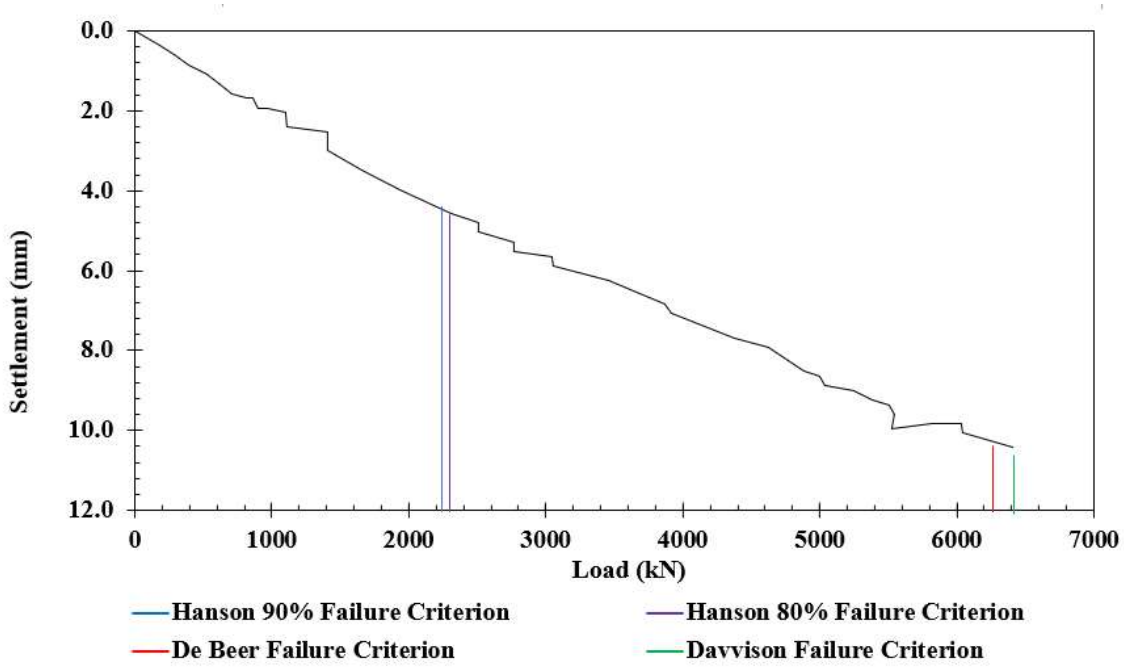

Figure 26. Pipe Pile Load-Settlement Curve

The load readings from the Enerpac ESS Synchronous Lift System and the calculated load from the pressure transducers were 2032.84 kN apart, indicating that the pile failed before it reached the design test load. When piles are loaded near failure, load-settlement data can become skewed. Table 7 lists the ultimate capacity predictions from the pipe pile static load test.

Table 7. Pipe Pile Static Test Ultimate Capacities

Failure Criterion	Ultimate Capacity
Hanson 90%	2,213 kN
Hanson 80%	2,236 kN
De Beer	6,309.6 kN
Davvison	6,410 kN

The Hanson failure criteria are extrapolation methods. The Hansen method assumes that when the failure load is approached, the load-settlement curve is hyperbolic in shape. The 90% (more conservative) Hanson failure method is the correct criteria for this load test because linear graphical derived failure criterion requires accurate load settlement readings. The deflection measured at the pile head during the pile load test never exceeded the calculated elastic shortening of the test pile. Thus, the FHWA failure criteria for a 30-inch-diameter steel pipe having a 1-inch wall thickness was not achieved at the maximum applied test load of 6418.78 kN.

2.13 Bearing Capacity Equations

2.13.1 H-Pile Bearing Capacity Equations Results

The bearing capacity equations prediction of the ultimate capacity of the H-Pile is 3,641kN. In the bearing capacity calculation, the effective earth coefficient (K) was assumed to be 1, and the soil/pile friction angle (δ) was assumed to be 0.65 φ (φ = effective internal angle of friction). The ultimate capacity predictions varied linearly over a range of assumed effective earth coefficients (δ=constant = 0.65 φ) and soil/pile friction angles (K=constant=1). This linear change is graphically demonstrated in Figure 27.

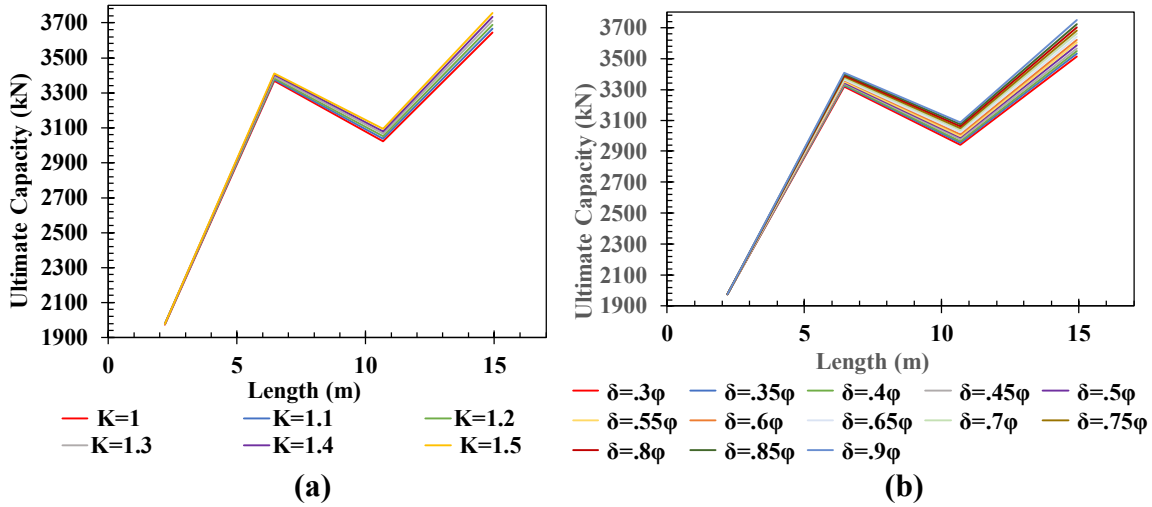

Figure 27. H-Pile Ultimate Capacity: (a) K= 1-1.5; (b) δ=0.3φ-0.9φ

The ultimate capacity ranged from 3,641 kN to 3,756 kN as the effective earth coefficient ranged from 1 to 1.5 (K=1-K=1.5) and ranged from 3,513 kN to 3,746 kN as the soil/pile friction angle ranged from 0.3φ to 0.9φ (δ=0.3φ- δ=0.9φ).

2.13.2 Pipe Pile Bearing Capacity Equation Results

The bearing capacity equations prediction of the ultimate capacity of the Pipe Pile is 12,045 kN. In the bearing capacity calculation, the effective earth coefficient (K) was assumed to be 1, and the soil/pile friction angle (δ) was assumed to be 0.65 φ (φ = effective internal angle of friction). The ultimate capacity predictions varied linearly over a range of assumed effective earth coefficients (δ=constant = 0.65 φ) and soil/pile friction angles (K=constant=1). This variation is shown in Figure 28.

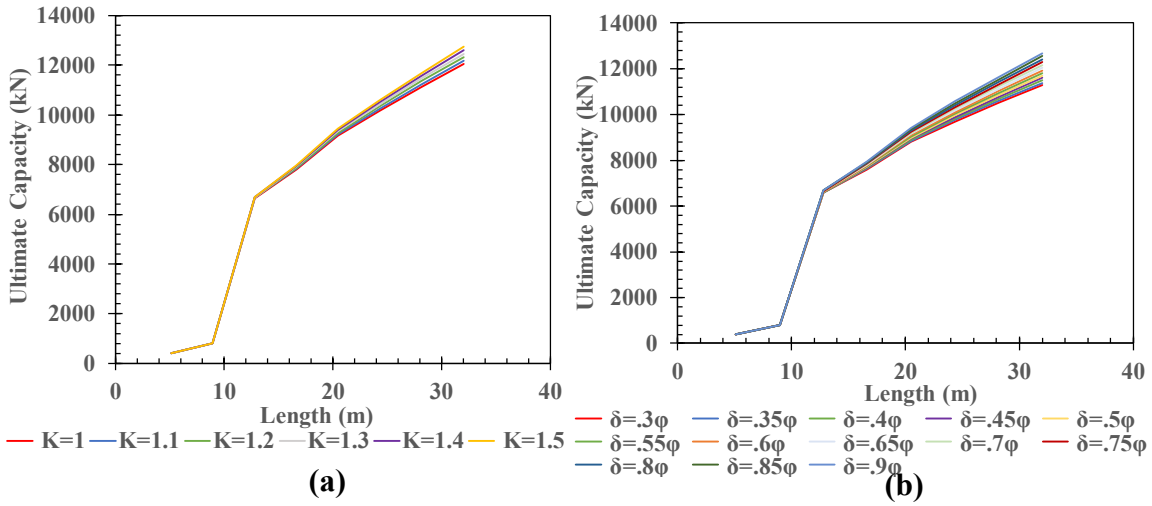

Figure 28. Pipe Pile Ultimate Capacity: (a) K= 1-1.5; (b) δ= 0.3φ-0.9φ

The ultimate capacity ranged from 12,405 kN to 12,732 kN as the effective earth coefficient ranged from 1 to 1.5 (K=1-K=1.5) and ranged from 11,278 kN to 12,679 kN as the soil/pile friction angle ranged from 0.3φ to 0.9φ (δ=0.3φ- δ=0.9φ).

2.14 Discussion of Pile Load Test Results

2.14.1 H-Pile Discussion

The Maximum Test Load (MTL) applied to the H-Pile was 5417.93 kN and exhibited a downward deflection of 0.7394 cm. The permanent displacement after unloading was 0.09144 cm. The H-Pile did not achieve geotechnical failure at 100% of the design test load, or the three additional load increments that were added up to the maximum test load. The GRLWEAP and Bearing Capacity Equations capacity calculations underestimated the ultimate capacities estimated by the load tests. The actual capacity for the H-Pile cannot be determined with certainty because failure did not occur during testing. This most likely due to partial soil plugging. If the soil does not plug during driving, the soil inside a pipe pile

or between H-pile flanges slips and produces internal shaft resistance. Slippage results in the limited toe resistance being the controlling variable in the capacity equation and the end bearing resistances being inaccurate. When the soil does not plug during driving, the soil inside a pipe pile or between H-pile flanges slips and produces internal shaft resistance. H-Piles can get soil trapped between the flange and affect the soil-pile interaction by changing the interface with additional sticking. This can have a significant impact on the accuracy of the predicted end-bearing capacity accuracy. The ultimate capacities estimations predicted in this study are summarized in Table 8.

Table 8. H-Pile Ultimate Capacity Summary

Dynamic Load Test	5,560 kN
Static Load Test	3,755 kN
Bearing Capacity Equations	3,641 kN
GRLWEAP	2,668 kN

2.14.2 Pipe Pile Discussion

The Maximum Test Load (MTL) applied to the pile was 6418.78 kN and exhibited a downward deflection of 1.05156 cm. The permanent displacement after unloading was .127 cm. The load readings were performed on the Enerpac ESS Synchronous Lift System, and the calculated load from the pressure transducers were 2032.84 kN apart, indicating that the pile failed before it reached the design test load. When a pile is loaded near failure, the load-settlement data can become skewed and make capacity estimations unreliable. Extrapolation methods assume that when the failure load is approached, the load-settlement curve is hyperbolic in shape. Extrapolation methods are practical solutions for capacity estimations when linear load-settlement data are not available. The Hanson 90% failure criterion provided the most accurate capacity corresponding to the applied load. The Davvison and De Beer failure criteria provided the most misleading capacity predictions. This is probably because the Davvison and De Beer failure criterion are derived from graphical methods that rely on linear relationships. The ultimate capacities estimations predicted in this study are summarized in Table 9.

Table 9. Pipe Pile Ultimate Capacity Summary

Dynamic Load Test	7,068 kN
Static Load Test	2,213 kN
Bearing Capacity Equations	12,045 kN
GRLWEAP	10,675 kN

2.15 Conclusions

The results of this study show that the dynamic methods for predicting the capacity of the pile do not match the measured results from the static load test. The study in the cases of both test piles show the dynamic test methods overpredicted the capacity pile. This study provides further support to the argument that further investigation and adjustment to dynamic methods are required before load test programs consisting of both static and dynamic load tests are not necessary to accurately predict the capacities of deep foundations using large diameter piles.

CHAPTER 3

3 Load Transfer Analysis of Load Test Program with Large Diameter Bridge Piles

3.1 Introduction

The method for predicting the load transfer behavior of driven piles is based on finite element analysis. The load transfer method treats the pile as a beam supported by non-linear springs. The active stresses at the soil-pile interface are represented by three loading mechanisms that are related by the internal angle of friction. The stress acting at the soil-pile interface can be represented with t-z and q-z curves. T-z and q-z curves define the soil-pile interaction with depth by quantifying the stresses brought forth with each load increment. T-z curves represent the load transfer relationship along the shaft of the pile, and q-z curves represent the soil-pile relationship at the pile toe.

The load-settlement data provided by dynamic load tests are generated by signal matching software that runs multiple iterations of the wave equation with measured strain and acceleration data. The theories and assumptions at the core of dynamic analysis were derived from research based on small diameter piles, homogenous soils, and ideal installation techniques. The use of different pile types, geometries, and soil mixtures creates uncertainty in the dynamic model of the soil-pile interface because of the variations that can occur to the active forces.

In high profile pile foundation designs, static tests subsequently performed after dynamic tests to supplement the dynamic results. A t-z analysis of the static load test data describes the soil-pile behavior over the entire length of the pile. The uncertainties reported in the literature associated with dynamic load transfer data for large diameter piles indicate that design failure is likely to occur unless back calculations and adjustments are made using static tests to account for soil plugging and elastic shortening.

This paper presents a load transfer analysis of static and dynamic load data from a load test program conducted on a bridge replacement project in western Kentucky. First, the site and soil conditions are described along with the dynamic and static load test procedures. The paper concludes by calculating and describing the approach used to develop the load transfer data, t-z, and q-z curves along with a discussion of the results.

3.2 Project Description

The Kentucky Transportation Cabinet (KYTC) has proposed bridge a replacement for an existing crossing at Kentucky Lake. The crossing follows the existing US 68/KY 80 highway corridor. The bridge is a multi-span structure that is served by causeways on the east and west banks of Kentucky Lake that extend into the lake and serve as approaches. The steel girder bridge will be supported on integral end bents and two interior piers. The interior piers are in turn supported on three columns that are connected to a single beam support. The proposed Bridge has a length of 176.80 m and a width of 19.6 m.

3.3 Site Conditions

A load test program is being conducted at two locations. The load test locations are designated L-1 and L-2. Several test borings and cone penetration tests (CPT) were performed in 2011 near the test pile locations. The geology of the site is influenced by the Mississippi Embayment to the west and is composed primarily of a cherty Mississippian-age residuum within the Ft. Payne Formation. This formation is described as a residual chert interbedded with residual clay. Existing grades currently slope from south to north over much of the site from the existing highway embankment to the existing lagoon. The load test locations are illustrated in Figure 29.

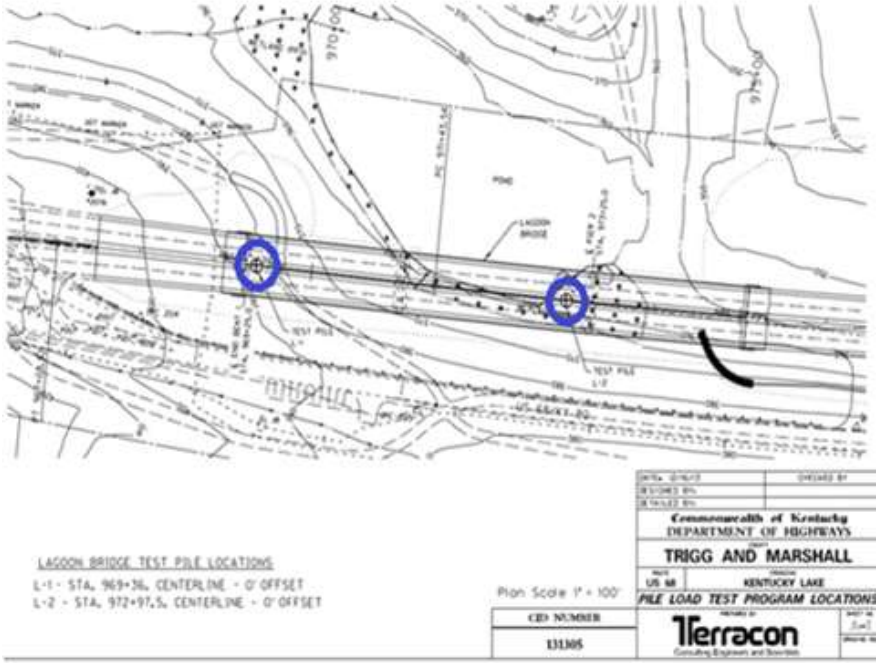

Figure 29. Project Site Test Locations

At the west end of the site, near the L-1 load test location, grades slope from southwest to northeast toward the lagoon. Grades at the site range from approximately 7H:1V near the lagoon to as steep as 3H:1V near the west end of the site (Figure 30). The groundwater has a summer pool elevation of 109.42 m and a winter pool elevation of 107.90 m.

The subsurface soil conditions at the L-1 test site are cohesive hard silt (ML) from ground surface to a depth of 2.1 m. Between depths of 2.1 m to 8.5 m boring logs documented cohesionless dense gravel with silt (GM). Between depths of 8.5 m to 10.05 m cohesive hard silt (ML) exists. From the depth of 10.05 m to the bottom of the boring (14 m), the test boring encountered cohesionless silty gravel with chert and bedded chert (GM-ML). The estimated soil properties from boring data for the L-1 test site are provided in Table 10.

Table 10. Estimated Soil Properties for L-1

Layer	Depth Interval (m)	Soil Type	Natural Moisture Content	Dry Unit Weight	Friction Angle (^{o})	qu/qp (kPa)	Average su (kPa)
I	0-2.13	Silt (ML)	46.54	2002	0	861/58	95.76
II	2.13-8.53	Silty/ Gravel (GM)	34.98	1842.12	34	6464/110	0
III	8.53-10.06	Silt (ML)	33.37	2002.307	0	862/67	95.76
IV	10.6-20.00	Silty/Gravel (GP- GM)	31.12	2002.307	36	7182/220	0

q_u = unconfined compression strength; q_p = pocket penetrometer strength; s_u = undrained shear strength.

At the L-2 load test site borings encountered alluvial clay (CL) and silt soils (ML) with some chert pieces from the muddy ground surface at a depth of 11.2 m. Within this depth test, a test boring encountered a layer of loose gravel with silt (GC) from a depth of 2.7 m to 4.2 m. Between the depths of 4.2 m to 20.4 m test borings encountered silty gravel with chert (GP-GM). From the depth of 20.4 m to 24.56 m at the bottom of the boring test,

borings encountered silty gravel with chert and chert layers (GC-GM). The estimated soil properties from boring data for the L-2 test site are provided in Table 11.

Table 11. Estimated Soil Properties for L-2

Layer	Depth Interval (m)	Soil Type	Natural Moisture Content	Dry Unit Weight	Friction Angle (°)	qu/qp (kPa)	Average su (kPa)
I	0-11.28	Clay/Silt (CL-ML)	26	2082	0	172/15	28.73
II	11.28-20.42	Silty Sand/Silty Gravel (GM)	21	2002	34	3519/48	0
III	20.42-26.21	Silty Gravel (GM)	30	2082	36	7182/110	0

q_u = unconfined compression strength; q_p = pocket penetrometer strength; s_u = undrained shear strength.

3.4 GRLWEAP Drive-Ability Results

The GRLWEAP results indicated a hammer with a rated energy of 37 kN-m to 66 kN-m will be required to drive unplugged H-piles, and a hammer with a rated energy of 206 kN-m to 217 kN-m will be required to drive unplugged H-Piles. The H-Pile GRLWEAP results are shown in Figure 30.

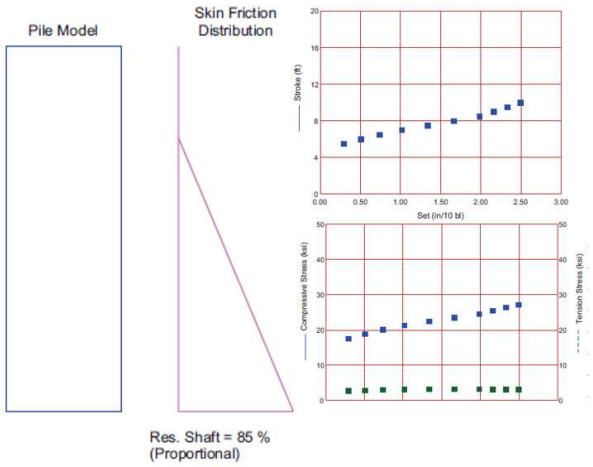

Figure 30. H-Pile GRLWEAP Hammer Information

The GRLWEAP results indicate that a hammer with a rated energy of 112.5 kN-m to 122 kN-m will be required to drive the unplugged pipe piles, and a hammer with a rated energy of 206 kN-m to 217 kN-m will be required to drive the plugged pipe piles to the necessary tip elevations without overstressing the piles. The Pipe Pile GRLWEAP results are shown in Figure 31.

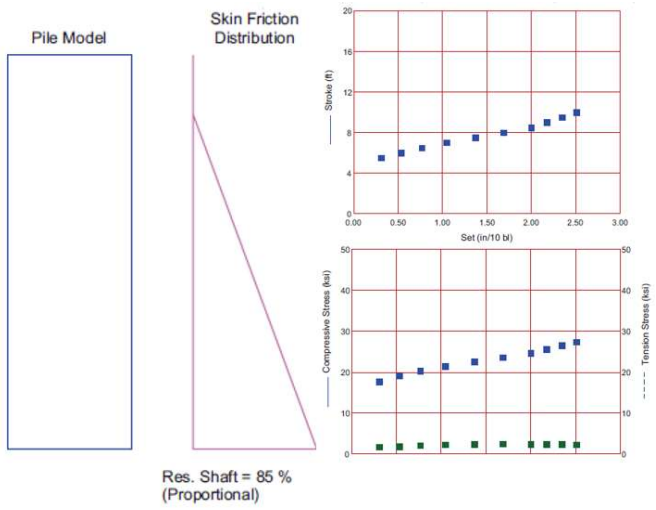

Figure 31. Pipe Pile GRLWEAP Hammer Information

3.5 Test Piles

3.5.1 Pile Selection

The pile load test program consisted of static and dynamic testing on two test piles designated as L-1 and L-2. Test pile L-1 was an HP18x204, ASTM A572, Grade 50 steel H-Pile with a length of 18.3 meters. Test pile L-2 was a 762 mm (O.D.) steel pipe pile with a wall thickness of 25.4 mm and had an overall length of 32 meters. The prescribed lengths assumed a water level elevation of 11.3 m plus an additional 6.1 m for instrumentation gages, leads/sleeves, and to provide sufficient stickup to perform pile testing. The analyses assumed all pipe piles would consist of ASTM A252 steel having a yield strength of at least 310 MPa, whereas the assumed yield strength is 344.7 MPa for the H-piles.

3.5.2 H-Pile Pile Instrumentation

The H-Pile arrived in one 18.3 m piece (area = 387 cm2). Strain gages were placed at ten different locations along the pile length. The strain gages were protected during driving with a welded steel angle over the gages and associated wires. The test pile was instrumented using vibrating wire strain gages at ten depth intervals along two vertical lines

located along the centerline of each side of the H-Pile web. A schematic depicting the instrumentation of the H-Pile is presented in Figure 32.

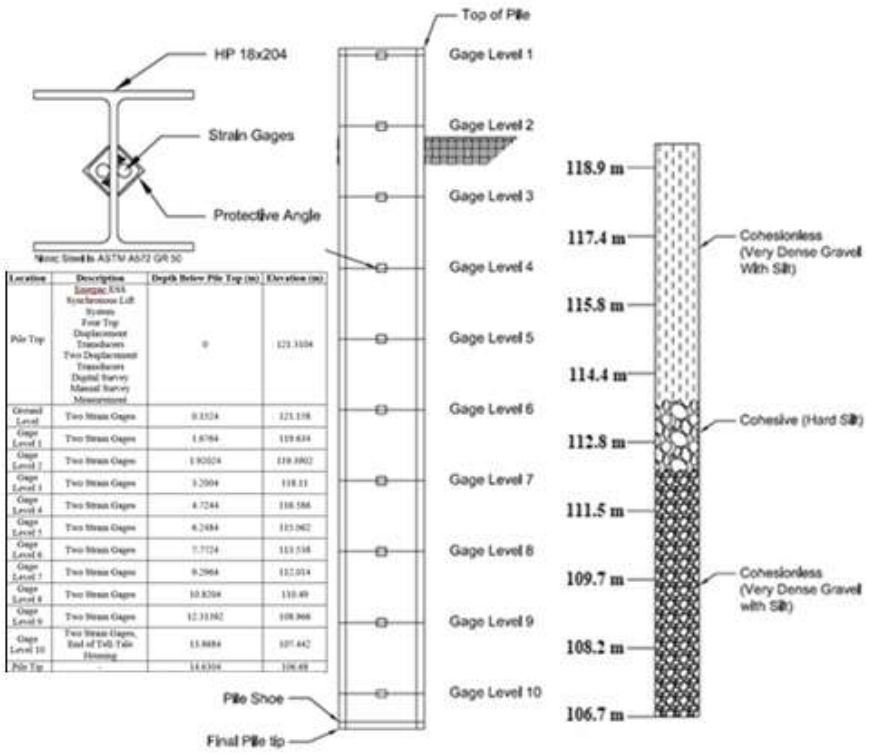

Figure 32. H-Pile Schematic

Before installing the test pile, a pre-probing program was implemented to determine if predrilling was extended to an elevation of 102.108 m. The pile was driven with an ICE I-30v2 open-ended diesel hammer to 350 ft before static testing proceeded.

3.5.3 Pipe Pile Instrumentation

The pipe pile was manufactured in two sections. The bottom part of the test pile was 4.65 m in length, and the top part was 5.11 m in length. The two pile sections were joined together with a field welded splice on the project site during installation. Strain gages placed at ten different locations along the pile length. A pile driving shoe was placed at the end of the pipe to improve driveability and durability. A schematic depicting the instrumentation of the Pipe Pile is presented in Figure 33.

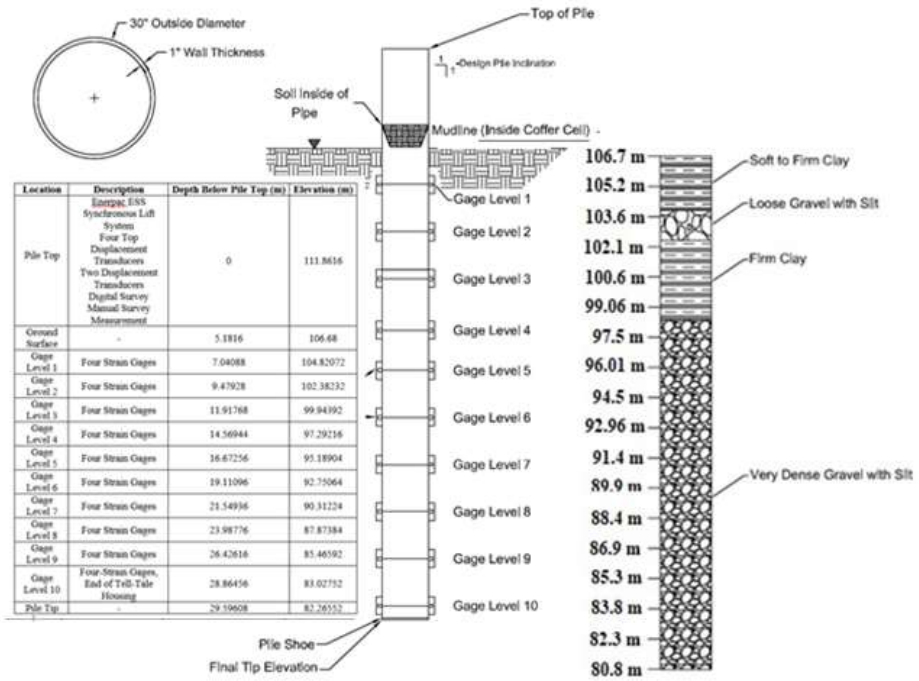

Location	Description	Depth Below Pile Top (m)	Elevation (m)
Pile Top	Energac ESS Synchronous Lift System Four Top Displacement Transducers Two Displacement Transducers Digital Survey Manual Survey Measurement	0	111.8616
Ground Surface	-	5.1816	106.68
Gage Level 1	Four Strain Gages	7.04088	104.82072
Gage Level 2	Four Strain Gages	9.47928	102.38232
Gage Level 3	Four Strain Gages	11.91768	99.94392
Gage Level 4	Four Strain Gages	14.56944	97.29216
Gage Level 5	Four Strain Gages	16.67256	95.18904
Gage Level 6	Four Strain Gages	19.11096	92.75064
Gage Level 7	Four Strain Gages	21.54936	90.31224
Gage Level 8	Four Strain Gages	23.98776	87.87384
Gage Level 9	Four Strain Gages	26.42616	85.46592
Gage Level 10	Four Strain Gages, End of Tell-Tale Housing	28.86456	83.02752
Pile Tip	-	29.19608	82.26552

Figure 33. Pipe Pile Schematic

Before installing the test pile, predrilling was performed using a 60.96 cm-diameter auger to Elevation 108.204 m. The test pile was driven using an ICE I-100v2 open-ended diesel hammer to a tip elevation of 84.7 m.

3.6 Dynamic Load Testing

3.6.1 H-Pile Dynamic Test Procedure

Before installing the test pile, a pre-probing program was implemented to determine if predrilling was required. This program determined that pre-drilling should be done due to the limited number of test borings at the site, and because of the presence of bedded chert. The predrilled hole extended to an elevation of 102.108 m. The pile was driven with an ICE I-30v2 open-ended diesel hammer. After completion of the initial drive, a restrike was performed 72 hours later. Dynamic testing data was recorded using pile driving monitoring equipment manufactured by Pile Dynamics Inc. (Model PAX, strain and accelerometer calibrations attached) and analyzed with the CAPWAP software during the initial drive and subsequent restrike.

Upon completion of dynamic testing (72-hour restrike), preparation for the axial static load test commenced. After preparation for the axial static load test, the tested pile length was

14.6304 m and had embedment length of 12.71 m within the soil. After the completion of the 72-hour restrike, the head of the pile elevation was +121.31 m, and the final pile tip elevation was +106.68 m; the final tested pile length was 14.60 m. The ground surface was at the height of +119.39 m, giving the pile an embedment length of 12.71 m within the soil.

3.6.2 Pipe Pile Dynamic Test Procedure

Before installing the test pile, predrilling was performed using a 60.96 cm-diameter auger to Elevation 108.204 meters. The decision to pre-drill made as a result of the presence of chert in the encountered soils during field exploration. Predrilling at the testing location was performed using a 60.96 cm-diameter auger to down to an elevation 108.204 m.

The test pile was driven using an ICE I-100v2 open-ended diesel hammer to a tip elevation of 84.7 m on the initial drive. Additional PDA restrikes were performed on August 19, 2013, and September 10, 2013. This corresponded to 72 hours after the completion of the redrive and four days after the completion of the static load test. Dynamic pile testing (PDA) was recorded during the initial drive, redrive, and subsequent restrikes. After the completion of the 72-hour restrike on August 19, 2013, the test pile was cut-off to bring the pile top to the required load testing elevation. The final tip elevation was +25.07 m and the top of pile elevation at the time of testing was +34.10 m, giving the tested pile a length of 9.02 m. The ground surface was at an elevation of +32.52 m, giving the pile an embedment length of 7.44 m within the soil. The surface was at an altitude of +32.52 m, which led to a pile embedment length of 7.44 m within the ground.

3.6.3 H-Pile Dynamic Test Results

The subject pile was monitored with dynamic pile testing equipment during initial drive, all subsequent re-strikes, and extended drive. The CAPWAP software was used to generate the load transfer information from the data collected during testing. Compression and tension pile driving stresses were below the acceptable limit of 279237 kPa. The acceptable limit of compression and tension driving stresses was defined as 90 percent of the applied load.

The GRLWEAP software determined estimated the unit side shear resistances in the dense to very dense gravel ranged from approximately 95.76 kPa to 191 kPa and generally increased with depth. The estimated unit end bearings at the pile tip (plugged condition)

ranged from approximately 636 to 911 kPa. The low hammer energy utilized during the final restrike did not mobilize the pile.

3.6.4 Pipe Pile Dynamic Test Results

The pile was monitored with dynamic pile testing equipment during initial drive, all subsequent re-strikes, and extended drive. Compression and tension pile driving stresses were below the acceptable limit of 279237 kPa. The match qualities (MQ) for the signal matching results were less than 4. Lower match qualities may be achievable; however, to achieve lower match qualities the ultimate capacity of the pile may be unrealistic given the soil conditions, transferred hammer energy, and the measured sets. The acceptable limit for compression and tension driving stresses was defined as 90 percent of Fy.

The CAPWAP software was used to generate the load transfer information from the data collected during testing. The unit side shear resistances in the dense to very dense gravel ranged from approximately 47.8 kPa to 311 kPa and increased with depth. The end bearing resistance ranged from approximately 5314 kPa to 5793.5 kPa. However, unit end bearings are likely much higher due to the pile likely only being partially plugged.

3.7 Static Load Testing

The load was applied using three hydraulic jacks equipped with a common manifold and single electric hydraulic pump. The hydraulic jacks had an effective area of 0.056 square meters. The hydraulic jacks acted against an engineered reaction frame with a total of 8 reactions placed in-line with the cylinders, then positioned adjacent to the pressure transducer supplied as part of the Synchronous Lift System. A sketch of the load test frame is shown in Figure 34.

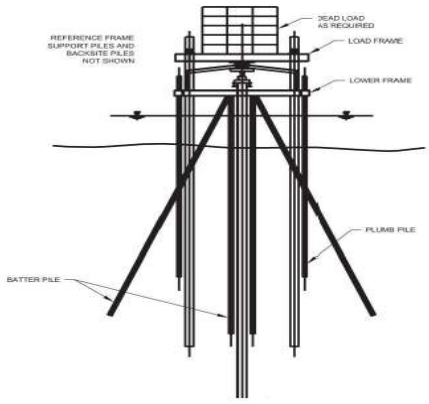

Figure 34. Load Test Frame

The applied load was measured with an Enerpac ESS Synchronous Lift System that records the applied load and hydraulic jack elongation data in real time. The top of the pile movement was measured using four displacement transducers mounted on a reference beam. Backup pile head measurements and measurements of reaction pile movements were measured using survey methods. Two telltales were installed along the exterior of the pile and terminated near the toe of the H-Pile. The H-Pile telltales housing is shown in Figure 35.

Figure 35. H-Pile Load Tell Tale Housing

The test load was applied in increments of 5% of the maximum applied test load. During each load interval, the load was maintained for a time interval of 10 minutes, using the same time interval for all loading increments except at 50% and 100 % on the applied test load. At 50% of the applied test load, the load was maintained for 30 minutes, and at 100% of the applied test load, the load was maintained for 1 hour. The applied test load was removed in ten, approximately equal, decrements. The load at each decrement was maintained for 15 minutes. The same time interval was utilized for all unloading decrements. Readings continued to be taken for 30 minutes after complete unloading of the test pile. The pile stiffness multiplied the average strain at each gage level.

3.8 Load Transfer Curves

Load transfer curves are derived from strain gage data using Hooke's Law. Hooke's Law states that stress can be interrupted as strain after multiplied by a modulus that correlates the two. Hooke's Law can be applied mathematically with Equation 16 where E is the modulus, ε is the strain, and σ is the stress.

$$\varepsilon = \frac{\sigma}{E} = \frac{F}{AE} \tag{16}$$

The data that strain gages provide during a load test can be easily converted into stress that when multiplied by the cross-sectional area of the pile outputs the desired axial force at the specified depth. Pile shortening is observed settlement and was calculated using telltale data in this study. Equation 17 mathematically represents this correlation with a variation of Hooke's Law where F is the force, and A is the area.

$$F = \sigma A \tag{17}$$

The load transfer curves presented in this study were constructed for each load increment at various depths by matching the strain gage reading at various depths to their respective load increment. The load transfer curves for the H-Pile and Pipe Pile are presented in Figure 36 (a) and Figure 36 (b), respectively. The load at a specified point in the pile was determined from the strain gage data using Equation 18 where P = applied load at the pile head; ε = strain at the gage level; A_p = cross-sectional area of the pile; E_p = composite elastic modulus of the pile.

$$P = \varepsilon A_p E_p \tag{18}$$

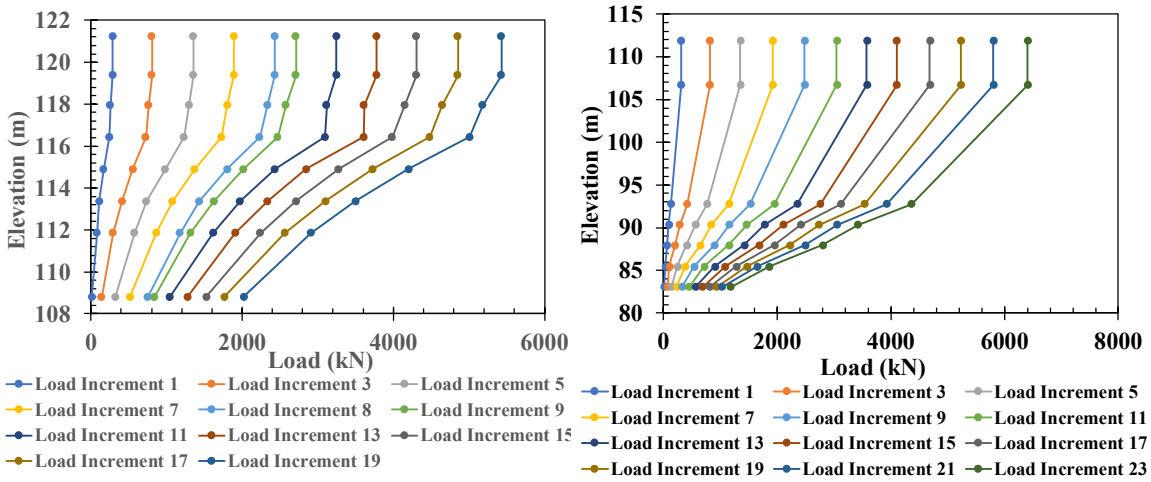

Figure 36. Load Transfer Curves: (a) H-Pile; (b) Pipe Pile

3.9 Unit Side Friction

The measured unit side shear resistance was calculated using the peak computed loads recorded by the strain gages at each depth interval and dividing the corresponding stress by the respective segment surface area. Equation 19 was used to calculate the unit side

shear resistance (T) where τ = soil unit skin friction (kPa) and A_S = surface area of the pile segment exterior in contact with soil in shear. It is important to note that the skin resistance was calculated at the mid-point of each interval between the strain gages in this calculation.

$$T = \tau * A_S \tag{19}$$

3.9.1 H-Pile Unit Side Friction

The unit side shear was measured to range from 62.24 in the predrilled zone to 287.3 kPa. The maximum unit shear resistance occurred a depth of 4.2 m. After the unit side shear resistance peaks, the shear resistance steadily decreases over the remaining length of the pile. The unit side shear resistance over the entire length of the H-Pile is plotted in Figure 37.

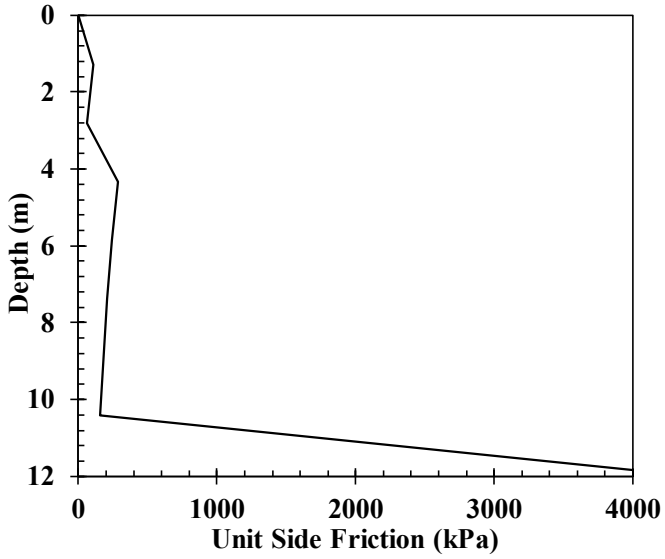

Figure 37. H-Pile Unit Side Friction

3.9.2 Pipe Pile Unit Side Friction

The measured unit side shear was measured to range from 105.34 to 167.58 kPa in the lower segments. The Pipe Pile unit shear resistance steadily increased with depth through the clay layers of soil to a depth of 14 m where very dense gravel and silt were present. The shear resistance at this point rapidly increased until it peaked at a depth of 16 m. The post-peak unit side shear resistance fluctuated over the remaining length of the pile. The unit side friction over the entire length of the Pipe Pile is plotted in Figure 38.

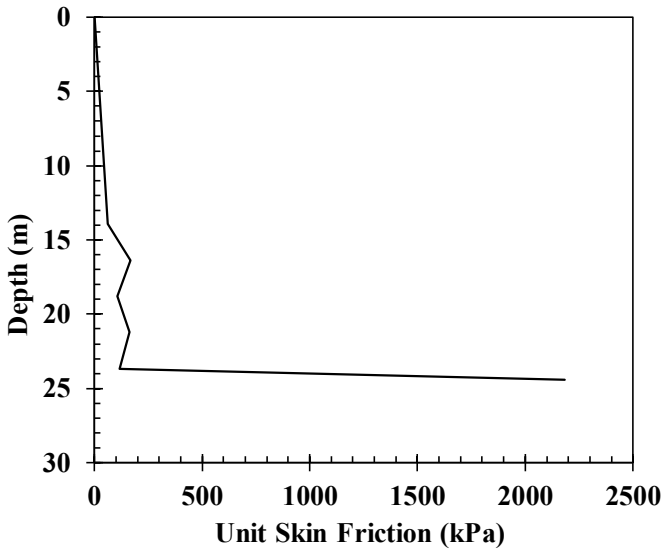

Figure 38. Pipe Pile Unit Side Friction

3.10 End Bearing Resistance

The potential to accumulate compacted soil must be considered in every subsurface profile. Piles that are hollow or have the potential to entrap soil can provide misleading test data because it can change the cross-sectional area of piles and expose them to additional resistive forces. This is often referred to as soil plugging and can potentially have a significant impact on the accuracy of the end-bearing capacity readings. In H-Piles it is possible that soil becomes trapped and compacted between the flange and web resulting in a larger surface area than the initially expected. This can also affect surface the soil-pile interaction by changing the interface that causes additional sticking or slipping. The plugged condition was assumed for both piles in all calculations. Equation 20 was used to calculate the unit side shear resistance (Q_{plug}).

$$Q_{plug} = q * A_{plug} \quad (20)$$

Q_{plug} =unit end bearing resistance (kPa)

A_{plug}=full cross-sectional area of pile toe

3.10.1 H-Pile End Bearing Resistance

The measured unit end bearing resistance ranged from 361 to 2275 kPa decreasing with depth. The mobilized toe resistance represents the load developed in side shear on the toe segment (bottom) coupled with the tip resistance component. The estimated mobilized toe

resistance represents the load developed in side shear on the toe segment coupled with the tip resistance component. The mobilized toe resistance accounted for the 2.3 m bottom of pile segment shear and assumed plugged pile end area of 387 cm^2. The toe segment resistance was estimated to be approximately 23,106.71kPa. The H-Pile load transfer information that describes the loads at other depths are charted in Table 12.

Table 12. H-Pile Static Load Transfer Results

Analysis Zone	Depth (m)	Load Transfer (kN)	Surface Area (m^2)	Unit Side Shear (kPa)
Segment 1	0-1.3	245	2.28	105
Segment 2	1.3-2.8	169	2.814	62
Segment 3	2.8-4.3	814	2.814	287
Segment 4	4.3-5.9	681	2.814	239
Segment 5	5.9-7.4	596	2.814	210
Segment 6	7.4-10.4	890	5.63	158
Toe Segment	10.4-12.7	2024	0.214	6349

The ultimate load in a pile is the sum of the unit skin friction and unit end bearing resistance in a pile at a specific depth. The ultimate load drops to zero when a pile fully mobilizes. The load test data suggests the lower four segments and tip resistance did not fully mobilize during the load test. The calculated ultimate loads measured over the entire length of the H-Pile are plotted in Figure 39.

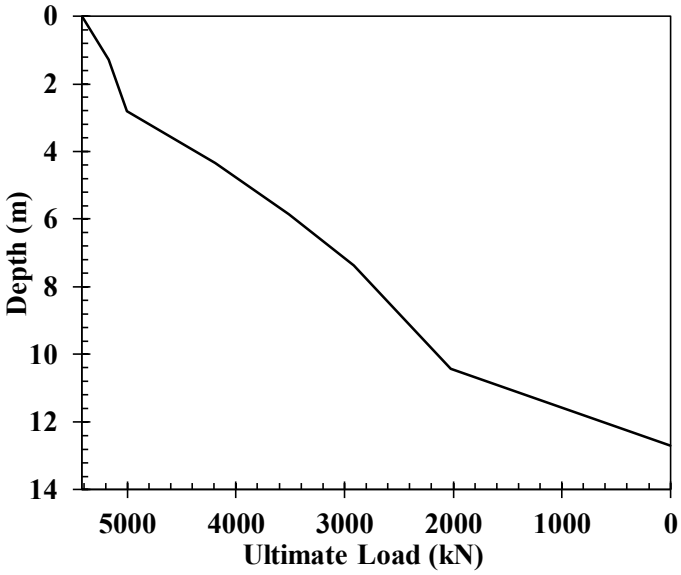

Figure 39. H-Pile Ultimate Load vs. Depth

3.10.2 Pipe Pile End Bearing Resistance

The measured unit end bearing resistance ranged from 130 kPa in the predrilled zone to 606 kPa. The maximum unit end bearing resistance occurred at a depth of 16 meters and steadily decreased over the remaining length of the pile embedded in the very dense gravel and silt. The calculated ultimate loads measured over the entire length of the Pipe Pile are plotted in Figure 40.

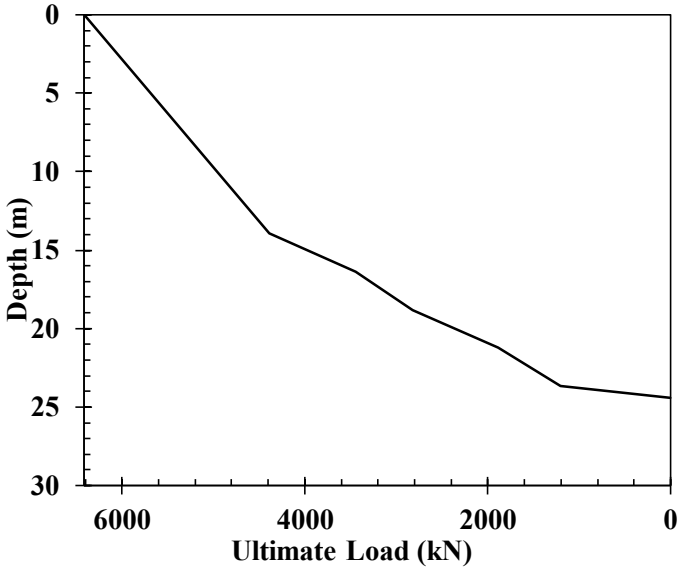

Figure 40. Pipe Pile Ultimate Load vs. Depth

The toe segment resistance represents the load developed from the side shear on the toe segment (bottom) coupled with the tip resistance component. The mobilized toe resistance accounted for the bottom of pile segment shear and assumed plugged pile end area. The estimated mobilized toe resistance is 2183.34 kPa. The Pipe Pile load transfer information that describes the loads at other depths are charted in Table 13.

Table 13. Pipe Pile Static Load Transfer Results

Analysis Zone	Depth (m)	Load Transfer (kN)	Surface Area (m^2)	Unit Side Shear (kPa)
Segment 1	0-13.93	2032.837271	33.32	62.24433656
Segment 2	13.93-16.37	943.0229792	5.61	167.5809061
Segment 3	16.37-18.81	622.751024	5.83	105.3365696
Segment 4	18.81-21.214	934.126536	5.76	162.7928802
Segment 5	21.214-23.65	680.5779048	5.83	114.9126213
Toe Segment	23.65-24.41	1205.468054	0.46	2183.339805

3.11 Development of t-z and q-z Curves

The formulation of t-z and q-z curves require the implementation of finite element analysis. Finite element analysis models the stress-strain relationship of a loaded pile using three loading mechanisms. The three mechanisms considered in the model are skin friction along the shaft of the pile, the resistance provided at the end of the pile, and deformation the pile undergoes as it is pressed down. To mathematically model the mechanisms acting on the pile the assumption that force created by the unit weight of the pile is negligible to the forces acting upon it. It is also assumed for analysis purposes that the integrity of the structural load-carrying capacity of the pile was preserved, and the materials properties of the pile are sufficient enough that failure will occur at the soil-pile interface due to slippage and not due to compression failure of the pile material.

The active forces transmitted on a pile subjected to axial loading can be conceptualized by sectionalizing the pile into manageable segments. It is generally assumed for derivation

purposes that the section is small and the forces acting on it are homogenous. A free-body diagram of a pile segment subjected to an axial load labeled with the active forces considered during finite element analysis is provided in Figure 41.

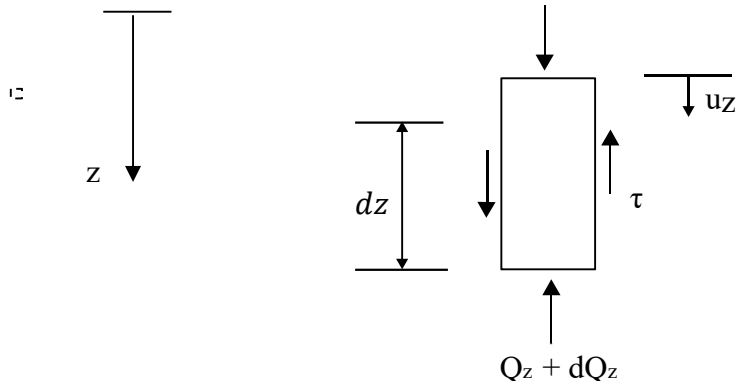

Figure 41. Pile Section Free Body Diagram.

Qz = The internal force acting on pile

C = Cicumference of the pile segment

τ = Unit skin friction

When force equilibrium principals are applied to the free-body diagram with the consideration of stress variation with depth, Equation 21 is formed. Equation 21 is the equilibrium equation for the general differential equation describing a pile under axial loading.

$$Qz = dQz + \tau * C * dz \tag{21}$$

If the unit skin friction and circumference of the pile segment are assumed constant over the pile segment, and the equilibrium equation is differentiated with respect to depth, Equation 22 is formed. Equation 22 is a particular solution to the governing differential equation that represents the load transfer of the applied loads to pile deformation, and skin friction.

$$\frac{dQz}{dz} = \tau * C \tag{22}$$

If the material properties are assumed to remain constant, the only entity that fluctuates with depth is the displacement of the pile segment due to applied loads. The mathematical

representation of how the internal forces change with depth in t-z and q-z analysis is Equation 23, where E = pile segment modulus of elasticity, A = the cross-sectional area of the pile segment, and $\frac{du_z}{dz}$ = pile segment displacement due to applied loads.

$$Qz = -EA\frac{du_z}{dz} \tag{23}$$

The method of substitution can be applied to solve this set of differential equations. When Equation 23 is plugged back into the equations above, the general solution that governs the load transfer mechanism can be obtained. Consequently, it governs t-z and q-z curve construction as well. The first order general solution of the differential equation that governs the pile-soil interaction during load transfer analysis is Equation 24.

$$-EA\frac{d^2u_z}{dz^2} + \tau * C = 0 \tag{24}$$

T-z curves represent the shear stress (t) and corresponding pile displacement (z) at locations along the pile shaft. The shear stress (t) is computed by taking the recorded axial force and dividing it by the pile sectional area. Various soil and pile parameters influence t-z behavior. The distribution of stiffness of both the pile and soil, pile geometry, and soil distribution are all influential factors. The load transfer information summarized in Table 11 and Table 12 of the previous section provided the data used to construct the t-z curves presented in this study. The average unit shaft resistance t was estimated between successive strain gages using Equation 25 where P_{i+1} and P_i are the axial loads in a pile at depths d_{i+1} and d_i, respectively; B = diameter of the pile.

$$t = \frac{P_{i+1} - P_i}{\pi \cdot B \cdot (d_{i+1} - d_i)} \tag{25}$$

3.12 Measured and Derived t-z Curves

The measured t-z curves presented in this study were plotted beside theoretical t-z curves for comparative analysis. The theoretically derived curves were formulated from load test the data of small piles (< 30 m long) with small diameters (< 0.5 m). The empirical t-z curves used in this study were generated using the API (1993) and Coyle and Reese (1966) methods. The API method (1993) uses the Davvison offset limit as its failure criterion.

Both methods consider plunging failure settlement cutoff equal to 5% of the shaft diameter first, but if this does not occur the methods yield different results. The Davvison offset limit defines the cutoff settlement as the elastic compression of the soil as well as the limiting plastic compression of the soil at the pile tip. The Coyle and Reese method (1966) uses the cutoff settlement as the ultimate axial capacity of undrained clays. Typically, the API (1993) method yields more conservative values than the Coyle and Reese (1966) method. The t-z curves generated by both methods tend to be softer when compared to measured data. For this reason, t-z analysis typically overpredicts the ultimate capacity of the pile. The t-z curves constructed for the H-Pile and Pipe Pile are presented in Figure 42 and Figure 44, respectively.

3.12.1 H-Pile t-z Curves

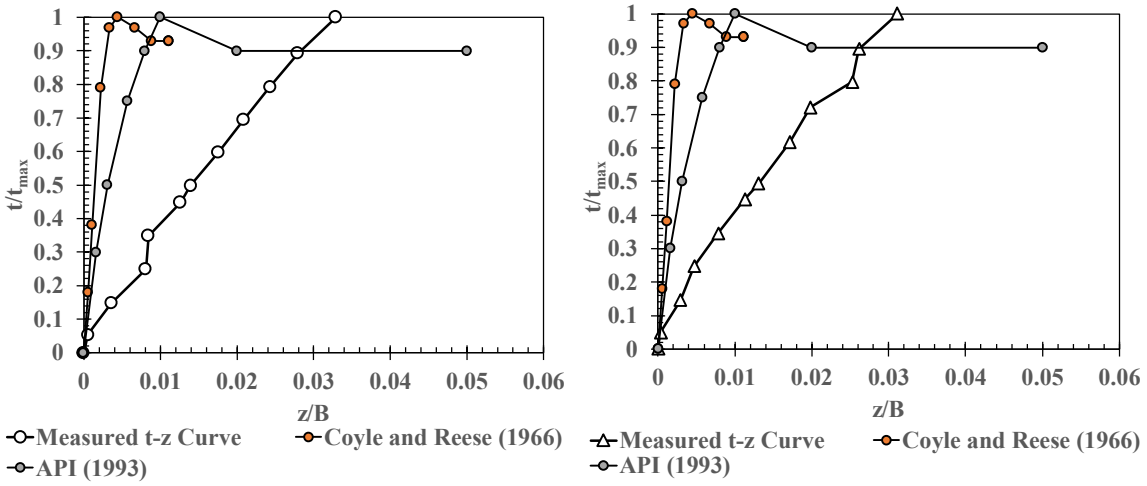

Figure 42. H-Pile t-z Curves: (a) Elevation 119 m; (b) Elevation 116 m.

The t-z curves presented in Figure 42 were constructed from the data collected by strain gages instrumented on the H-Pile. The initial slope (stiffness) of the measured t-z curves is not represented well by the API (1993) or Coyle and Reese (1966) theoretical curves. The measured t-z curves reach their peak values at a greater shaft movement than both theoretical curves. This is probably due to insufficient loading resulting in geotechnical failure not being achieved. The actual yield resistance for the H-Pile is unknown because the load required for the pile to mobilize is uncertain. The t-z curves were constructed from the data recorded at each strain gage elevation to model the soil-pile interaction at the soil-pile interface over the entire length of the H-Pile. The t-z curves constructed for each strain

location can be found in APPENDIX E. The frictional resistive force measured along the entire length of the H-Pile is plotted in Figure 43.

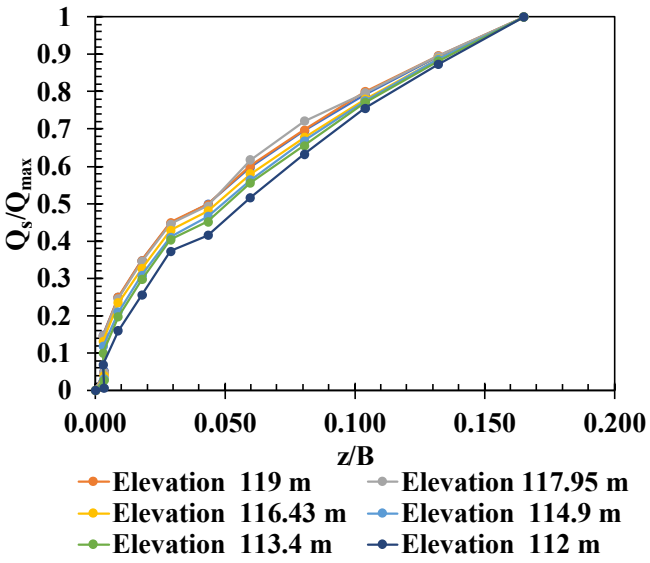

Figure 43. H-Pile Side Friction Force vs. Depth

3.12.2 Pipe Pile t-z Curves

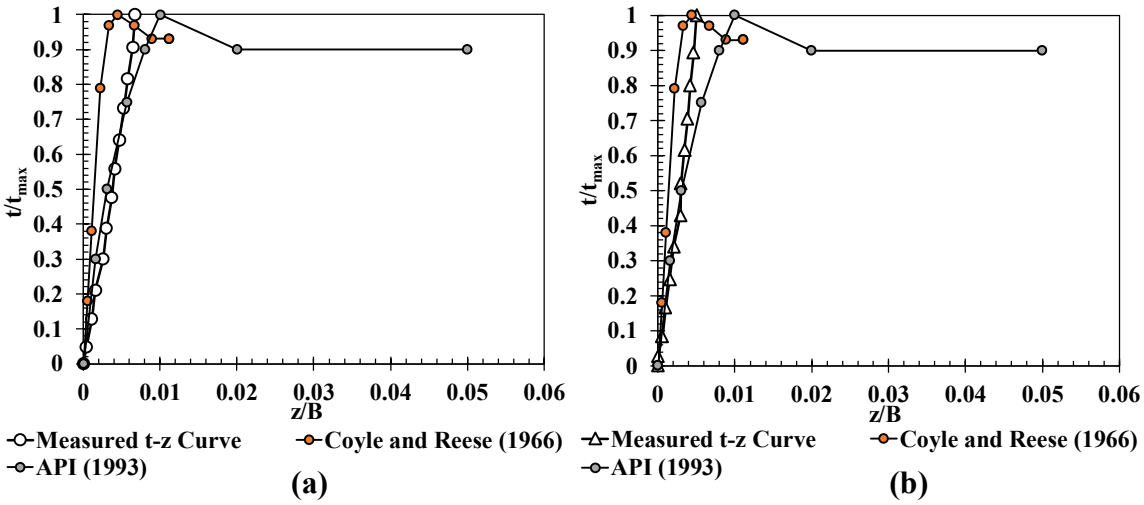

Figure 44. Pipe Pile t-z Curves: (a) Elevation 107 m.; (b) Elevation 90 m.

The t-z curves shown in Figure 44 were constructed from the data collected by strain gages instrumented on the Pipe Pile. The measured t-z curves reach their peak values at greater shaft movements than the Coyle and Reese (1966) theoretical curves and smaller shaft movements than the API (1993) theoretical curves. The initial slope (stiffness) of the measured t-z curves are well represented by both theoretical curves. The measure t-z curves

correlate better to the Coyle and Reese (1966) theoretical curves. This is probably due to the clay layers present in the upper segments of the Pipe Pile subsurface profile. The API (1993) theoretical curves assume the elastic compression of soil. The t-z curves presented in Figure 46 illustrate that the soil response stiffens as the shear stress increases. The elastic shortening that occurs when the slope of the curve is increased contributes to the measured t-z curve correlating better with the Coyle and Reese (1966) method. T-z curves were constructed from data recorded at all strain gage elevations to model the interaction at the soil-pile interface over the entire length of the Pipe Pile. The t-z curves constructed for each strain location can be found in Appendix E. The frictional resistive force measured along the entire length of the Pipe Pile is plotted in Figure 45.

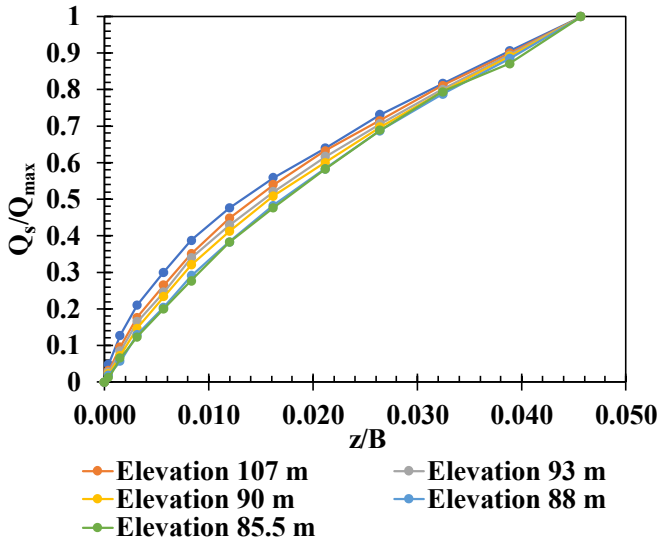

Figure 45. Pipe Pile Side Friction Force vs. Depth

3.13 Measured q-z Curves

For q-z curves, the q value is obtained from the axial load at the pile tip divided by the pile cross-section area, and the z is obtained from the pile tip movement measured using tell-tale data. The q-z plots for the H-Pile and Pipe Pile indicate that their respective corresponding t-z analyses are accurate. The q-z data for both piles demonstrate increasing q values with increasing axial loads. The H-Pile and Pipe Pile q-z curves plotted in Figure 46 illustrate the positive trend in the q-z data and support the t-z analyses for both piles.

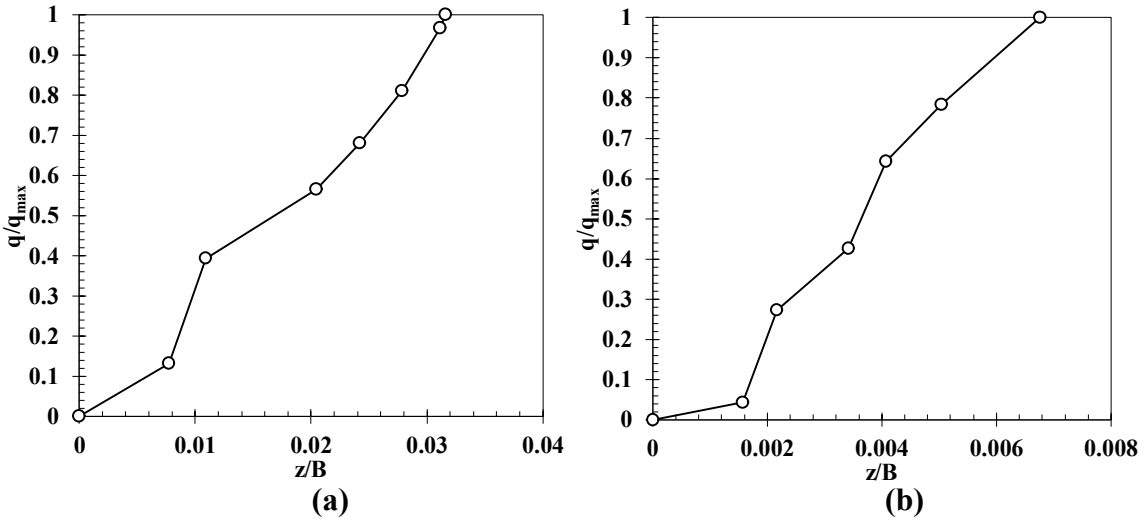

Figure 46. q-z Curves: (a) H-Pile; (b) Pipe Pile

3.14 Discussion of Load Transfer Analyses

3.14.1 H-Pile Load Transfer Discussion

The measured unit side shear resistances were calculated using the peak computed loads recorded by the vibrating wire strain gages at each depth interval and dividing the corresponding stress by the respective segment surface area. The measured unit end bearing resistance ranged from 391 to 2274 kPa along the exterior of the embedded test pile. The measured unit end bearing resistance ranged from 60 to 290 kPa. The estimated mobilized toe resistance represents the load developed in side shear on the toe segment coupled with the tip resistance component. The toe segment resistance was estimated to be approximately 23,106.71kPa.The static test data suggests the lower four segments and tip resistance did not fully mobilize during the load test.

The dynamically determined unit side shear resistances in the dense to very dense gravel ranged from approximately 95.76 kPa to 191 kPa and generally increased with depth. The dynamic test unit end bearing resistances ranged from approximately 636 to 911 kPa. The low hammer energy utilized during the final restrike did not mobilize the pile. The ultimate load in a pile did not wholly transfer before it reached the end of the pile.

The t-z analysis of the static load test data supports the load transfer analysis of the dynamic load test data performed with the CAPWAP software. The dynamic testing unit end bearing resistances predictions are smaller but still fall within the lower range of the measured unit end bearing resistances. This most likely due to the pile only being partially plugged. H-

Piles can get soil trapped between the flange and web that results in an additional sticking force acting on the pile. This can have a significant impact on the accuracy of the end-bearing capacity readings because the additional resistance behaves as a wedging force that supports the pile. The H-Pile load transfer results are summarized in Table 14.

Table 14. H-Pile Static and Dynamic Load Transfer Summary

Resistance	Dynamic Load test	Static Load Test
Unit Side Friction	95.76 - 191 kPa	62.24-167 kPa
Unit End Bearing	630 – 911 kPa	361- 2274 kPa

3.14.2 Pipe Pile Load Transfer Discussion

The measured unit end bearing resistance ranged from 105.34 to 167 kPa along the exterior of the embedded test pile. The measured unit end bearing resistance ranged from 130 kPa in the predrilled zone to 606 kPa. The maximum unit end bearing resistance occurred at a depth of 16 meters and steadily decreased over the remaining length of the pile. The estimated mobilized toe resistance is 2183.34 kPa.

The dynamically determined unit side shear resistances in the dense to very dense gravel ranged from approximately 47.8 – 311 kPa and generally increased with depth. The dynamic test unit end bearing resistances ranged from approximately 5314-5793 kPa.

The t-z analysis does not support the CAPWAP load transfer analysis. The dynamic unit end bearing resistances are significantly larger than the measured static data. This is probably due to the soft to firm clay layers present in the upper segments of the Pipe Pile subsurface profile. When piles are driven into soft to firm clay, the pore water pressure increases causing the effective stress to decrease. This results in a reduction of the unit bearing stress and is often accompanied by ground heave. If the clay is very stiff, small amounts of consolidation will occur. The H-Pile load transfer results are summarized in Table 15.

Table 15. Pipe Pile Static and Dynamic Load Transfer Summary

Resistance	Dynamic Load test	Static Load Test
Unit Side Friction	47.8 – 311 kPa	105.34-167 kPa
Unit End Bearing	5314-5793 kPa	130-606 kPa

3.15 Conclusion of The Load Transfer Analyses

The results of this study show that the dynamic testing methods for predicting the load transfer characteristics should be supplemented with static testing for large diameter piles driven in mixed soils. The dynamic load transfer analyses provided very accurate unit side friction values for both piles. However; the dynamic unit bearing results were not as satisfactory. The dynamic analysis was not able to accurately model the plugging the plunging behavior of the H-Pile or account for the elastic shortening in the Pipe Pile. This study concludes that further research needs to be done on this topic to better model large diameter in cohesive soils using dynamic methods

CHAPTER 4

4 Comparison of Static and Dynamic Test Results

4.1 Introduction

This case study reviews a pile load test program completed for the proposed Lagoon Bridge as part of the Kentucky Lake Bridge Advance Contract (CID 131305) in Marshall and Trigg Counties, Kentucky. The Kentucky Transportation Cabinet (KYTC) has proposed bridge replacements for existing crossings of Kentucky Lake and Lake Barkley. These crossings follow the existing US 68/KY 80 highway corridor. The existing bridge is multi-span structures served by causeways on both ends of each structure. The design load test program was intended to gather information through dynamic pile load testing and static load testing methods to use in the design of the proposed Kentucky Lake Bridge pile foundations.

4.2 Project Information

The pile load test program consisted of static and dynamic testing on two test piles designated as L-1 and L-2. Test pile L-1 was an HP18x204, ASTM A572, Grade 50 steel H-Pile with a length of 18.3 meters. Test pile L-2 was a 762 mm (O.D.) steel pipe pile with a wall thickness of 25.4 mm and had an overall length of 32 meters. Inserts were placed in the interior of the piles to force a plugged condition to occur in the test piles. This was done to take advantage of higher axial pile resistances in the piles. The test piles that were used in the load test program are shown in Figure 47.

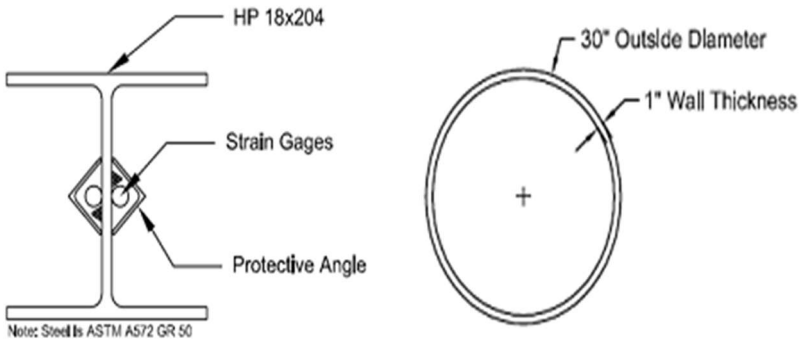

Figure 47. Test Piles

Initially, test piles for the Design Load Test Program will be driven to tip elevations that achieve the target nominal axial resistances that represent the estimated axial resistances.

The test piles subjected to dynamic and static axial load testing were instrumented to estimate the unit skin resistance and end bearing resistance components of the pile resistance and to develop t-z and q-z data for the foundation analyses.

4.3 Subsurface Conditions

The generalized soil conditions at the pile test locations were based on subsurface conditions encountered in nearby test borings. Several test borings and cone penetration tests (CPT) were performed in 2011 near the test pile locations. The soil borings and CPT soundings provided the data and intact samples for testing in the upper lean clay soils.

The effective strength parameters of the granular soils for Test Pile Location L-1 were estimated using the SPT N-value data from the test borings. Where SPT N-values was obtained that did not appear to be skewed by the chert gravel, the shear strength parameters of the granular soils were estimated using published AASHTO correlations. Unit weights of some of the granular soils were based upon previous triaxial consolidated-undrained shear test results performed by F&H consulting. Compression and recompression indices and over-consolidation ratios (OCR) were estimated from CPT data. Where laboratory data or CPT data were not available, corrected N-values from SPT borings were used to estimate compression and recompression indices.

At testing location L-2, the results of consolidated-undrained (CU) triaxial shear tests and unconsolidated undrained triaxial (UU) shear tests were used to estimate the effective and total soil shear strength parameters in the fine-grained soil samples collected in the test borings. Data from these tests supplemented with data from CPT soundings were also used to estimate the unit weight parameters of the fine-grained soils at the site.

4.3.1 Test Pile L-1 Area

The geology of the Test Pile L-1 site is influenced by the Mississippi Embayment to the west and is composed primarily of a cherty Mississippian-age residuum within the Ft. Payne Formation. This formation is described as a residual chert interbedded with residual clay. Test borings in the area of the Test Pile L-1 indicate that the soils in the area beginning at the ground surface (119.48 m elevation at the test pile) generally consist of approximately 5.18 m of alluvial clay (CL) and silt soils (ML) with some chert pieces to an elevation of approximately 114.3 m. The clay and silt are underlain by about 4.57 m of

silty gravel (GM) to an elevation of approximately 109.73 m. Beginning around an elevation of 109.73 m there is a 1.5 m thick layer of silt (ML). Around 11.23 m below the ground surface, silty gravel with chert layers (GM or GP-GM soils) exists, and it extends all the way down to the bottom of the boring. The subsurface profile for Test Pile L-1 is shown in Figure 48.

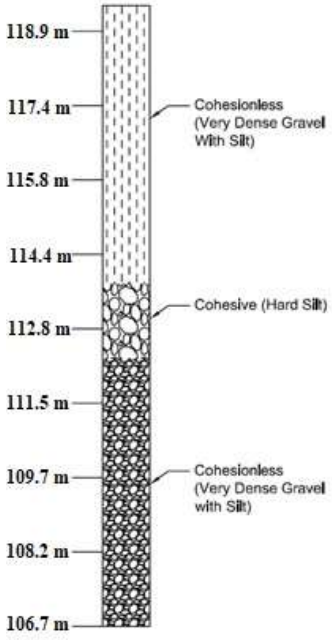

Figure 48. L-1 Subsurface Profile

4.3.2 Test Pile L-2 Area

The geology of the western part of the site is influenced by the Mississippi Embayment to the west and is composed primarily of a cherty Mississippian-age residuum within the Ft. Payne Formation. This formation is described as a residual chert interbedded with residual clay. The geology of the eastern part of the site transitions to a cap of Cretaceous-age materials over the Ft. Payne Formation. The foundation soil under the existing causeways and bridge are composed of river alluvium as influenced by the Tennessee River before being dammed to form Kentucky Lake in 1944. The alluvium is described as sand and gravel, which grades coarser and denser with depth. At the L-2 load test site borings encountered alluvial clay (CL) and silt soils (ML) with some chert pieces from the muddy ground surface at a depth of 11.2 m. Within this depth test, a test boring encountered a

layer of loose gravel with silt (GC) from a depth of 2.7 m to 4.2 m. Between the depths of 4.2 m to 20.4 m test borings encountered silty gravel with chert (GP-GM). From the depth of 20.4 m to 24.56 m at the bottom of the boring test, borings encountered silty gravel with chert and chert layers (GC-GM). The subsurface profile for Test Pile L-1 is shown in Figure 49.

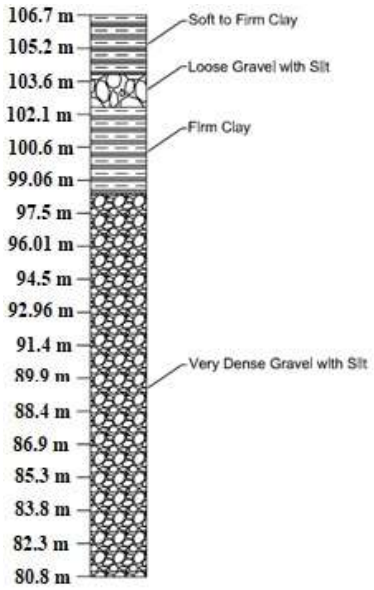

Figure 49. L-2 Subsurface Profile

4.4 Load Test Program

The pile load test program consisted of dynamic and axial static load testing. Dynamic load testing was performed by Applied Foundation Testing between August 12, 2013, and September 27, 2013, on each test pile during the initial drive, restrike, and extended drive. The test pile was driven using an ICE I-100v2 open-ended diesel hammer. Static load testing was also performed on both test piles. Due to the different pile types and local geology of the two sites, the testing procedure varied at each testing location. The load test frame was designed by Genesis Structures, a subconsultant to Jim Smith Contracting. The top of pile movement was measured using four displacement transducers mounted on a reference beam. Backup pile head measurements and measurements of reaction pile movements were measured using survey methods. An Enerpac Synchronous Lift System provided the applied load and hydraulic jack elongation using three – 800-kip hydraulic jacks.

4.4.1 Test Pile L-1 Load Test Results

The H-Pile ultimate capacity prediction for the static load test data was 3,755 kN. The Maximum Test Load (MTL) applied to the H-Pile was 5417.93 kN and exhibited a downward deflection of 0.7394 cm. The permanent displacement after unloading was 0.09144 cm. The static capacity of the H-Pile exceeded the nominal resistance of 2,668 kN. The deflection measured at the pile head during the pile load test never exceeded the calculated elastic shortening of the test pile. Thus, the FHWA failure criteria for an HP18x204 pile was not achieved.

The ultimate capacities predictions CAPWAP produced were made using the case method. The ultimate capacities ranged from approximately 5160kN at the end of the initial drive to approximately 5560 kN during the 72-hour re-strike. The ultimate capacity or the H-Pile exceeded the nominal resistance of 2,668 kN. The H-Pile load-settlement curves from the dynamic and static load tests are plotted in Figure 50.

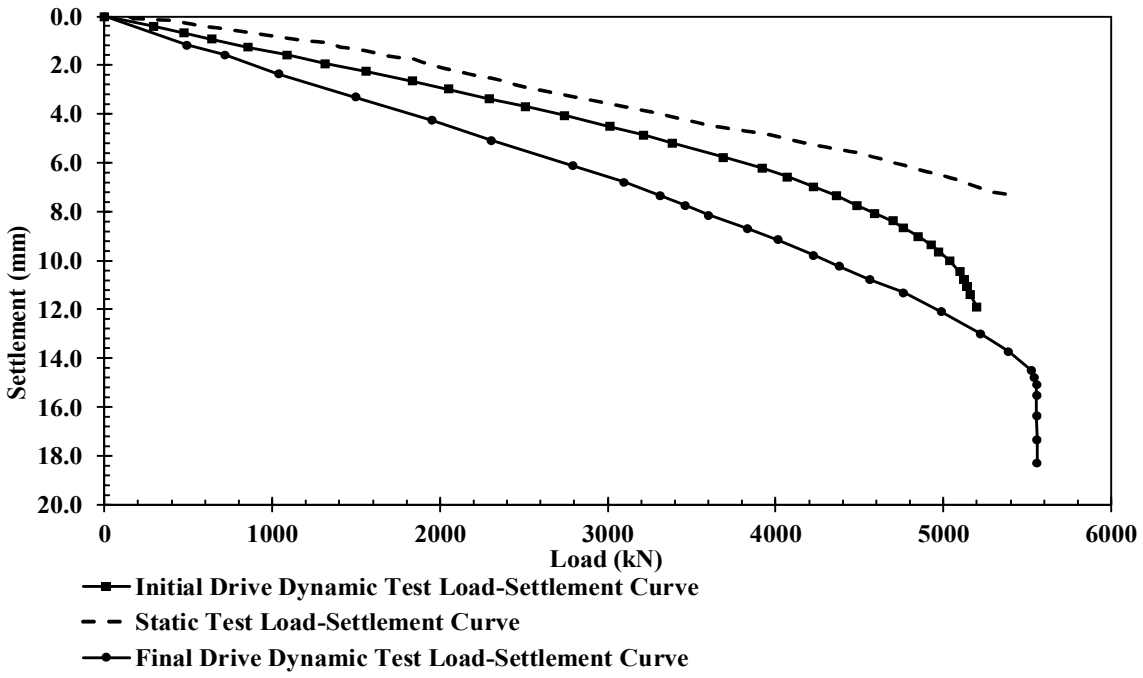

Figure 50. H-Pile Load-Settlement Curves

The measured unit side shear resistance was calculated using the peak computed loads recorded by the vibrating wire strain gages at each depth interval and dividing the corresponding stress by the respective segment surface area. The measured unit end bearing resistance ranged from 60 to 290 kPa along the exterior of the embedded test pile. The

measured unit end bearing resistance ranged from 60 to 290 kPa. The unit end bearing resistance rapidly increased from the top of the pile through cohesionless gravel and silt until it peaked at a depth of 4.3 m. The unit end bearing resistances steadily decreased over the remaining length of the pile. The estimated mobilized toe resistance represents the load developed in side shear on the toe segment coupled with the tip resistance component. The toe segment resistance was estimated to be approximately 23,106.71kPa.The static test data suggests the lower four segments and tip resistance did not fully mobilize during the load test.

The dynamically determined unit side shear resistances in the dense to very dense gravel ranged from approximately 95.76 kPa to 191 kPa and generally increased with depth. Unit end bearing resistances (using an end area based on a plugged condition) ranged from approximately 636 to 911 kPa. The low hammer energy utilized during the final restrike did not mobilize the pile. The ultimate load in the pile did not completely transfer before it reached the end of the pile. The H-Pile load transfer analysis data from the dynamic and static load tests are plotted in Figure 51.

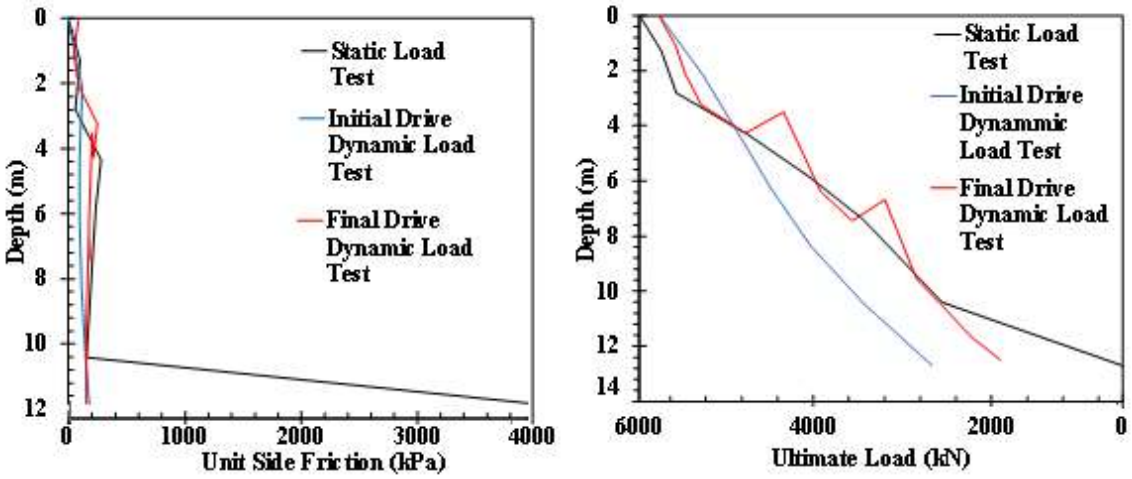

Figure 51. H-Pile Load Transfer: (a) Unit Side Friction; (b) Ultimate Load

4.4.2 Test Pile L-2 Load Test Results

The Pipe Pile ultimate capacity estimation for the static load test data was 2,213 kN. The ultimate capacity prediction applied Hanson's 90% failure criterion. The Hanson's 90% failure criterion selected because the load–settlement data was hyperbolic due to the loading of the pile. The Maximum Test Load (MTL) applied to the pile was 6418.78 kN

and exhibited a downward deflection of 1.05156 cm. The permanent displacement after unloading was .127 cm. The static capacity of the Pipe Pile failed to exceed the nominal resistance of 10,675 kN. The deflection measured at the pile head during the pile load test never exceeded the calculated elastic shortening of the test pile. Thus, the FHWA failure criteria for a 30-inch-diameter steel pipe having a 1-inch wall thickness was not achieved.

The ultimate capacities predicted by CAPWAP ranged from approximately 5947.27 kN at the end of the initial drive to approximately 10675.73 kN during the final re-strike. The re-strike capacities for the first (48 hour) and second (72 hour) re-strike showed an increase in capacity of approximately 1120.95 kN and 271.34 kN, respectively. The dynamic capacity of the H-Pile exceeded the nominal resistance of 10,675 kN. The H-Pile load-settlement curves from the dynamic and static load tests are plotted in Figure 52.

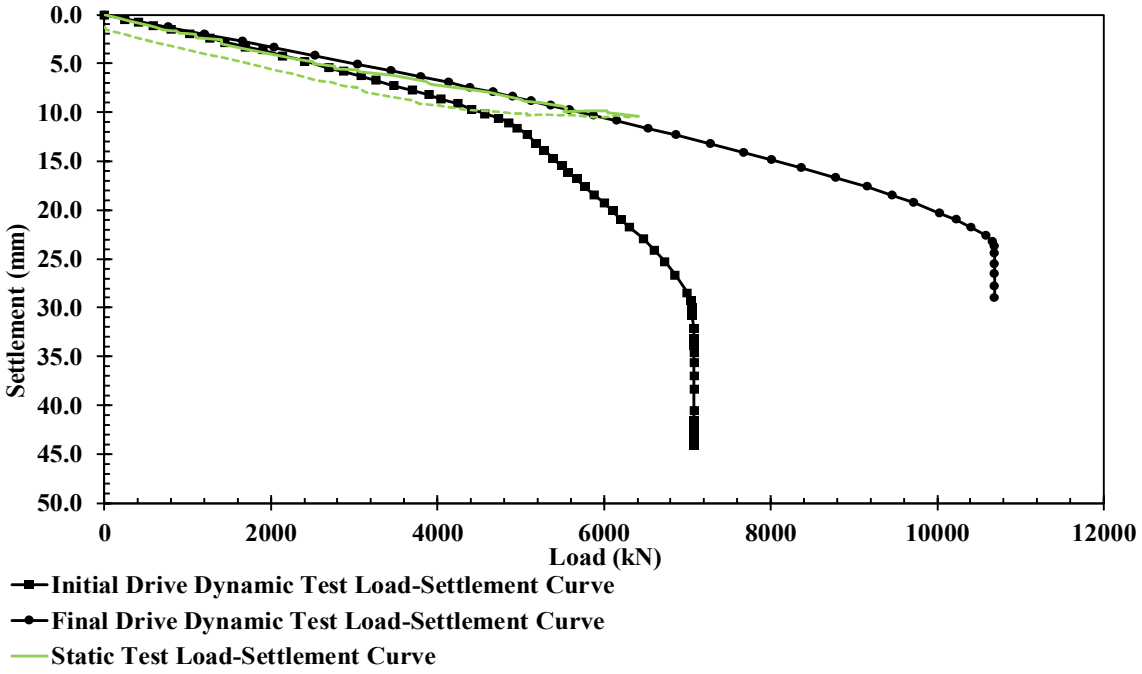

Figure 52. Pipe Pile Load-Settlement Curves

The measured unit side shear resistance was calculated using the peak computed loads recorded by the vibrating wire strain gages at each depth interval and dividing the corresponding stress by the respective segment surface area. The unit side shear was measured to range from 62.24 in the predrilled zone to 287.3 kPa. The maximum unit shear resistance occurred a depth of 4.2 m. After the unit side shear resistance peaks, the shear resistance steadily decreases over the remaining length of the pile. The measured unit end

bearing resistance ranged from 130 kPa in the predrilled zone to 606 kPa. The maximum unit end bearing resistance occurred at a depth of 16 meters and steadily decreased over the remaining length of the pile embedded in the very dense gravel and silt.

The GRLWEAP software estimated the unit side shear resistances in the dense to very dense gravel ranged from approximately 47.8 kPa to 311 kPa and increased with depth. Figure 24 plots the shear resistance against depth. The end bearing resistance (using an end area based on a plugged condition) ranged from approximately 5314 kPa to 5793.5 kPa. The Pipe Pile load transfer analysis data from the dynamic and static load tests are plotted in Figure 53.

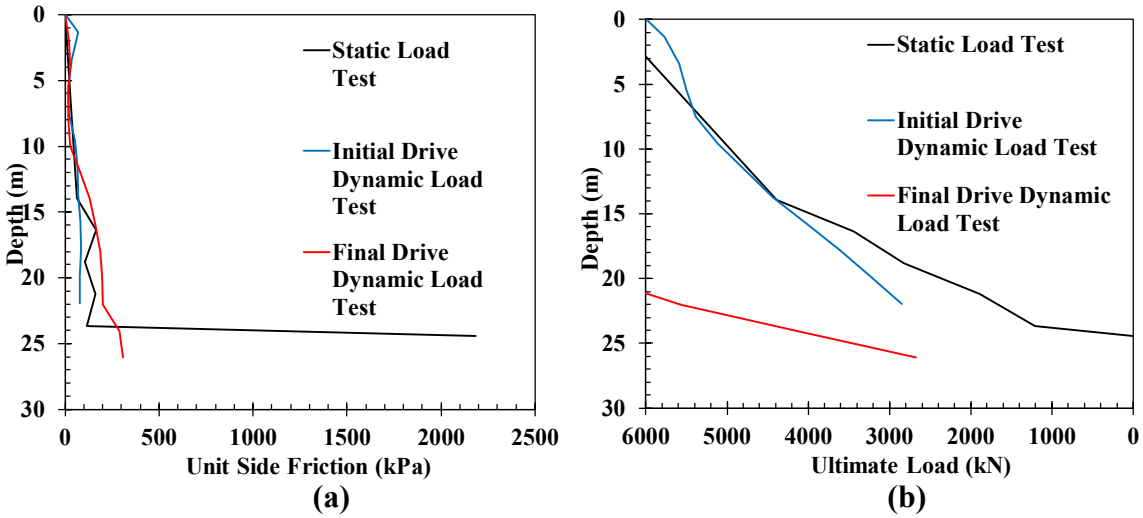

Figure 53. Pipe Pile Load Transfer: (a) Unit Side Friction; (b) Ultimate Load

APPENDIX A

Soil Data

A.1 H-Pile CPT

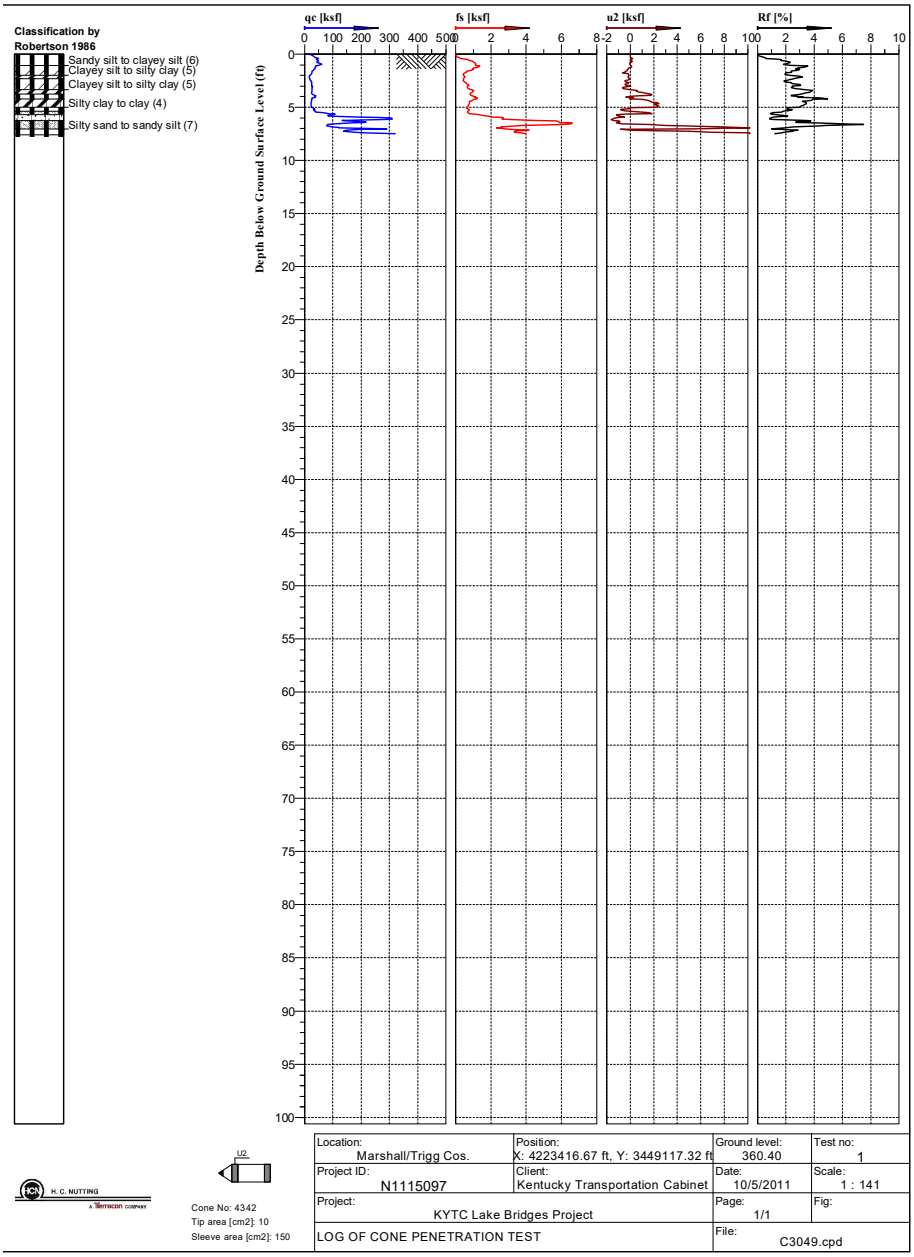

Figure A.1. H-Pile CPT

A.2 Driller's Subsurface Log

Drilling Firm: Kentucky Transportation Cabinet
For: Division of Structural Design
Geotechnical Branch

DRILLER'S SUBSURFACE LOG

Printed: 7/8/11

Project ID: ***SA-015-2010***	***Marshall - US-68***	Project Type: ***Structure Addendum State Bri***
Item Number: ***01-0180.70***	***Kentucky Lake***	Project Manager: ***Darrin Beckett***

Hole Number ***3051***	Immediate Water Depth ***NA***	Start Date ***06/15/2011***	Hole Type ***sample***
Surface Elevation ***359.9'***	Static Water Depth ***NA***	End Date ***06/19/2011***	Rig_Number ***300404***
Total Depth ***85.8'***	Driller ***Cayton, Bill***	Latitude(83) ***36.771046***	
Location ***973+50.00 CL***		Longitude(83) ***-88.131662***	

Lithology Elevation	Lithology Depth	Description	Overburden / Rock Core	Sample No.	Depth (ft) Std/Ky RQD	Depth (ft) Run (ft)	Rec. (ft) Rec (ft)	SPT Blows Rec (%)	Sample Type SDI (JS)	Remarks
		Sand with gravel.								
354.9	5.0			SS-1		5.0-6.5		2-3-5	SPT	
		Brown, gravel with clay.		ST-1		10.0-12.0	1.5		ST	
346.4	13.5									
		Very soft, gray, clay.		ST-2		15.0-17.0	0.0		ST	
				SS-2		17.0-18.5		2-2-2	SPT	
340.6	19.3									
				SS-3		20.0-21.5		4-4-5	SPT	
		Gray and brown, clay with gravel.		ST-3		25.0-27.0	1.5		ST	
				SS-4		29.2-30.7		2-2-2	SPT	
				ST-4		34.2-35.2	1.0		ST	
322.7	37.2									
				SS-5		39.2-40.7		16-18-23	SPT	
		Gray, sandy clay with gravel.		SS-6		44.2-45.7		16-29-24	SPT	
				SS-7		49.2-50.0		50/4"/0.3"	SPT	

A.3 H-Pile Soil Classification and Gradation Test Results

Geotech Firm: HCN/F&H
For: Division of Structural Design
Geotechnical Branch

Printed: 7/20/12

Soil Classification and Gradation Test Results

Page 1 of 93

Project ID: ***SA-015-2010***	***Marshall - US-68***	Project Type: ***Structure Addendum State Bridg***
Item Number: ***01-0180.70***	***Kentucky Lake***	Project Manager: ***Darrin Beckett***

Location:	969+03 45.0' Lt.	Hole #:	3001
Lab ID#:	SS-1	Depth (ft):	5.1-5.4

Sieve Size	%Passing	Sieve Size	%Passing	Sieve Size	%Passing
3"	100.0	2"	100.0	1"	100.0
3/4"	100.0	3/8"	90.0	No. 4	81.4
No. 10	76.4	No. 40	74.2	No. 200	70.6
0.002 mm					

Gravel (-3" + No. 10)	23.6	Coarse Sand (-No. 10 + No. 40)	2.3
Fine Sand (-No. 40 +No. 200)	3.5	Silts (-No. 200 + 0.002mm)	
Clay (-0.002mm)		Colloids (-0.001mm)	

Liquid Limit:	0	Plastic Limit:	0	Plasticity Index:	0
		Activity:	0.00	Spec. Gravity:	

AASHTO Classification:	A-4 (0)
Unified Classification:	ML

D 10 (mm):	0.003	NAT MT =	46.54
D 30 (mm):	0.009	LIQ =	0.00000
D 50 (mm):	0.026		
D 60 (mm):	0.043		
D 90 (mm):	9.481		
D 95 (mm):	13.423		
		Cu =	13.01060
Sieve Type:	Wash Grad		
Notes:		Cc =	0.59861
Silts + Clays + Colloids:	70.6		

Remarks:

Copies:

Figure A.3. H-Pile Soil Classification and Gradation Test Results

A.4 Pipe Pile CPT

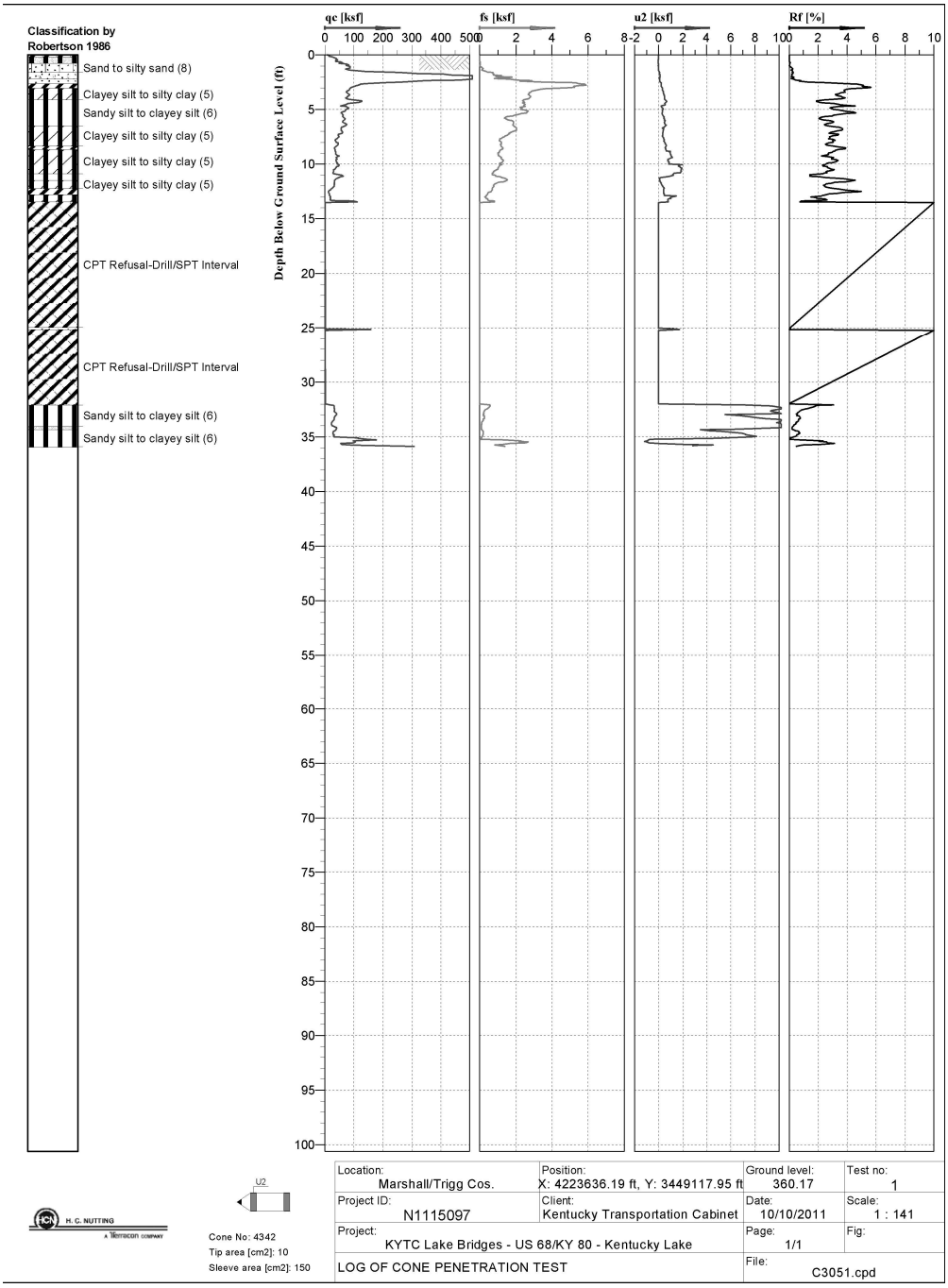

Figure A.4. Pipe Pile CPT

A.5 Driller's Subsurface Log

Drilling Firm:
For: Division of Structural Design
Geotechnical Branch

DRILLER'S SUBSURFACE LOG

Printed: 7/20/12

Project ID: [redacted]	[redacted]	Project Type: ***Structure Addendum State Bridge***
Item Number: [redacted]	[redacted]	Project Manager:

Hole Number ***C3051***	Immediate Water Depth ***(10/10/11)***	Start Date ***10/10/2011***	Hole Type ***CPT/Sample***
Surface Elevation ***360.2'***	Static Water Depth ***NA***	End Date ***10/12/2011***	Rig_Number ***HCN 7253***
Total Depth ***81.4'***	Driller ***Johnson***	Latitude(83) ***36.771034***	
Location ***973+25.12 1.7' Rt.***		Longitude(83) ***-88.131746***	

Lithology Elevation	Depth	Description	Overburden / Rock Core	Sample No. / Std/Ky RQD	Depth (ft) / Run (ft)	Rec. (ft) / Rec (ft)	SPT Blows / Rec (%)	Sample Type / SDI (JS)	Remarks
		(CONE PENETRATION TEST - Refer to CPT log C3051 - Test terminated due to bending rods).							
346.7	13.5								
		(Brown SILTY GRAVEL, with sand, loose, moist, water noted between 18-19.5').		1	18.0-19.5	0.7	3-2-3	SPT	
337.2	23.0								
335.0	25.1	(CONE PENETRATION TEST - Refer to CPT log C3051 - Test terminated due to bending rods).		2	23.0-24.5	1.3	7-4-5	SPT	
		(Gray LEAN CLAY, stiff, moist).		3	30.0-31.5	1.5	3-6-8	SPT	
328.2	32.0								
		(CONE PENETRATION TEST - Refer to CPT log C3051 - Test terminated due to bending rods).							
324.3	35.9								
		(Light brown SILTY CHERT GRAVEL, with sand, very dense, moist, grades wet at 45').		4	40.0-41.5	1.0	17-20-34	SPT	
				5	45.0-45.9	0.7	22/0.7/0	SPT	
310.2	50.0								

A.6 Pipe Pile Soil Classification and Gradation Test Results

Geotech Firm: HCN/F&H
For: Division of Structural Design
Geotechnical Branch

Printed: 7/20/12

Soil Classification and Gradation Test Results

Project ID: ***SA-015-2010***	***Marshall - US-68***	Project Type: ***Structure Addendum State Bridc***
Item Number: ***01-0180.70***	***Kentucky Lake***	Project Manager: ***Darrin Beckett***

Location:	973+50 CL	Hole #:	3051
Lab ID#:	SS-1	Depth (ft):	5-6.5

Sieve Size	%Passing	Sieve Size	%Passing	Sieve Size	%Passing
3"	100.0	2"	100.0	1"	100.0
3/4"	100.0	3/8"	91.2	No. 4	72.2
No. 10	53.6	No. 40	51.6	No. 200	42.8
0.002 mm	14.3				

Gravel (-3" + No. 10)	46.4	Coarse Sand (-No. 10 + No. 40)	2.0
Fine Sand (-No. 40 +No. 200)	8.8	Silts (-No. 200 + 0.002mm)	28.5
Clay (-0.002mm)	14.3	Colloids (-0.001mm)	11.0

Liquid Limit:	33	Plastic Limit:	18	Plasticity Index:	15
		Activity:	1.05	Spec. Gravity:	2.731

AASHTO Classification:	A-6 (3)
Unified Classification:	SC

D 10 (mm):	0.000	NAT MT =	23.54
D 30 (mm):	0.015	LIQ =	0.36914
D 50 (mm):	0.311		
D 60 (mm):	2.695		
D 90 (mm):	9.082		
D 95 (mm):	12.793		
		Cu =	
Sieve Type:	With Gravel		
Notes:		Cc =	
Silts + Clays + Colloids:	N/A		

Remarks:

Copies:

Figure A.6. Pipe Pile Soil Classification and Gradation Test Results

A.7 CU Test Results

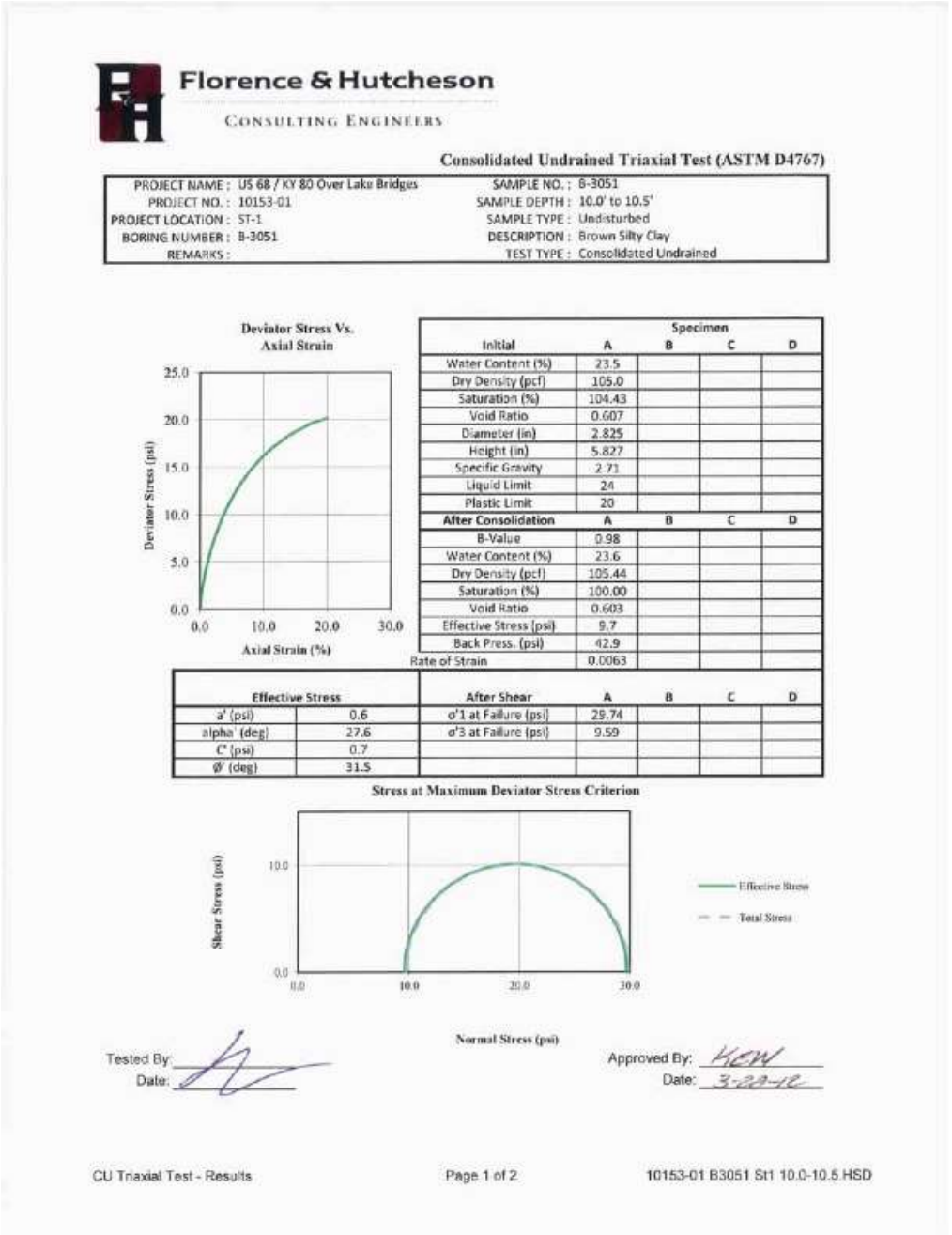

Florence & Hutcheson
CONSULTING ENGINEERS

Consolidated Undrained Triaxial Test (ASTM D4767)

PROJECT NAME : US 68 / KY 80 Over Lake Bridges	SAMPLE NO. : B-3051
PROJECT NO. : 10153-01	SAMPLE DEPTH : 10.0' to 10.5'
PROJECT LOCATION : ST-1	SAMPLE TYPE : Undisturbed
BORING NUMBER : B-3051	DESCRIPTION : Brown Silty Clay
REMARKS :	TEST TYPE : Consolidated Undrained

Deviator Stress Vs. Axial Strain

Initial	A	B	C	D
Water Content (%)	23.5			
Dry Density (pcf)	105.0			
Saturation (%)	104.43			
Void Ratio	0.607			
Diameter (in)	2.825			
Height (in)	5.827			
Specific Gravity	2.71			
Liquid Limit	24			
Plastic Limit	20			
After Consolidation	**A**	**B**	**C**	**D**
B-Value	0.98			
Water Content (%)	23.6			
Dry Density (pcf)	105.44			
Saturation (%)	100.00			
Void Ratio	0.603			
Effective Stress (psi)	9.7			
Back Press. (psi)	42.9			
Rate of Strain	0.0063			

Effective Stress		After Shear	A	B	C	D
a' (psi)	0.6	σ'1 at Failure (psi)	29.74			
alpha' (deg)	27.6	σ'3 at Failure (psi)	9.59			
C' (psi)	0.7					
Ø' (deg)	31.5					

Stress at Maximum Deviator Stress Criterion

Tested By:
Date:

Approved By: KCW
Date: 3-29-12

CU Triaxial Test - Results Page 1 of 2 10153-01 B3051 St1 10.0-10.5.HSD

Figure A.7. CU Test Results

Florence & Hutcheson, Inc.

CONSULTING ENGINEERS

TRIAXIAL COMPRESSION TEST

Project Name : US 68/KY 80 Over Lake Bridges
Project No. : 10153-01
Project County : Marshall
Project State : Kentucky
Laboratory No. : 10153-01
Submitted By : Florence & Hutcheson
Soil Type : Gray & Brown Lean Clay

Point No. : 1
Sample Loc. : B-3051 ST-3
Sample Depth : 25.5' to 26.0'
Date Tested : 9-16-11
Date Reported : 10-18-11

Wet Density : 126.8 pcf
Dry Density : 101.5 pcf
Moisture : 25.0 %

Delta Height : NA
Delta Volume : NA
Chamber Pressure : 27.0 psi

Initial Height : 14.84 cm
Initial Diameter : 7.17 cm
Init. Pore Pres. : NA

RESULTS:

	ε a	σ 3 (psi)	σ 1 (psi)	σ1 / σ3
1	0.00	27.00	27.00	1.00
2	0.86	27.00	29.66	1.10
3	1.71	27.00	31.40	1.16
4	2.57	27.00	32.67	1.21
5	3.42	27.00	33.49	1.24
6	4.28	27.00	34.28	1.27
7	5.13	27.00	34.86	1.29
8	10.27	27.00	37.64	1.39
9	15.40	27.00	40.01	1.48
10	20.54	27.00	41.85	1.55
11	25.67	27.00	43.03	1.59
12	30.81	27.00	43.56	1.61
13	34.23	27.00	43.73	1.62
14	42.79	27.00	43.27	1.60
15	51.34	27.00	41.88	1.55
16	59.90	27.00	40.03	1.48
17	68.46	27.00	37.70	1.40
18	77.02	27.00	35.07	1.30
19	85.57	27.00	32.27	1.20
20	94.13	27.00	29.19	1.08
21	102.69	27.00	25.98	0.96
22	111.25	27.00	22.65	0.84
23	119.80	27.00	19.26	0.71
24	128.36	27.00	15.80	0.59
25	136.92	27.00	12.35	0.46
26	145.48	27.00	8.78	0.33
27	154.03	27.00	5.03	0.19
28	162.59	27.00	1.30	0.05
29	171.15	27.00	-2.36	-0.09
30	179.71	27.00	-6.20	-0.23
31	188.26	27.00	-10.29	-0.38
32	196.82	27.00	-14.29	-0.53

P O Box 7267 • Paducah, KY 42002 • 2550 Irvin Cobb Dr • Paducah, KY 42003 • 270/444-9691 • fax 270/443-3943
mail@flohut.com

Figure A.8. UU Test Results

A.9 H-Pile Geotechnical Parameters

Project: Kentucky Lake Lagoon Bridge - End Bent 1
Borings: B-3001

Soil Layer	Layer 1	Layer 2	Layer 3	Layer 4
Soil Type	Cohesive	Cohesionless	Cohesive	Cohesionless
Moist Unit Weight (pcf)	125	125		
Saturated Unit Weight (pcf)			125	130
Elevation @ top of layer (ft.)*	32.51 (391.51)**	21(380)	1 (360)	-4 (355)
Elevation @ bottom of layer (ft.)*	21(380)	1 (360)	-4 (355)	-100 (259)
Water Table (Normal Pool) (ft.)*	0 (359)	0 (359)	0 (359)	0 (359)
Lateral Soil Layer Model	Clay, Stiff w/o water	Sand (Reese)	Clay, Stiff w/water	Sand (Reese)
Internal Friction Angle (degree)	0	34	0	36
Undrained Shear Strength (psf)	2000		2000	
k (p-y) static (pci)		70	1000	125
ε50	0.005		0.005	
Top of Layer Ultimate Unit End Bearing (ksf)	18	135	18	150
Top of Layer Ultimate Unit Skin Friction (ksf)	1.21	2.13	1.41	4.6
At Depth Ultimate Unit End Bearing (ksf)***	18 @ 375	150 @ 365	18 @ 355	150 @ 340
At Depth Ultimate Unit Skin Friction (ksf)***	1.21 @375	3.79 @ 360	1.41 @ 355	5.0 @ 340

Note: *First number is relative to 0 = Normal Pool Elevation = 359 ft. MSL. Second number in parentheses is Mean Sea Elevation.
** Bottom of Pile Cap Elevation
Calculated using Norlund Method for cohesionless soils and Tomlinson method for cohesive soils.
*** Second number is elevation in MSL at which the unit end bearing or unit skin friction occurs. If the elevation is not the bottom of the layer, the unit bearing or unit skin friction is constant for the remaining portion of the layer below the MSL elevation.

Table A.1 H-Pile Geotechnical Parameters

A.10 Pipe Piles Geotechnical Parameters

Project: Kentucky Lake Lagoon Bridge - Pier 2
Borings: B-3051 and C-3051

Soil Layer	Layer 1	Layer 2	Layer 3
Soil Type	Cohesive	Cohesionless	Cohesionless
Saturated Unit Weight (pcf)	130	125	130
Elevation @ top of layer (ft.)*	-10.03 (349.97)**	-36 (323)	-66 (293)
Elevation @ bottom of layer (ft.)*	-36 (323)	-66 (293)	-119 (240)
Water Table (Normal Pool) (ft.)*	0	0	0
Lateral Soil Layer Model	Clay, soft w/water	Sand (Reese)	Sand (Reese)
Internal Friction Angle (degree)	0	34	36
Undrained Shear Strength (psf)	600		
k (p-y) static (pci)		75	150
ε50	0.01		
Top of Layer Ultimate Unit End Bearing (ksf)	3.6	73.5	150
Top of Layer Ultimate Unit Skin Friction (ksf)	0.32	1	2.3
At Depth Ultimate Unit End Bearing (ksf)**	3.6 @ 323	73.5 @ 293	150 @ 275
At Depth Ultimate Unit Skin Friction (ksf)**	0.32 @ 323	2.3 @ 293	5.5 @ 275

Note: *First number is relative to 0 = Normal Pool Elevation = 359 ft. MSL. Second number in parentheses is Mean Sea Elevation.
**Bottom of pile cap elevation.
Calculated using Norlund Method for cohesionless soils and Tomlinson method for cohesive soils.
*** Second number is elevation in MSL at which the unit end bearing or unit skin friction occurs. If the elevation is not the bottom of the layer, the unit bearing or unit skin friction is constant for the remaining portion of the layer below the MSL elevation.

Table A.2. Pipe Piles Geotechnical Parameters

APPENDIX B

Maps

B.1 Project Maps

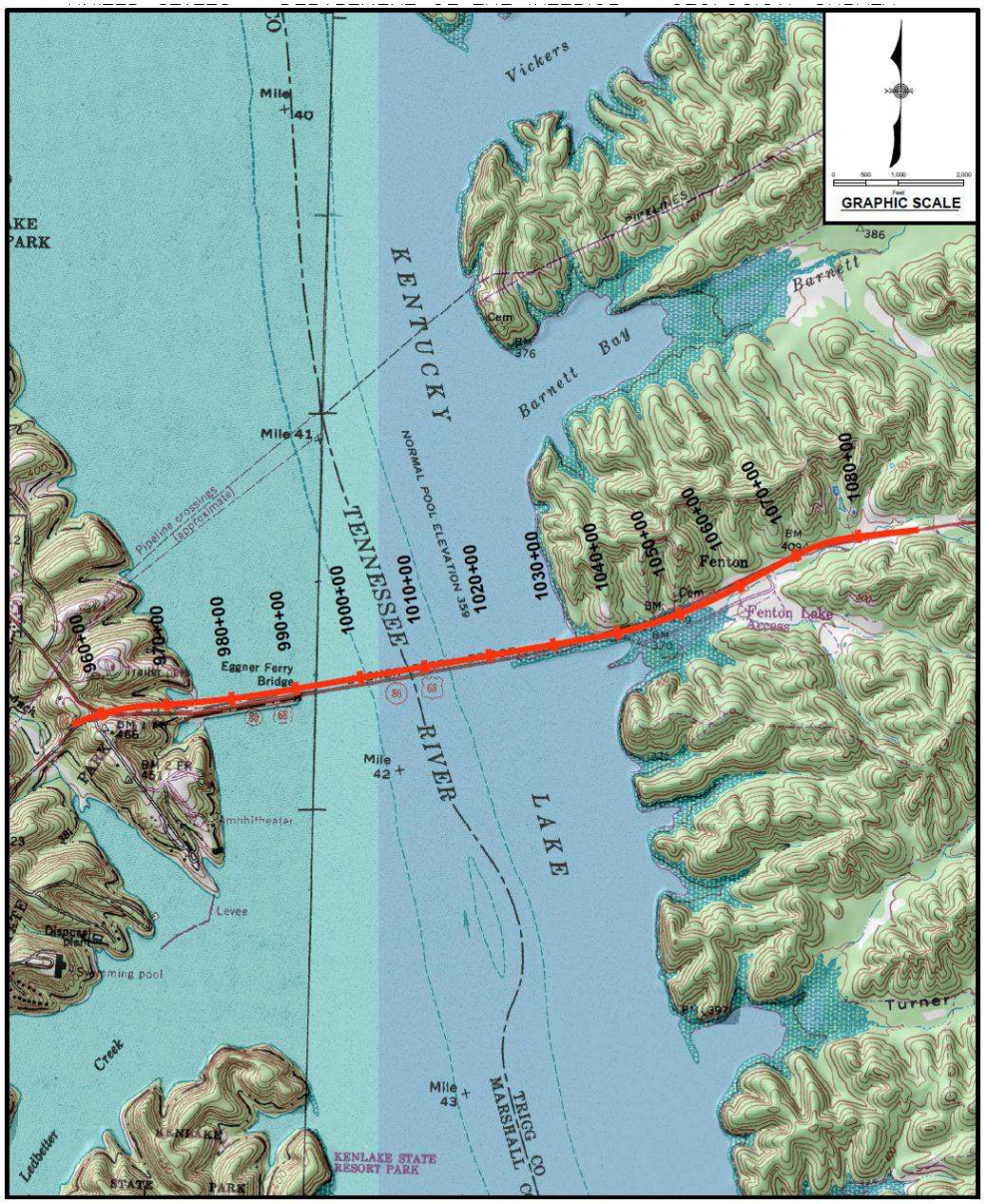

Figure B.1. Quadrangle Topo Map

B.2 Cross Sectional Profile

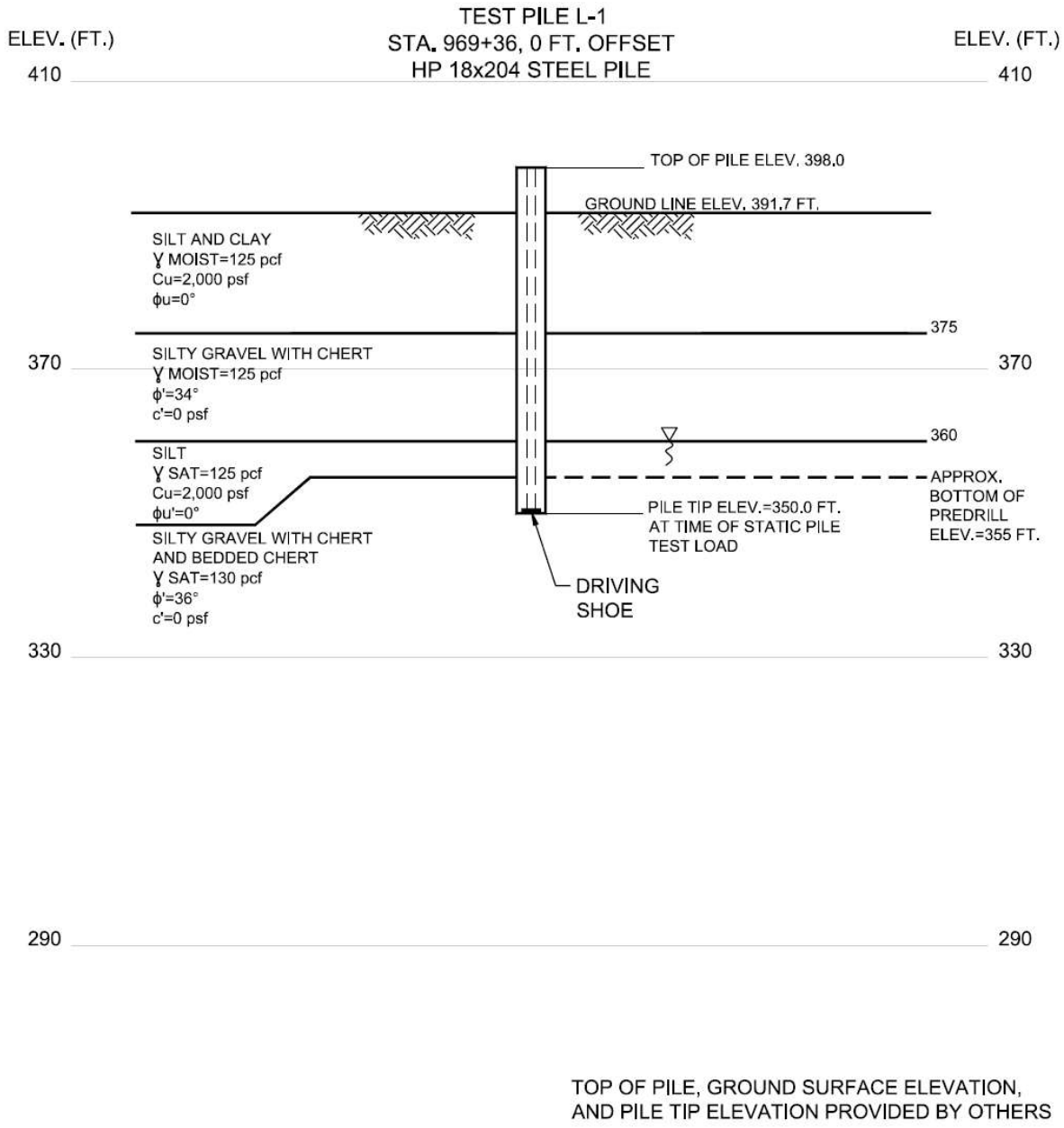

Figure B.2. H-Pile Cross Sectional Profile

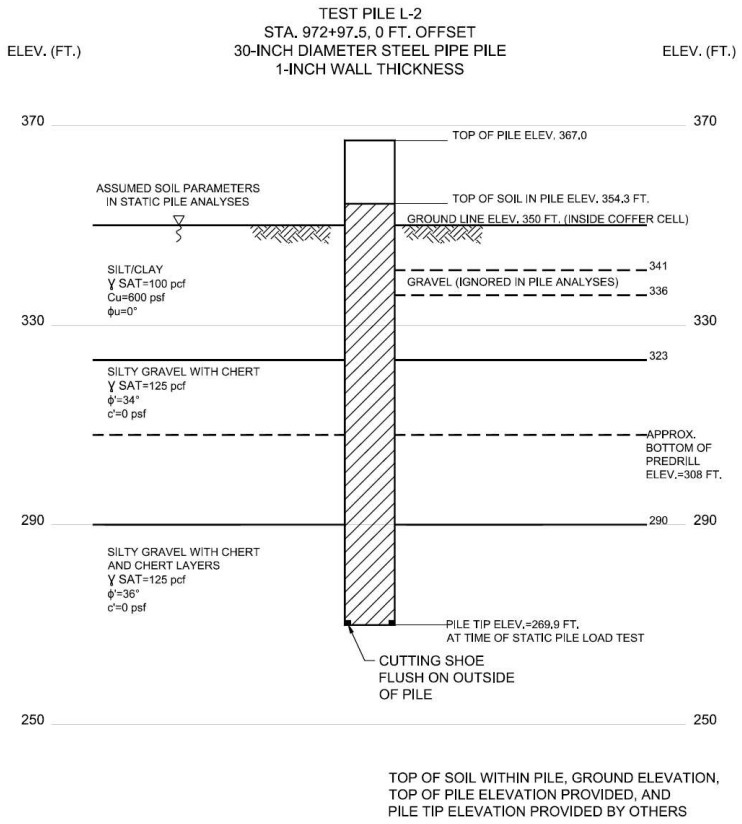

Figure B.3. Pipe Pile Cross Sectional Profile

B.3 H-Pile Instrumentation

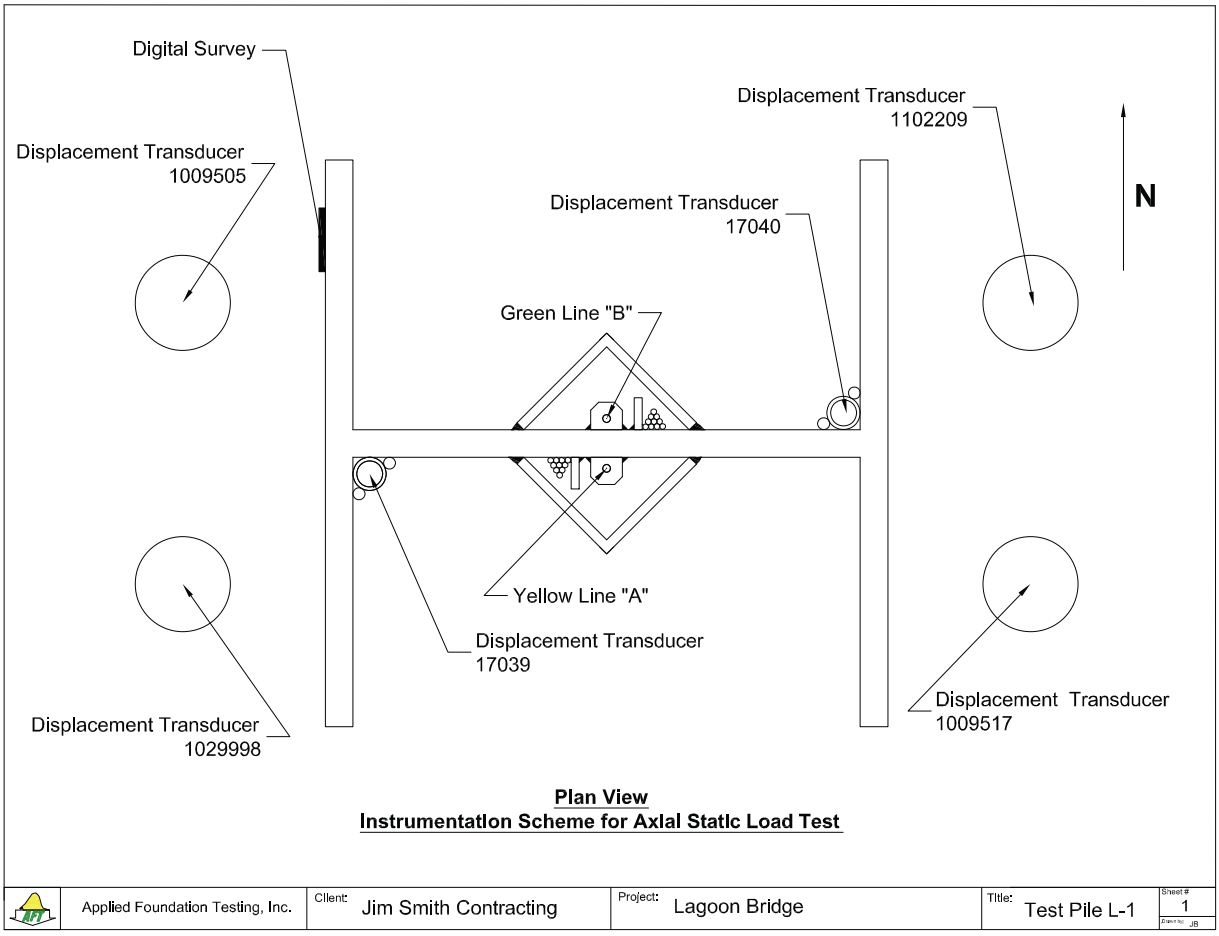

Figure B.4. H-Pile Instrumentation Scheme

Table B.1. B-3 H-Pile Manufacturer Sizing Information

skylinesteelI
a NUCOR company

HP

Steel H-Pile

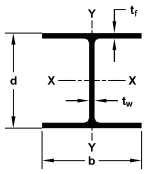

SECTION	Weight lb/ft (kg/m)	Area in² (cm²)	Depth d in (mm)	Flange Width b in (mm)	THICKNESS Flange (t_f) in (mm)	THICKNESS Web (t_w) in (mm)	Coating Area ft²/ft (m²/m)	ELASTIC PROPERTIES AXIS X-X I in⁴ (cm⁴)	S in³ (cm³)	Z in³ (cm³)	r in (cm)	AXIS Y-Y I in⁴ (cm⁴)	S in³ (cm³)	Z in³ (cm³)	r in (cm)
HP 8 HP 200	36 54	10.6 68.4	8.02 204	8.16 207	0.445 11.3	0.445 11.3	3.92 1.19	119 4953	29.8 488	33.6 550.6	3.36 8.53	40.3 1677	9.88 162	15.2 249.1	1.95 4.95
HP 10 HP 250	42 63	12.4 80.0	9.70 246	10.10 257	0.420 10.7	0.415 10.5	4.83 1.47	210 8741	43.4 711	48.3 791.5	4.13 10.5	71.7 2984	14.2 233	21.8 357.2	2.41 6.12
	57 85	16.7 108	9.99 254	10.20 259	0.565 14.4	0.565 14.4	4.91 1.50	294 12237	58.8 964	66.5 1089.7	4.18 10.6	101 4204	19.7 323	30.3 496.5	2.45 6.22
HP 12 HP 310	53 79	15.5 100	11.80 300	12.00 305	0.435 11.0	0.435 11.0	5.82 1.77	393 16358	66.7 1093	74.0 1212.6	5.03 12.8	127 5286	21.1 346	32.2 527.7	2.86 7.26
	63 94	18.4 119	11.90 302	12.10 307	0.515 13.1	0.515 13.1	5.86 1.79	472 19646	79.1 1296	88.3 1447.0	5.06 12.9	153 6368	25.3 415	38.7 634.2	2.88 7.32
	74 110	21.8 141	12.10 307	12.20 310	0.610 15.5	0.605 15.4	5.91 1.80	569 23683	93.8 1537	105 1720.6	5.11 13.0	186 7742	30.4 498	46.6 763.6	2.92 7.42
	84 125	24.6 159	12.30 312	12.30 312	0.685 17.4	0.685 17.4	5.97 1.82	650 27055	106 1737	120 1966.4	5.14 13.1	213 8866	34.6 567	53.2 871.8	2.94 7.47
HP 14 HP 360	73 109	21.4 138	13.60 345	14.60 371	0.505 12.8	0.505 12.8	6.96 2.12	729 30343	107 1753	118 1933.7	5.84 14.8	261 10864	35.8 587	54.6 894.7	3.49 8.86
	89 132	26.1 168	13.80 351	14.70 373	0.615 15.6	0.615 15.6	7.02 2.14	904 37627	131 2147	146 2392.5	5.88 14.9	326 13569	44.3 726	67.7 1109.4	3.53 8.97
	102 152	30.1 194	14.00 356	14.80 376	0.705 17.9	0.705 17.9	7.06 2.15	1050 43704	150 2458	169 2769.4	5.92 15.0	380 15817	51.4 842	78.8 1291.3	3.56 9.04
	117 174	34.4 222	14.20 361	14.90 378	0.805 20.4	0.805 20.4	7.12 2.34	1220 50780	172 2819	194 3179.1	5.96 15.1	443 18439	59.5 975	91.4 1497.8	3.59 9.12
HP 16 HP 410	88 131	25.8 167	15.30 389	15.70 399	0.540 13.7	0.540 13.7	7.52 2.29	1110 46201	145 2376	161 2638.3	6.56 16.7	349 14526	44.5 729	68.2 1117.6	3.68 9.35
	101 150	29.9 193	15.50 394	15.80 401	0.625 15.9	0.625 15.9	7.56 2.30	1300 54110	168 2753	187 3064.4	6.59 16.7	412 17149	52.2 855	80.1 1312.6	3.71 9.42
	121 180	35.8 231	15.80 401	15.90 404	0.750 19.1	0.750 19.1	7.62 2.32	1590 66180	201 3294	226 3703.5	6.66 16.9	504 20978	63.4 1039	97.6 1599.4	3.75 9.53
	141 210	41.7 269	16.00 406	16.00 406	0.875 22.2	0.875 22.2	7.69 2.34	1870 77835	234 3835	264 4326.2	6.70 17.0	599 24932	74.9 1227	116 1900.9	3.79 9.63
	162 241	47.7 308	16.30 414	16.10 409	1.000 25.4	1.000 25.4	7.75 2.36	2190 91154	269 4408	306 5014.4	6.78 17.2	697 29011	86.6 1419	134 2195.9	3.82 9.70
	183 272	54.1 349	16.50 419	16.30 414	1.130 28.7	1.130 28.7	7.81 2.38	2510 104473	304 4982	349 5719.1	6.81 17.3	818 34047	100.0 1639	156 2556.4	3.89 9.88
HP 18 HP 460	135 201	39.9 257	17.50 445	17.80 452	0.750 19.1	0.750 19.1	8.54 2.60	2200 91570	251 4113	281 4604.7	7.43 18.9	706 29386	79.3 1299	122 1999.2	4.21 10.7
	157 234	46.2 298	17.70 450	17.90 455	0.870 22.1	0.870 22.1	8.60 2.62	2570 106971	290 4752	327 5358.5	7.46 18.9	833 34672	93.1 1526	143 2343.3	4.25 10.8
	181 269	53.2 343	18.00 457	18.00 457	1.000 25.4	1.000 25.4	8.66 2.64	3020 125701	336 5506	379 6210.7	7.53 19.1	974 40541	108.0 1770	167 2736.6	4.28 10.9
	204 304	60.2 388	18.30 465	18.10 460	1.130 28.7	1.130 28.7	8.73 2.66	3480 144847	380 6227	433 7095.6	7.60 19.3	1120 46618	124.0 2032	191 3129.9	4.31 11.0

B.4 Pipe Pile Instrumentation Scheme

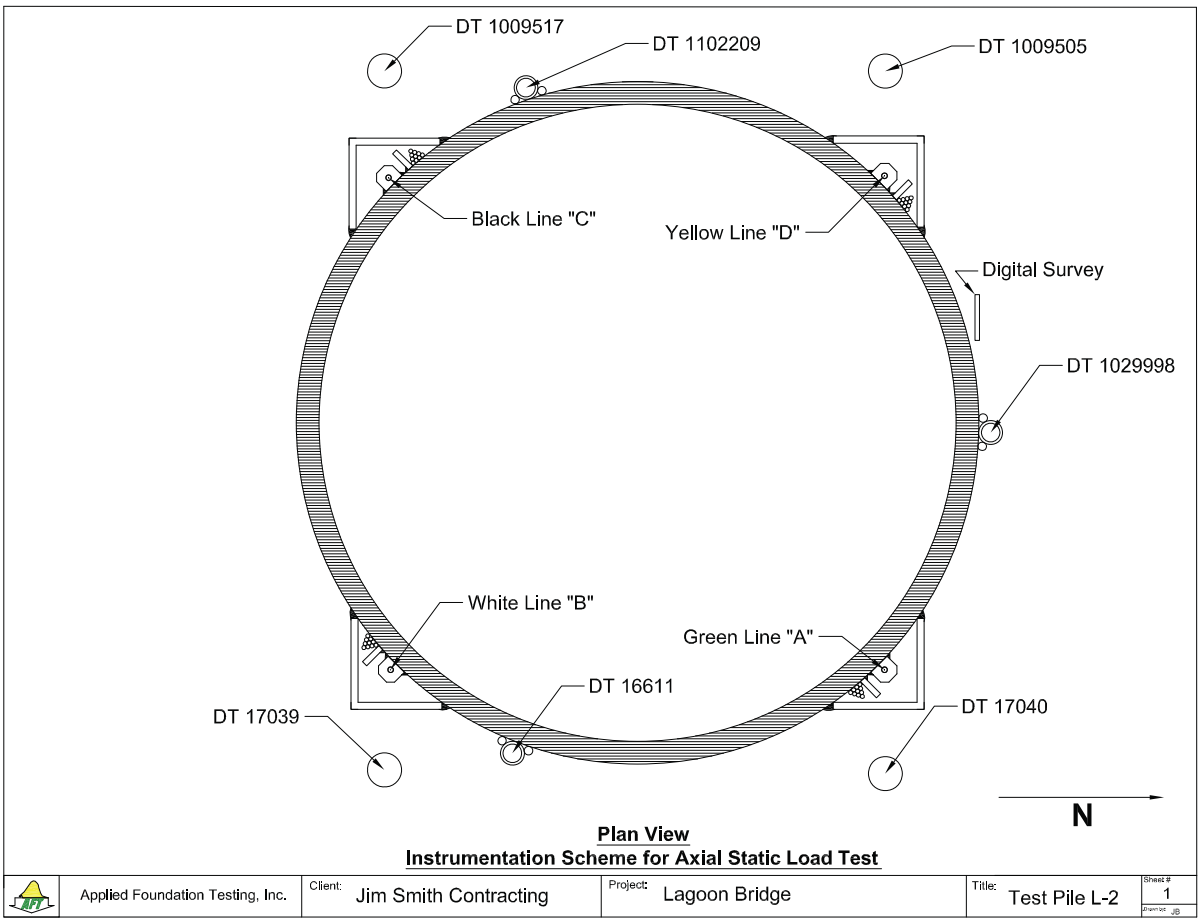

Figure B.5. Pipe Pile Instrumentation Scheme

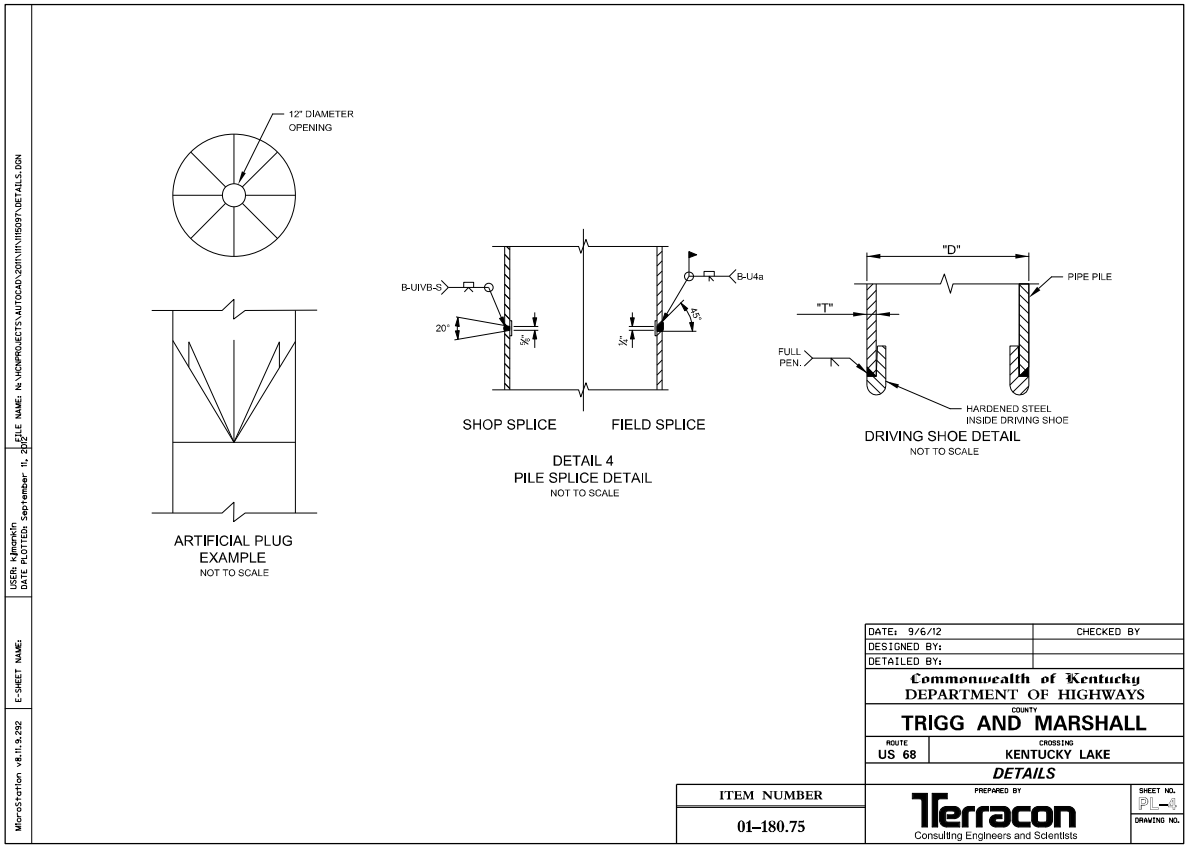

Figure B.6. B-4 Additional

B.5 H-Pile Final Schematic

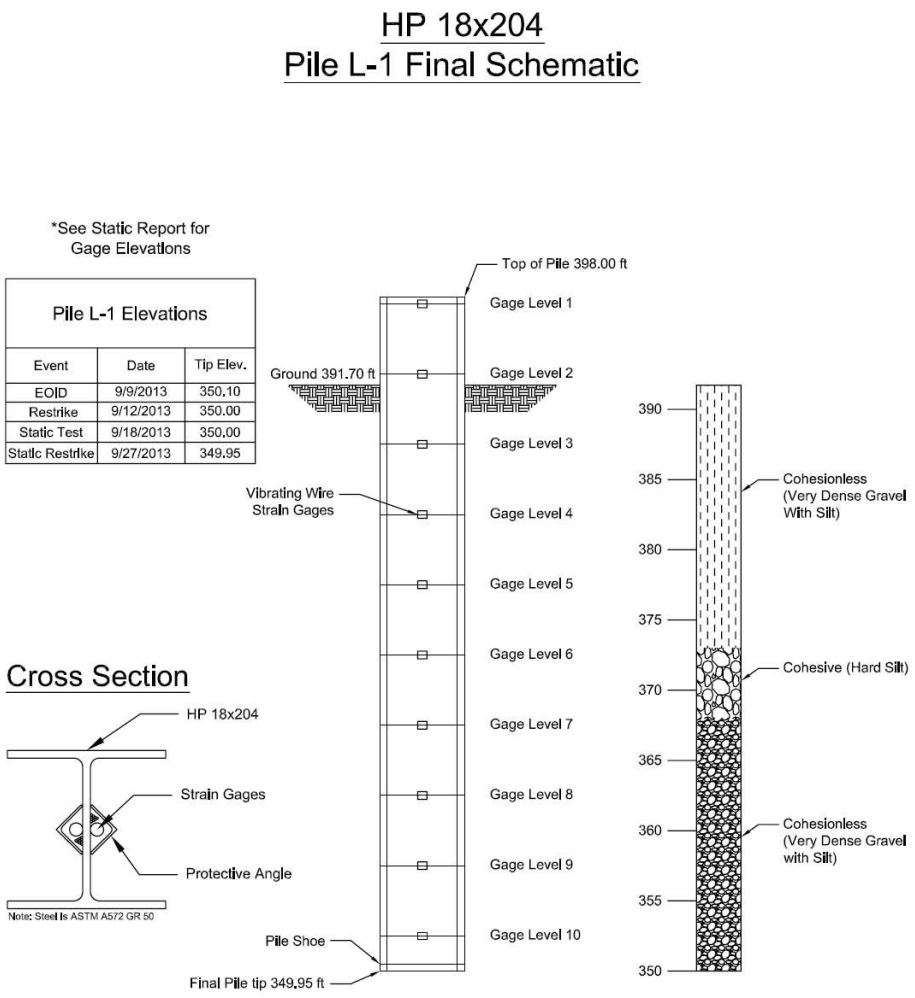

Figure B.7. H-Pile Final Schematic

B.6 Pipe Pile Final Schematic

Final 30" Test Pile L-2 Schematic

*See Static Report for Gage Elevations

Pile L-2 Elevations			
Event	Date	Plug Elev.	Tip Elev.
EOID	8/12/2013	N/A	277.6
1st Restrike	8/14/2013	N/A	277.2
2nd Restrike	8/15/2013	353.3	277.0
Ext. Drive	8/16/2013	354.3	270.0
Ext. Drive RS	8/19/2013	354.3	269.9
After Static	9/6/2013	354.3	269.8
Static Restrike	9/10/2013	N/A	269.7

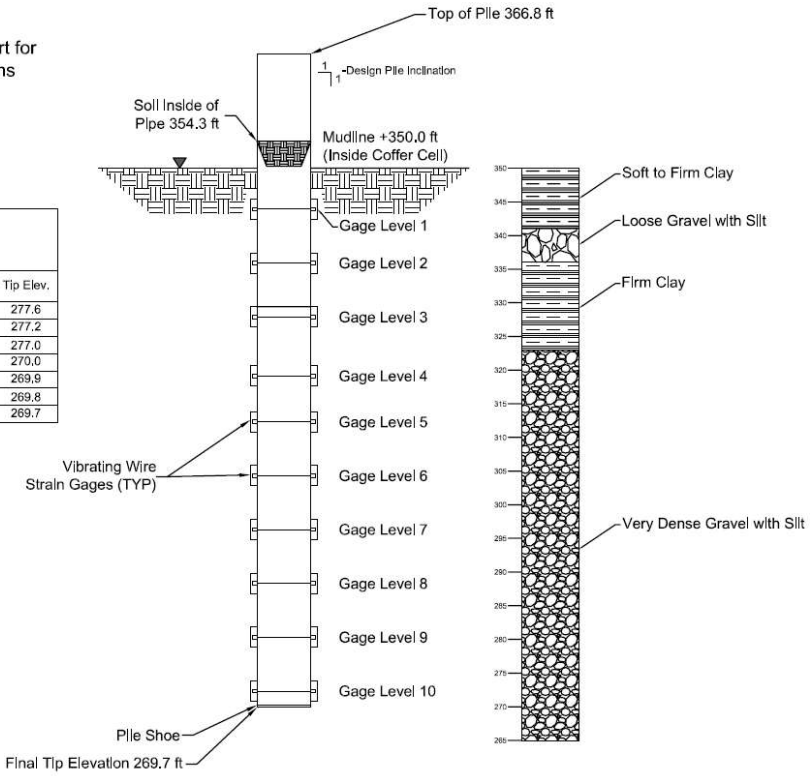

Cross Section View

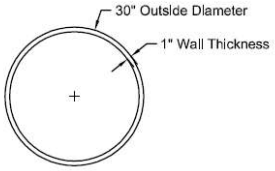

Notes:
1. All Steel is Grade 3 (Minimum yield strength of 45KSI)

APPENDIX C

Dynamic Testing

C.1 H-Pile CAPWAP Results

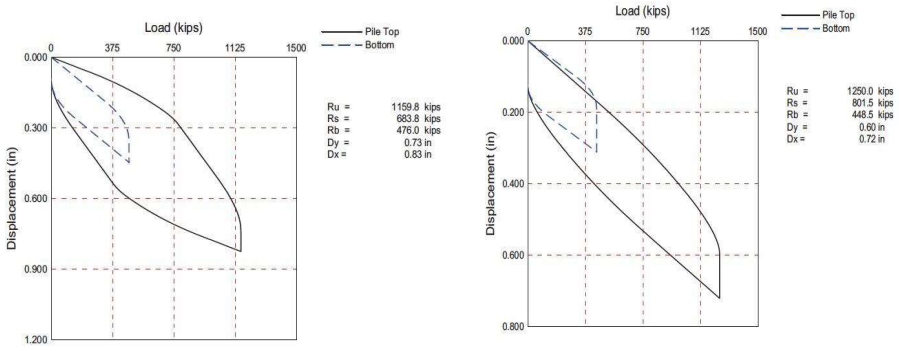

The subject pile was monitored with dynamic pile testing equipment during initial drive, all subsequent re-strikes, and extended drive. Compression and tension pile driving stresses were below the acceptable limit of 40.5 ksi. The acceptable limit for compression and tension driving stresses is defined as 90 percent of Fy. The ultimate capacities ranged from approximately 1,160 kips at the end of initial drive to approximately 1,250 kips during the 72 hour re-strike. The 72 hour re-strike capacity showed an increase of approximately 90 kips. However, the subsequent final restrike (after the static load test) showed a slight decrease in capacity with respect to the initial drive. This was most likely caused by the lower hammer energy utilized during the final re-strike not fully mobilizing the pile capacity.

The unit side shear resistances in the dense to very dense gravel ranged from approximately 2 to 4 ksf and generally increased with depth. Unit end bearings at the pile tip (using an end area based on a plugged condition) ranged from approximately 133 to 207 ksf. However the end bearings are likely much higher due to the pile likely only being partially plugged.

Figure C.1. H-Pile CAPWAP Results

C.2 Pipe Pile CAPWAP Results

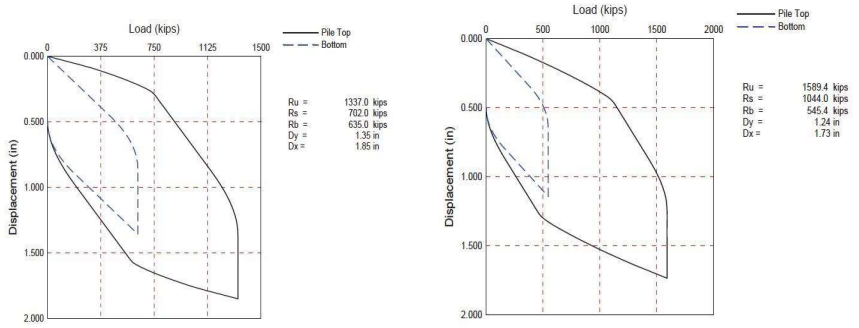

The pile was monitored with dynamic pile testing equipment during initial drive, all subsequent re-strikes, and extended drive. Compression and tension pile driving stresses were below the acceptable limit of 40.5 ksi. The acceptable limit for compression and tension driving stresses is defined as 90 percent of Fy. It should be noted the driving shoe located at the pile tip was not included as part of the pile model within the CAPWAP software. The signal matching results would only be marginally affected even if the pile shoe was included, given the size and depth of the driving shoe relative to the pile. The impedance changes in the bottom few inches would have been very small.

The match qualities (MQ) for the signal matching results were less than 4. Lower match qualities may be achievable; however, to achieve lower match qualities the ultimate capacity of the pile may be unrealistic given the soil conditions, transferred hammer energy, and the measured sets.

The ultimate capacities ranged from approximately 1,337 kips at the end of initial drive to approximately 2,400 kips during the final re-strike. The re-strike capacities for the first (48 hour) and second (72 hour) re-strikes showed an increase in capacity of approximately 252 and 61 kips, respectively.

The unit side shear resistances in the dense to very dense gravel ranged from approximately 1 to 6.5 ksf and increased with depth. The end bearing resistance (using an end area based on a plugged condition) ranged from approximately 111 to 121 ksf. However, unit end bearings are likely much higher due to the pile likely only being partially plugged.

Figure C.2. Pipe Pile CAPWAP Results

C.3 H-Pile Signal Matching Analysis

Blow Location	R_{ult} (k)	R_{skn} (k)	Approx. Blows per foot	EMX (k-ft)	QS (in)	QT (in)	SS (sec/ft)	ST (sec/ft)	Match Quality
End of Initial Drive (BN 2155)	1,160	684	127	37.6	0.04	0.27	0.06	0.10	1.6
09/12/13 RS (BN 2)	1,250	802	96	36.2	0.13	0.14	0.23	0.03	1.99
09/27/13 RS (BN 3)	1,160	852	250	31.0	0.12	0.17	0.12	0.19	1.32

RMX (kN)	EMX (kN/m)	CSX (kPa)	CSB (kPa)	Match Quality
5529.14	548.7231496	215116.43	111005.59	1.99
5066.524	528.2919685	169611.03	102731.88	1.32

The RMX (maximum case method) data indicated that the ultimate capacitates dropped from a capacity of approximately 5530kN during the first re-strike to 5066.524 kN during the final re-strike. This was most likely caused by the lower hammer energy utilized during the final re-strike not fully mobilizing the pile capacity.

The unit side shears ranged from 95 .6 to 191 kPa and generally increased with depth as the pile proceeded through dense to very dense gravel. The unit end bearing at the pile tip assumed plugged conditions. The unit end bearings ranged from approximately 6368.07 to 9911.21 kPa. The maximum compression stress at the gage level ranged from 169611.03 kPa to 215116.43 kPa, and the maximum compression stress at the toe reached 111005.59 kPa to 102731.88 kPa. The maximum energy transferred to a gage location was 548.723 kPa. The amount of energy transferred lost during the final re-strike was 20.3 kPa.

Figure C.3. H-Pile Signal Matching Analysis

C.4. Pipe Pile Signal Matching Analysis

Blow Location	R_{ult} (k)	R_{skn} (k)	Approx. Blows per foot	EMX (k-ft)	QS (in)	QT (in)	SS (sec/ft)	ST (sec/ft)	Match Quality
End of Initial Drive (BN 575)	1,337	702	24	104.1	0.04	0.66	0.05	0.05	3.59
08/14/13 RS (BN 1)	1,589	1,044	24	124.5	0.06	0.50	0.11	0.05	2.96
08/15/13 RS (BN 3)	1,650	1,100	46	144.3	0.04	0.60	0.07	0.12	3.96
08/16/13 ED (BN 235)	1,660	1,079	38	92.8	0.10	0.34	0.08	0.05	3.14
08/19/13 RS (BN 2)	2,300	1,713	60	94.5	0.06	0.18	0.11	0.03	2.77
09/23/13 RS (BN 2)	2,400	1,803	60	91.1	0.16	0.06	0.11	0.14	2.66

The ultimate capacities ranged from approximately 7148.3kN first re-strike to 10675.7kN during the final re-strike.The capacities showed an increase of roughly 3527 kN.

The subsurface conditions consisting of dense to very dense gravel resulted in the unit shear ranging from 47.88kPa to 311.22 kPa as the depth. The unit end bearings at the pile tip were calculated considering plugged condition even though they are likely only to be partially plugged. The pile only being partially plugged will yield much higher end bearings in the field. With the assumed conditions, the end bearing pressures ranged from approximately 5314.71 to 5793.51 kPa.

RMX (kN)	EMX (kN/m)	CSX (kPa)	CSB (kPa)	Match Quality
7148.3	1816.915748	247521.79	124795.12	2.96
10675	1329.486142	235110.7985	177884.4165	2.66

The signal matching results provide quality information about the state of the pile at the time of the final restrike. The compression stress acting at the toe of the pile has significantly increased, the energy transferred to the gage location has decreased considerably, and the maximum compression stress at that gage location has been relieved by approximately 1200 kPa. This indicates that the pile has mobilized.

Figure C.4. Pipe Pile Signal Matching Analysis

C.5 H-Pile Dynamic Testing Results Summary

Table C.1. H-Pile Dynamic Testing Results Summary

Drive	Maximum Case Method (kips)	Max. Comp. Stress (ksi)	Average Comp. Stress (ksi)	Max. Comp. Stress at Bottom (ksi)	Average Comp. Stress at Bottom (ksi)	Average Transferred Energy (k-ft)	Average Hammer Stroke (ft)
Initial	@ End 1,196	31.5	26.5	21.6	14.6	33.9	10.02
09/12/13 RS	1,243	31.2	23.8	19.9	16.1	29.0	9.74
09/27/13 RS	1,139	24.6	19.3	19.0	14.9	20.3	8.76

C.6 Pipe Pile Dynamic Testing Results Summary

Table C.2. Pipe Pile Dynamic Testing Results Summary

Drive	Maximum Case Method (kips)		Max. Comp. Stress (ksi)	Average Comp. Stress (ksi)	Max. Comp. Stress at Bottom (ksi)	Average Comp. Stress at Bottom (ksi)	Average Transferred Energy (k-ft)	Average Hammer Stroke (ft)
Initial	@ End 1,320		33.5	28.4	32.4	27.0	104.4	9.3
08/14/13 RS	1,607		35.9	31.8	18.1	16.7	122.6	10.0
08/15/13 RS	1,575		37.2	29.2	19.4	17.4	94.0	8.8
08/16/13 ED	@ Start 1,598	@ End 1,643	39.4	30.1	21.6	17.8	93.6	8.6
08/19/13 RS	2,141		34.6	28.9	22.8	21.3	97.2	9.4
09/10/13 RS	2,622		34.1	28.4	25.8	21.7	97.2	10.2

C.7 GRLWEAP

KYTC Lake Bridges Project Marshall/Trigg Counties, KY
HCN/Terracon Project No. N1115097

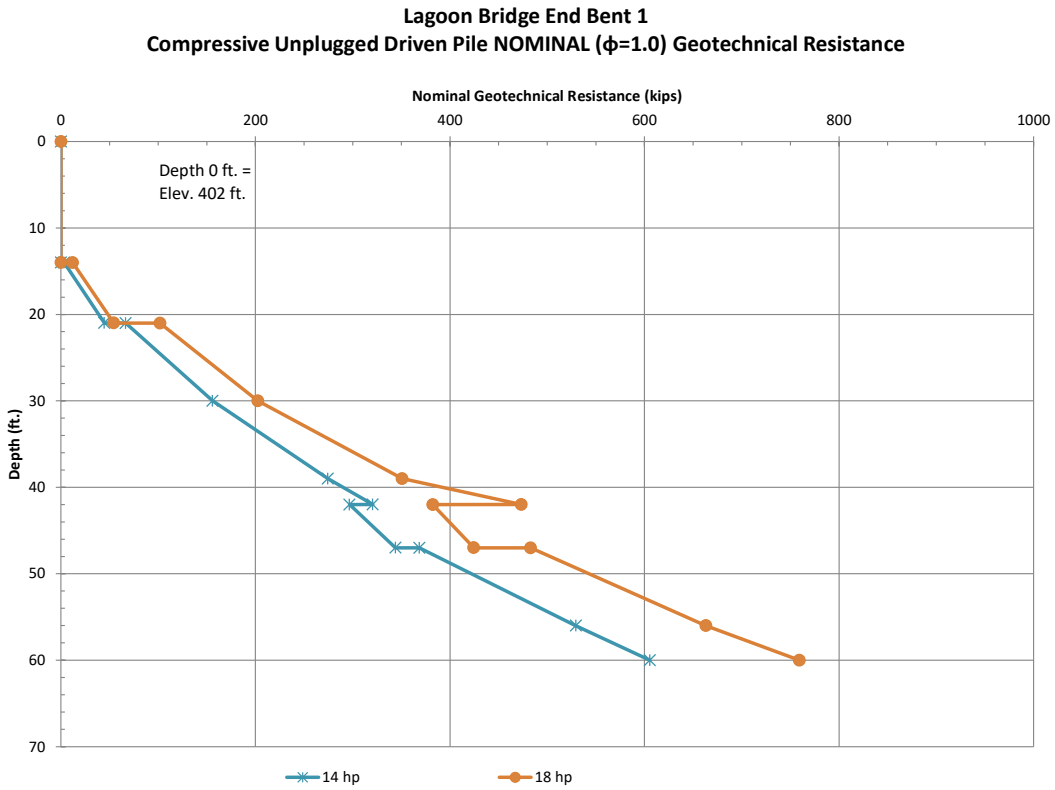

Exhibit E-1

Figure C.5. GRLWEAP Plots

C.8 Hammer Information

ICE

Model I-30^{v2}

Single-Acting Diesel Hammer

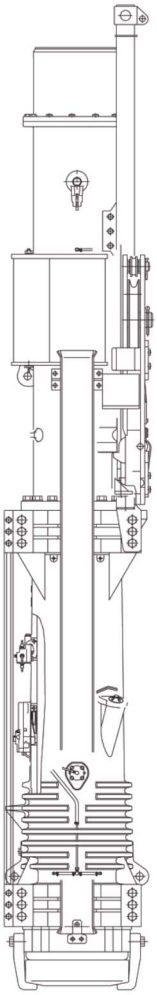

- **Simple and reliable low-pressure impact-atomization fuel injection system ensures maximum uptime.**
- **Excellent cylinder scavenging ensures cooler operation.**
- **Automatic oil lubrication to both the upper and lower cylinders eliminates greasing and increases productivity.**
- **Remote hydraulic fuel control system available.**
- **Electronic energy output monitoring system available.**

Working Specifications		
Ram weight	6615 lbs	3000 kg
Maximum geometric stroke	13.73 ft	4185 mm
Energy at maximum stroke	90824 ft-lbs	123 kJ
Rated continuous stroke	10.84 ft	3304 mm
Energy at rated stroke	71700 ft-lbs	97 kJ
Blow rate	33-53 bpm	33-53 bpm
Weights		
Hammer with box-lead guides	14250 lbs	6462 kg
Typical helmet weight	1785 lbs	809 kg
Typical operating weight	16035 lbs	7272 kg
Capacities		
Diesel fuel tank	16.8 gal	63.6 liters
Lube oil tank	4.6 gal	17.4 liters
Ether tank	0.5 gal	1.9 liters
Dimensions		
Length	17.7 ft	5395 mm
Length with trip guides	20.8 ft	6340 mm
Overall width	25.3 in	643 mm
Standard box leads	26 in	660 mm
Overall depth	32.7 in	831 mm
Centerline to rear	17.7 in	450 mm
Centerline to front	15.0 in	381 mm

ICE INTERNATIONAL CONSTRUCTION EQUIPMENT, LLC

Figure C.6. Hammer Information

APPENDIX D

Static Testing

D.1 Pile Load Test Profile Schematic

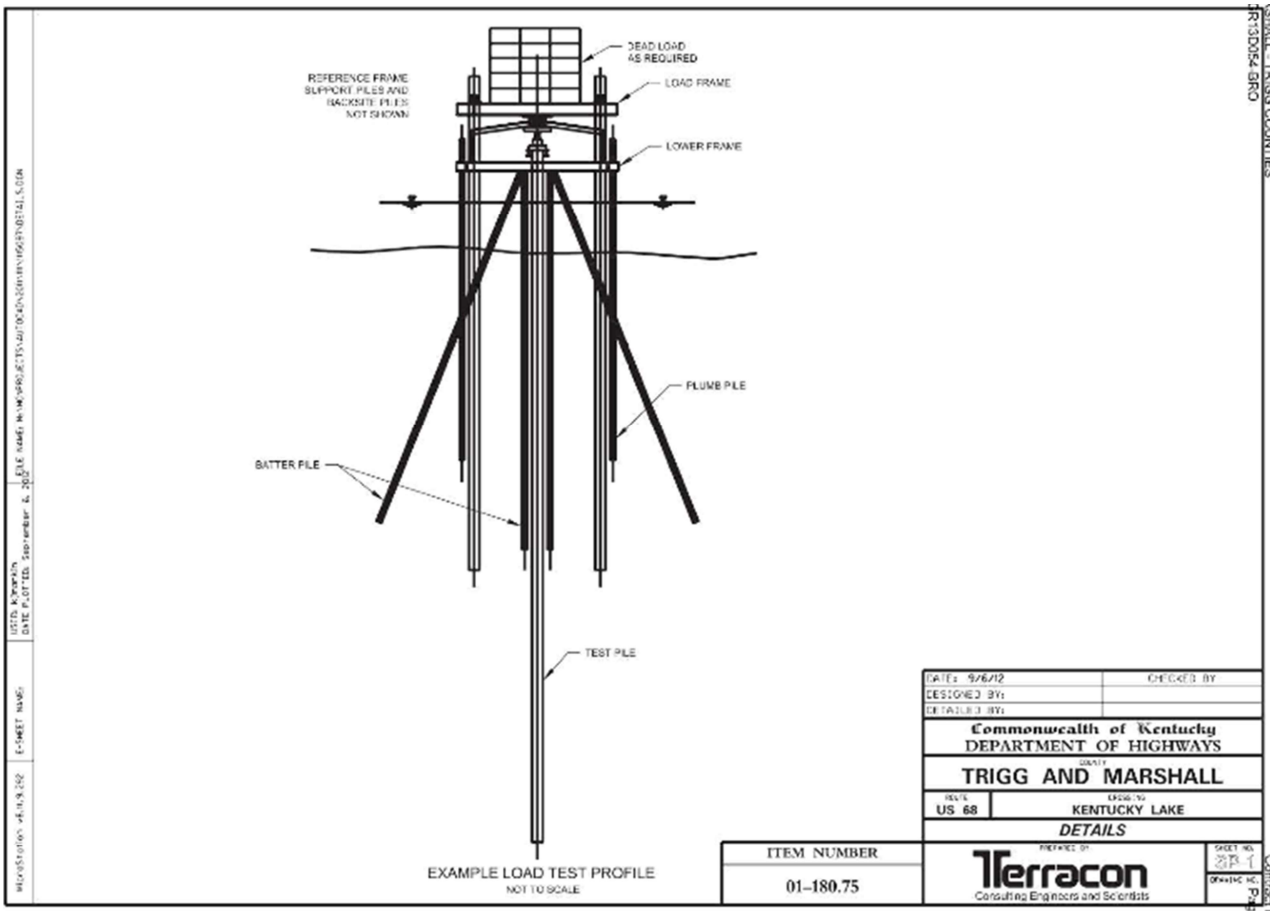

Figure D.1. Pile Load Test Profile Schematic

D.2 H-Pile Bearing Capacity Using Various Failure Criterion

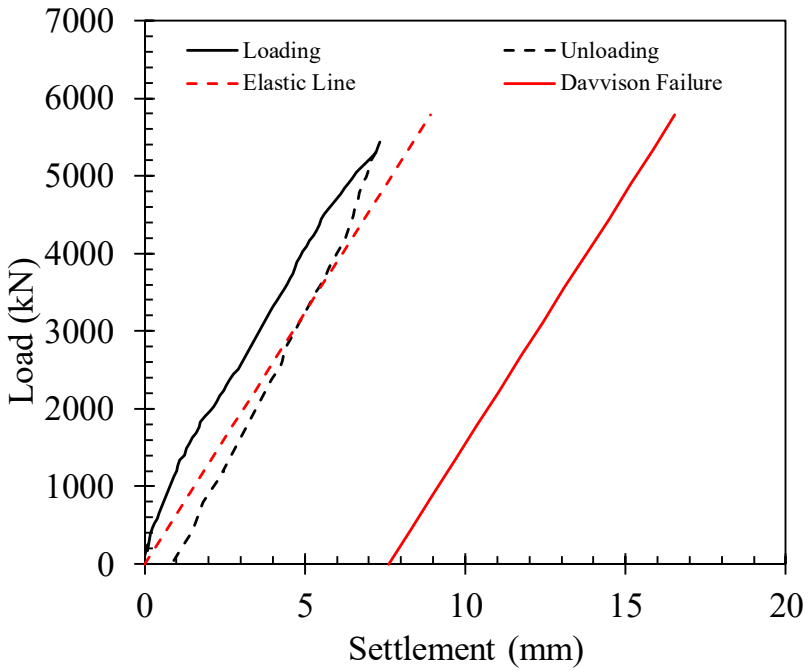

Figure D.2. H-Pile Bearing Capacity Using Davisson Method Failure Criterion

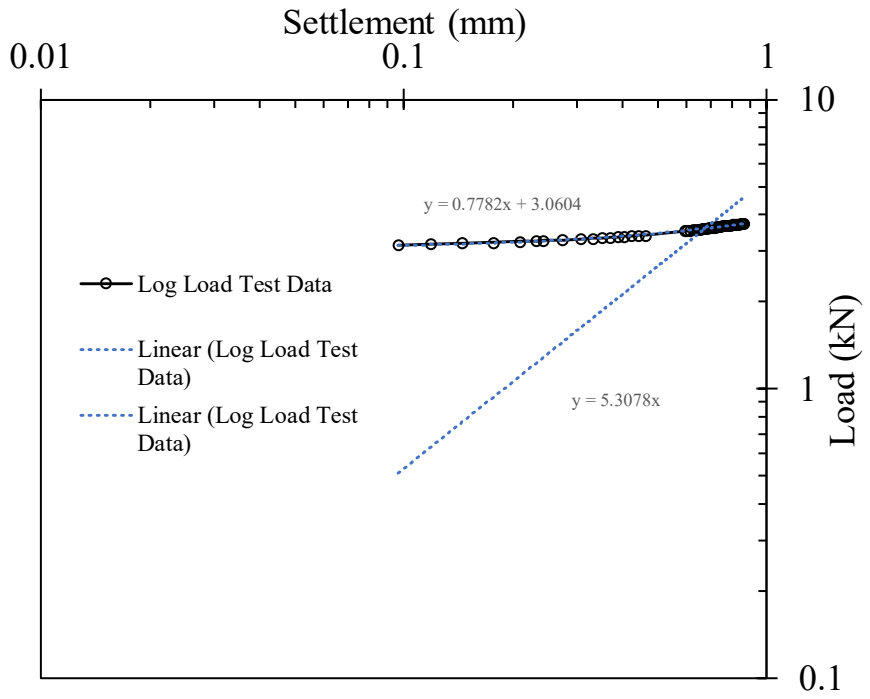

(1)Best fit linear line to the load-settlement curve		(2) Best Fit line y intercept =0	
C11	0.7782	C21	5.3078
C12	3.0604		

To find the x coordinate where the lines intersect equation (1) and (2) are set equal to each other. To the y coordinate of the intersection point, the x coordinate solved for in last step was plugged into equation (2)

x	0.675644649	y	3.586186665

10^3.58612

Qu=	3856.441

Figure D.3. D-2 H-Pile Bearing Capacity Using De Bear Failure Criterion

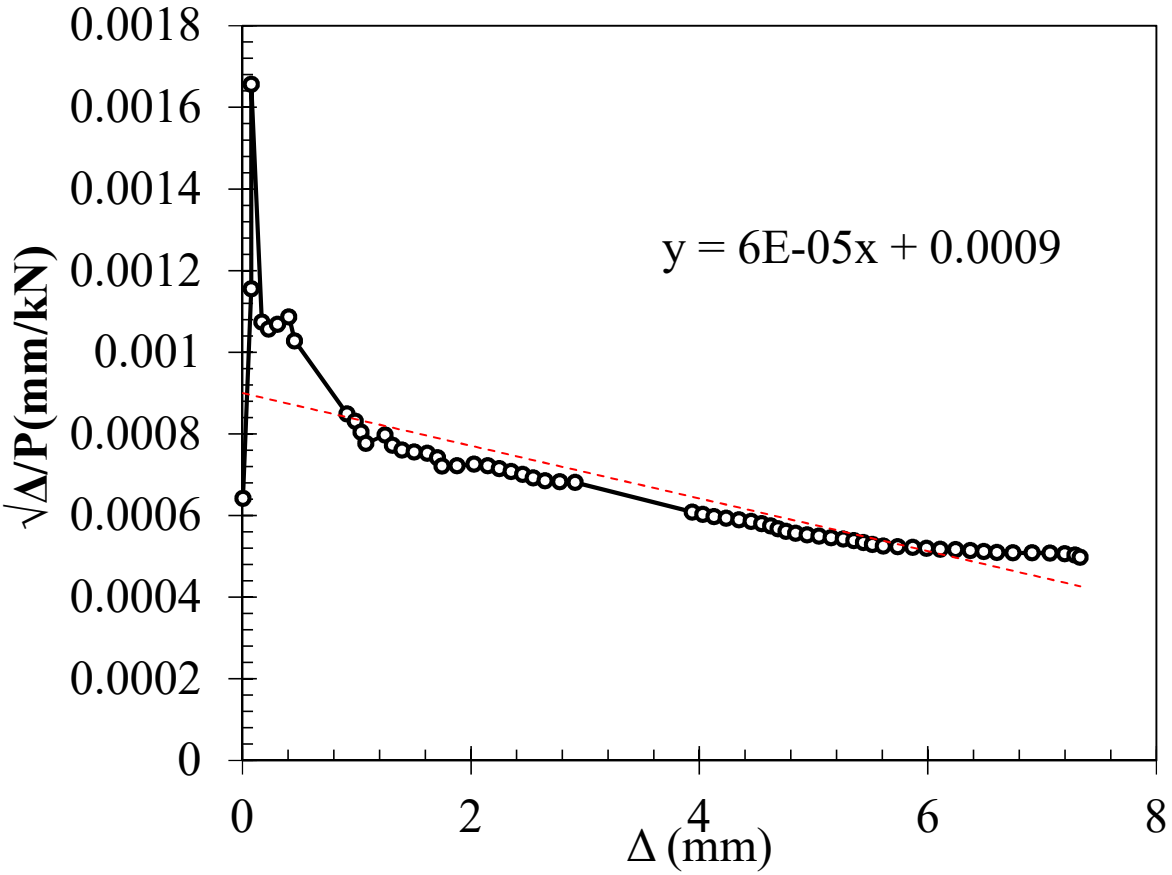

Figure D.3. D-2 H-Pile Bearing Capacity Using Various Failure Criterion

Figure D.4. D-2 H-Pile Bearing Capacity Using Various Failure Criterion

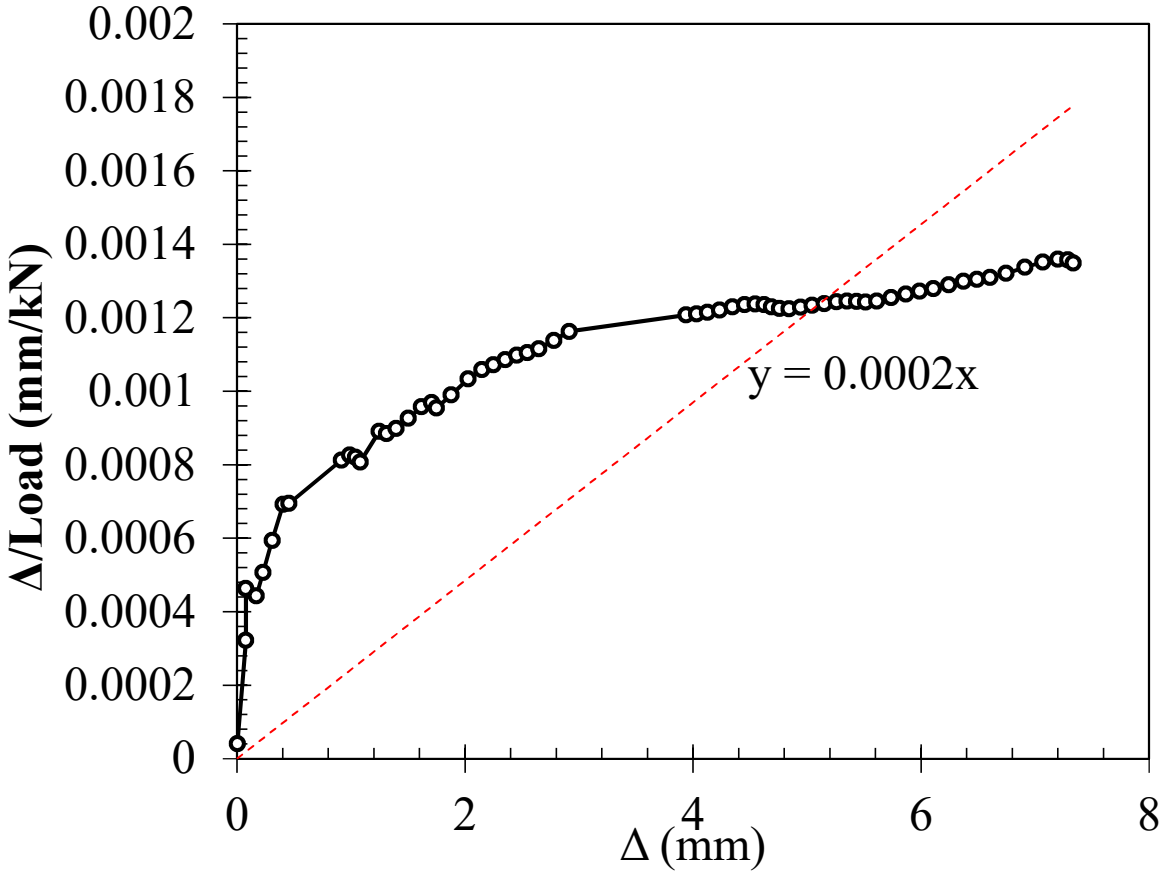

D.3 Pipe Pile Bearing Capacity Using Various Failure Criterion

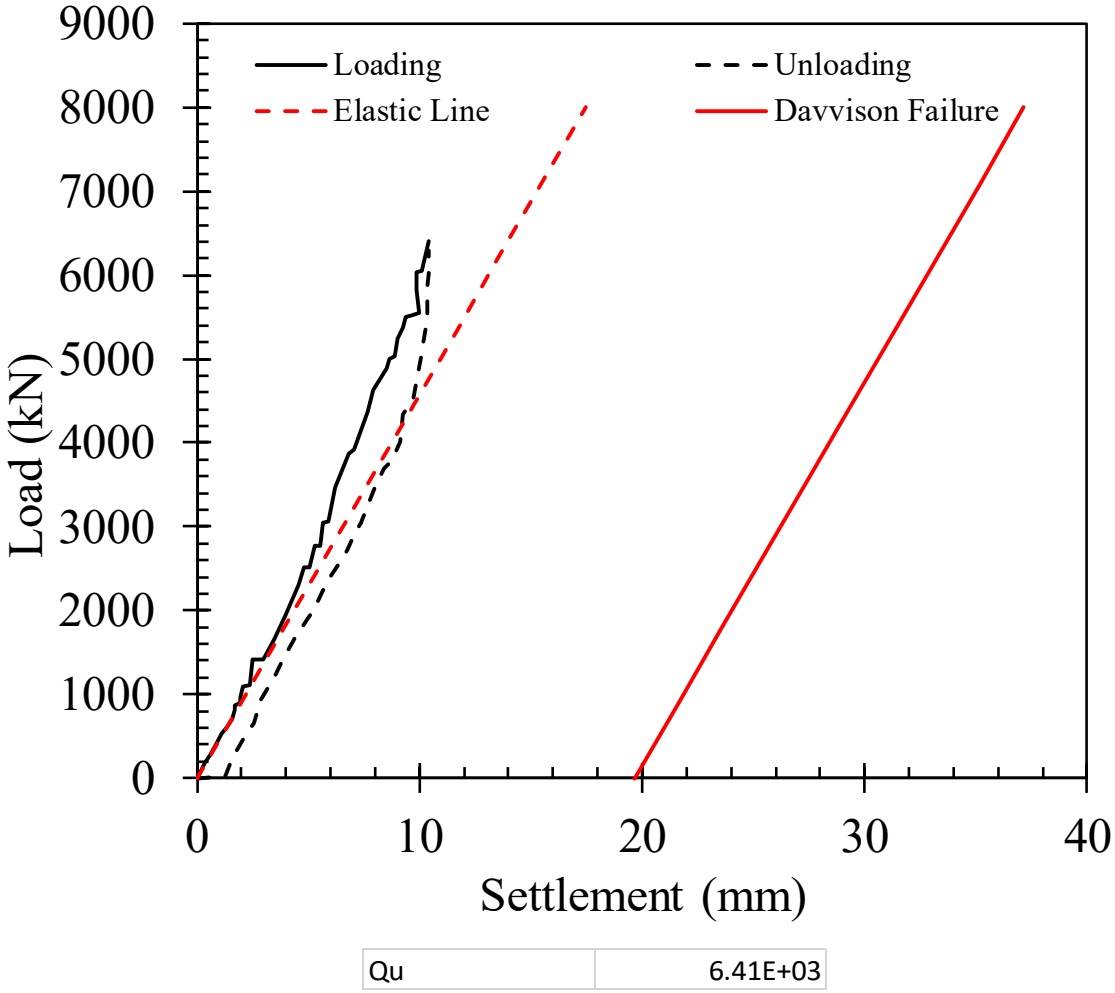

Figure D.5. Pipe Pile Bearing Capacity Using Davisson Failure Criterion

Figure D.6. Pipe Pile Bearing Capacity Using Various Failure Criterion

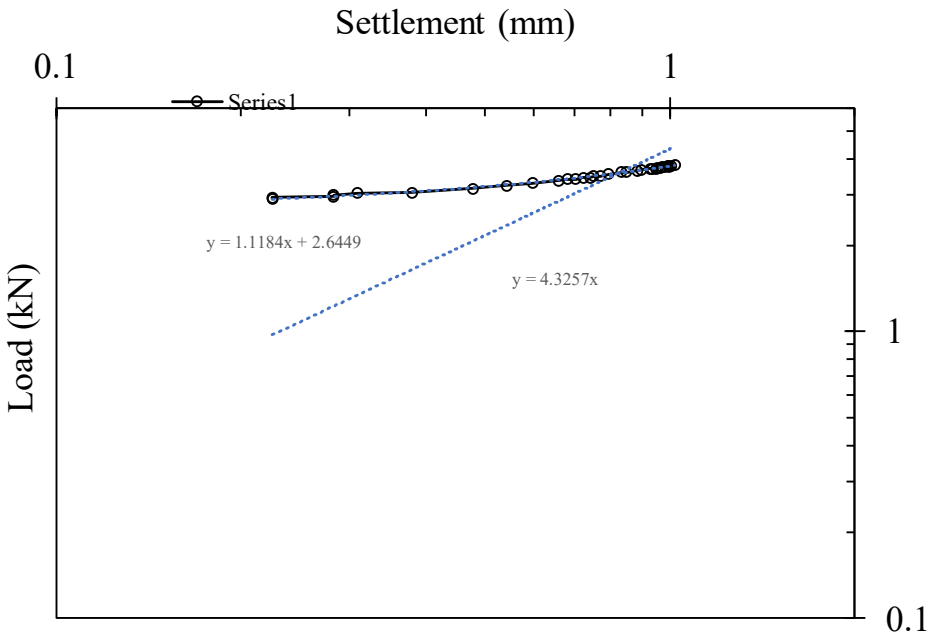

(1)Best fit linear line to the load-settlement curve		(2) Best Fit line y intercept =0	
C11	1.1184	C21	4.3257
C12	2.6449		

To find the x coordinate where the lines intersect equation (1) and (2) are set equal to each other. To the y coordinate of the intersection point, the x coordinate solved for in last step was plugged into equation (2)

x	0.824650017	y	3.567188579

10^3.567

Qu=	3691.379

Figure D.7 Pipe Pile Bearing Capacity Using Various Failure Criterion

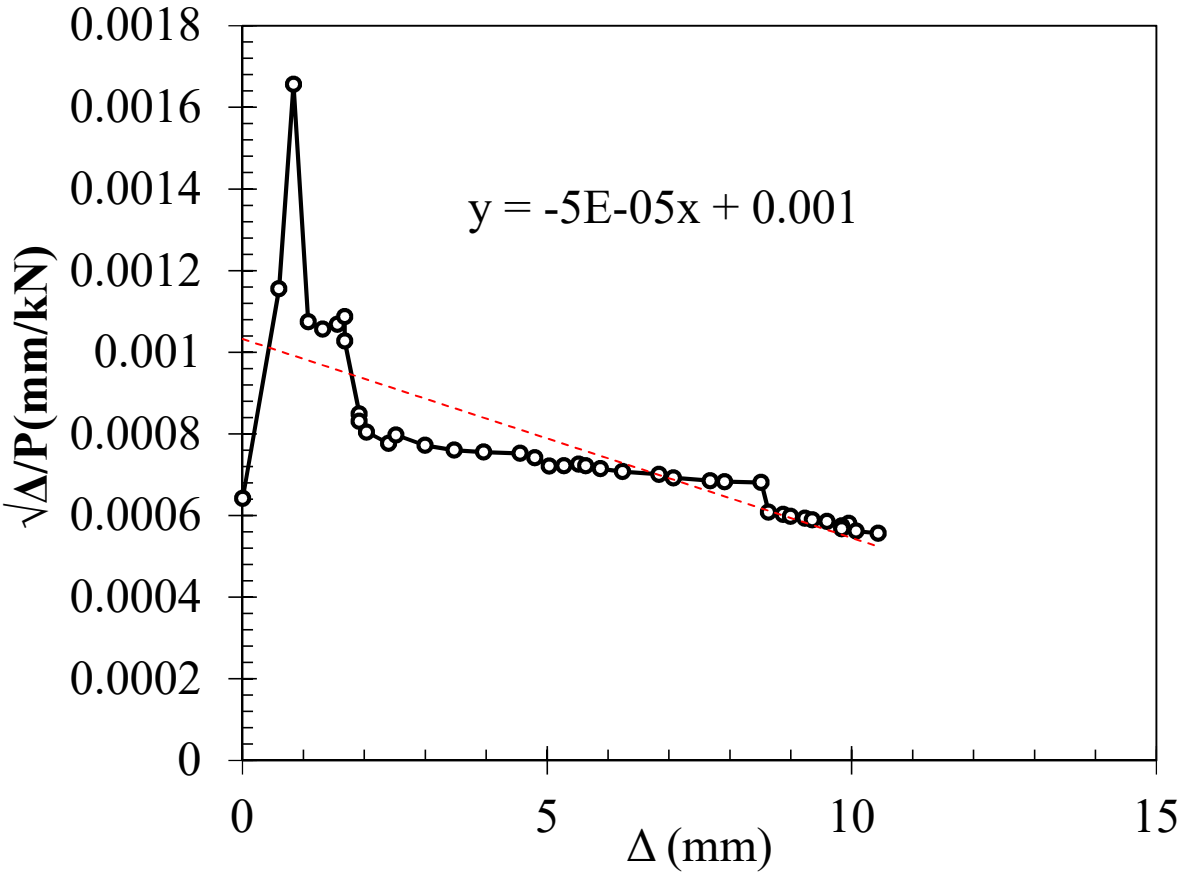
0.0018
0.0016
0.0014
0.0012
0.001
0.0008
0.0006
0.0004
0.0002
0
√Δ/P(mm/kN)
y = -5E-05x + 0.001
0
5
10
15
Δ (mm)

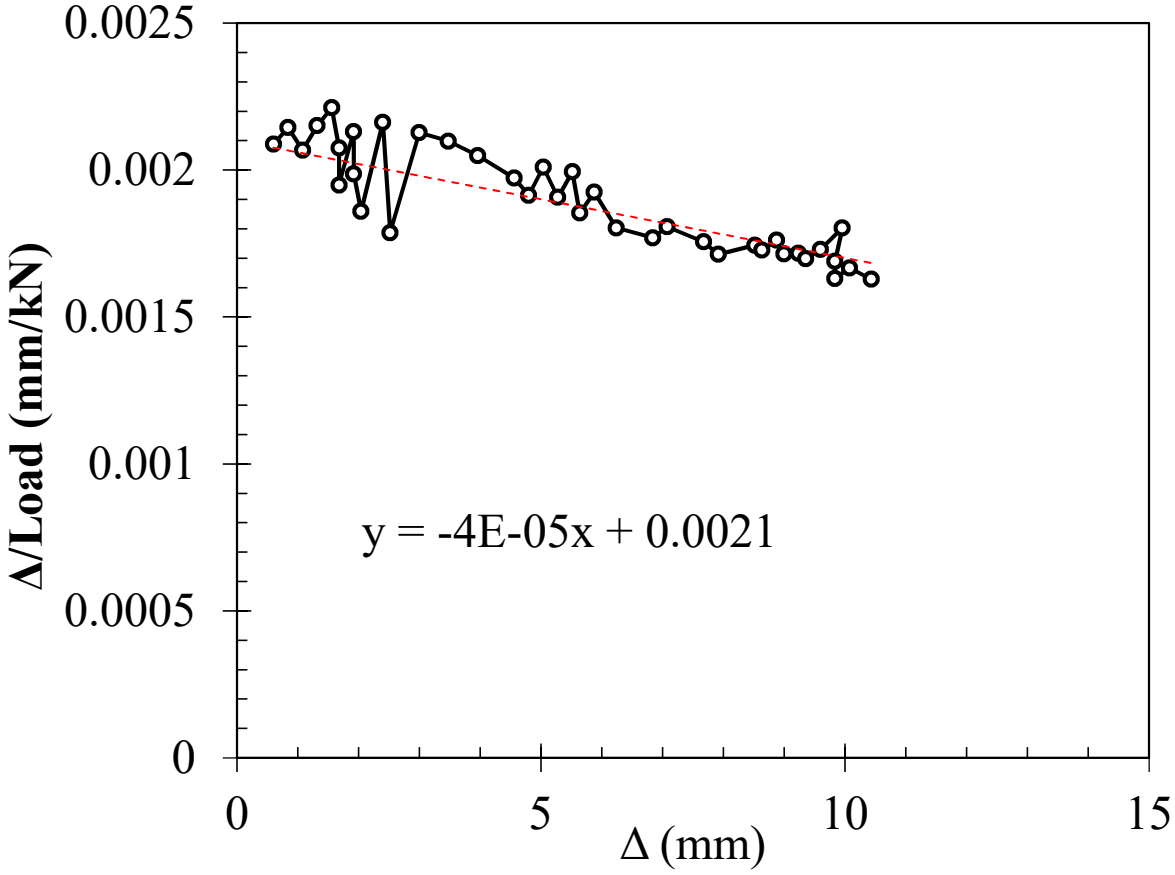
0.0025
0.002
0.0015
0.001
0.0005
0
Δ/Load (mm/kN)
y = -4E-05x + 0.0021
0
5
10
15
Δ (mm)

APPENDIX E

t-z curves

E.1 H-Pile t-z curves

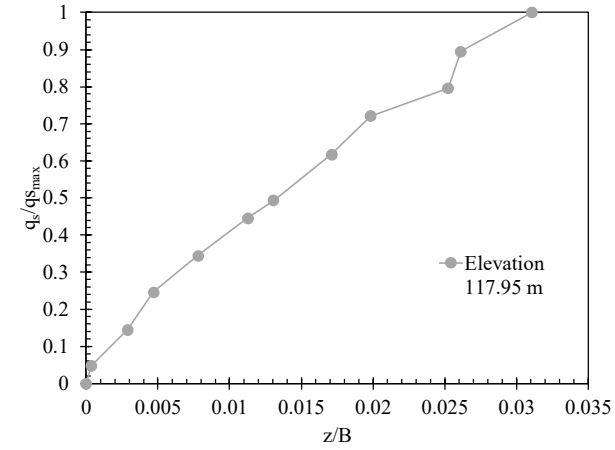

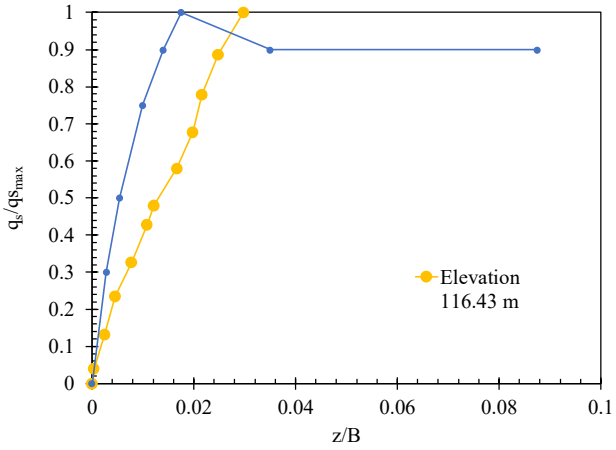

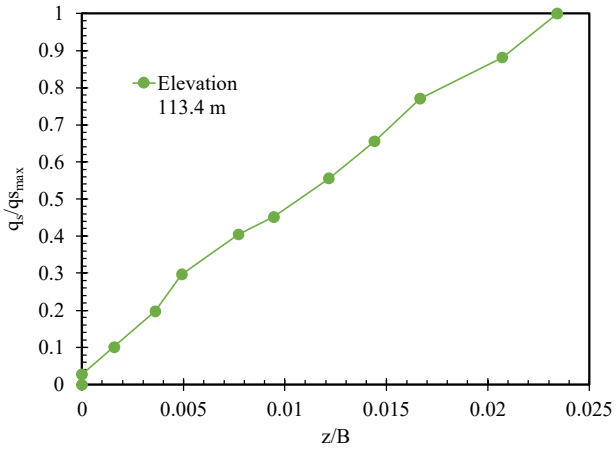

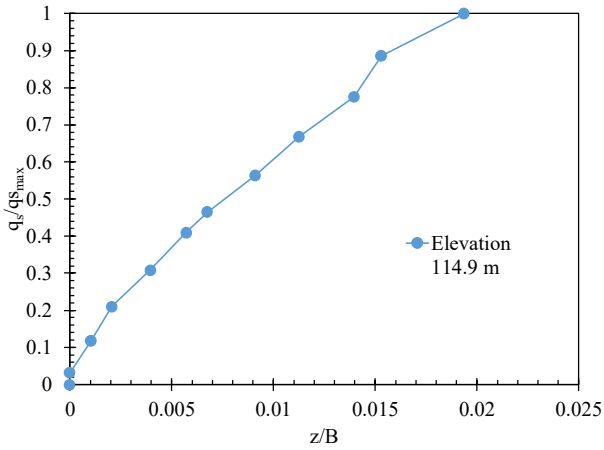

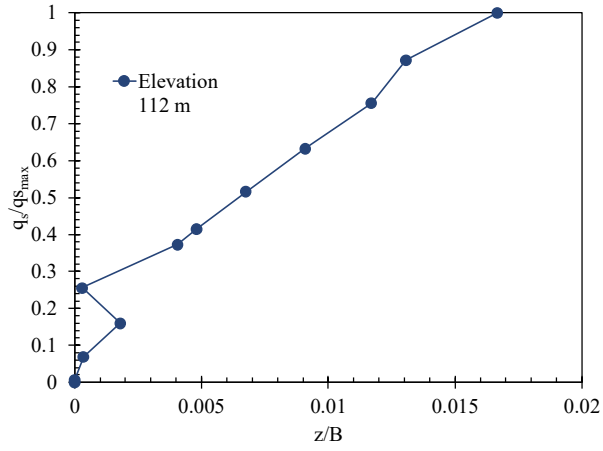

E.2 Pipe Pile t-z curves

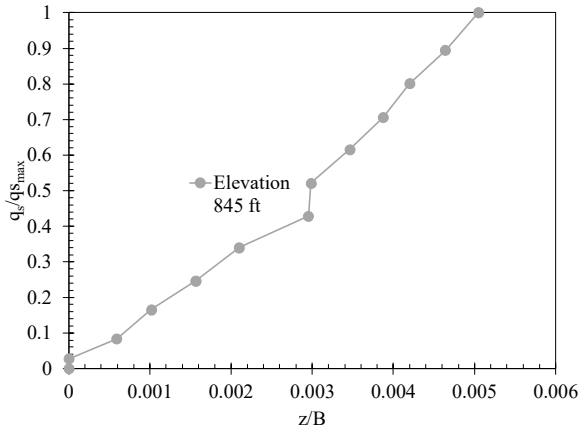

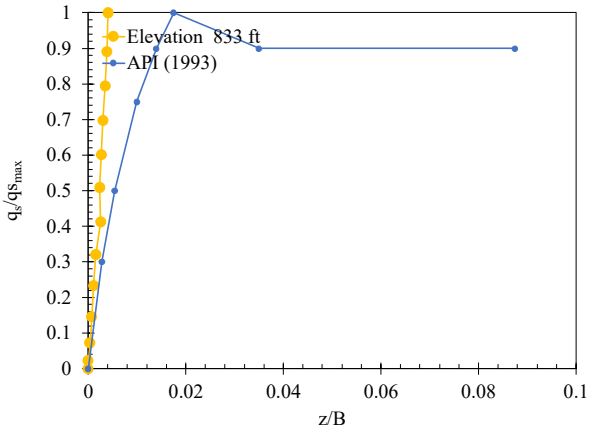

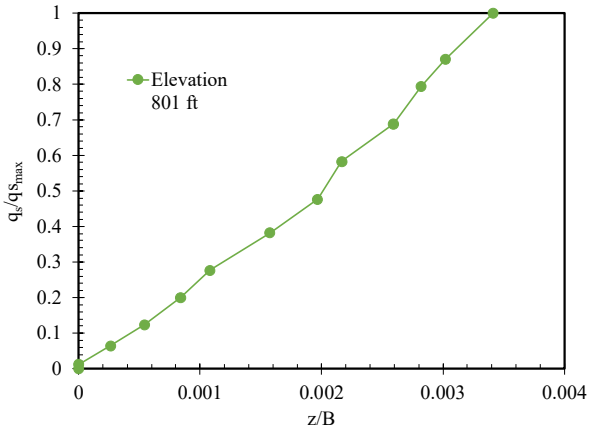

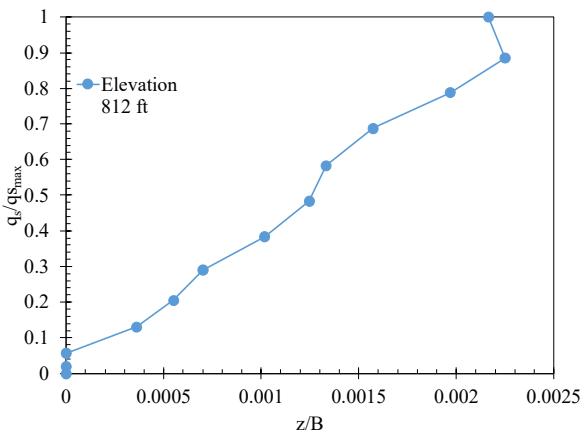

REFERENCES

API (American Petroleum Institute). (1993). *Recommended practice for planning, designing and constructing fixed offshore platforms–Working stress design*, 20th Ed., Washington, DC.

AASHTO LRFD Bridge Design Specifications (2007). Customary U.S. Units, 4th edition (2008 Interim), American Association of State Highway Transportation Officials, Washington, D.C.

Allen, T. M., Nowak, A. S., and Bathurst, R. J. (2005). ―Calibration to Determine Load and Resistance Factors for Geotechnical and Structural Design.‖ *Transportation Research Circular Number E-C079*, TRB, Washington, DC.

Argo, D. E. (1987). ―Dynamic Formulas to Predict Driven Pile Capacity.‖ Department of Civil and Environmental Engineering, Washington State University, Pullman, WA.

ASTM D1143 (2007). ―Standard Test Methods for Deep Foundations under Static Axial Compressive Load.‖ *American Society for Testing and Materials, ASTM*, Philadelphia, PA.

Burland, J. B., (1973). ―Shaft Friction of Piles in Clay.‖ Ground Engineering, London, Vol.6., No.3, pp.3042.

Butler, H. D., and Hoy, H. E. (1977). ―Users Manual for the Texas Quick-Load Method for Foundation Load Testing.‖ *FHWA-IP- 77-8, FHWA*, Office of Development, Washington, DC.

Canadian Foundation Engineering Manual, (1985). ―Second Edition, Part 3: Deep Foundations.‖ *Canadian Geotechnical Society*, BiTech Publishers, Vancouver.

Cheney, R. S. and Chassie, R. G. (1993). ―Soils and Foundations Workshop Manual.‖ *FHWA Report No. FHWA-HI-88-009*.

Chin, F. V. (1970). ‗‗Estimation of the Ultimate Load of Piles Not Carried to Failure.‘‘ *Proceeding: The 2nd Southeast Asian Conference on Soil Engineering*, pp. 81–90.

Coduto, D. P. (2001). ―Foundation design: principles and practices.‖ Prentice-Hall Inc. Englewood Cliffs, N.J.

Cummings, A. E. (1940). ―Dynamic Pile Driving Formulas.‖ *Journal of the Boston Society of Civil Engineers*, No. 27:6-27.

Davisson, M. (1972). ―High Capacity Piles.‖ *Proceeding: Soil Mechanics Lecture Series on Innovations in Foundation Construction*, ASCE, IL Section, Chicago, IL, pp. 81–112.

DiMaggio, J., Saad, T., Allen, T., Barry, R., Al Dimillio, Goble, G., Passe, P., Shike, T., and Person, G. (1999). ―FHWA International Technology Exchange Program.‖ *FHWA Report Number FHWA-PL-99-013*.

Dirks, K. and Kam P. (2003). ―Foundation Soils Information Chart – Pile Foundation.*"* *Iowa Department of Transportation*, Office of Road Design, Ames, Iowa, United States.

Fellenius, B. H., (1991). ―Summary of Pile Capacity Predictions and Comparison with Observed Behavior.‖ ASCE: American Society of Civil Engineers, ASCE, *Journal of Geotechnical Engineering*, Vol. 117, No. 1, pp. 192 - 195.

FHWA (1997). ―Design and Construction of Driven Pile Foundations.‖ *Workshop manual*, Volumes I, publication FHWA-HI-97-013.

FHWA (2007). ―Load and Resistance Factor Design (LRFD) for Highway Bridge Superstructures.‖ *FHWA Publication number*: FHWA-NHI-07-03

Fragaszy, Richard J., Douglas E., Argo, and Higgins, J. D. (1989). ―Comparison of Formula Predictions with Pile Load Tests.‖ Transportation Research Record: *Journal of the Transportation Research Board*

Gates, M. (1957). ―Empirical Formula for Predicting Pile Bearing Capacity.‖ *Civil Engineering*, 65-66.

GRL, Inc. (1999). ―Pile-Driving Analyzer, PAK Users Manual.‖ Goble, Rausche, Likins and Associates

Gulhati, Sahashi, K., and Manoj, D. (2005). ―Geotechnical Engineering.‖ New Delhi, Haryana India: Tata McGraw-Hill Publishing Company Limited.

Hannigan, P. J., Goble, G. G., Thendean, G., Likins, G. E., and Rausche, F. (2005). ―Design and Construction of Driven Pile Foundations.‖ Vol. I and II, *Federal Highway Administration Report No. FHWA-HI-05*, Federal Highway Administration, Washington, D.C.

Hansen, J. B. (1963). ―Hyperbolic Stress-strain Response: Cohesive Soils,‖ *Discussion Journal of the Soil Mechanics and Foundations Division*, American Society of Civil Engineers, New York, NY

Hara, A., Ohta, T., Niwa, M., Tanaka, S., and Banno, T. (1974). ―Shear Modulus and Shear Strength of Cohesive Soils.‖ *Soils and Foundations*, Vol. 14, No. 3, Sept. 1974.

Jardine R. J, Chow, F. C, Overy, R., and Standing, J. (2005). ―ICP Design Methods for Driven Piles in Sands and Clays.‖ Publishers Thomas Telford Inc.

Kulhawy, F. H. and Mayne, P. W., (1990). ―Manual on Estimating Soil Properties for Foundation Design.‖ *Report. EL-6800*, Electric Power Research Ins., Palo Alto.

McVay, M., Birgisson, B., Zhang, L., Perez., A, and Putcha, S. (2000). ―Load and Resistance Factor Design (LRFD) for Driven Piles Using Dynamic Methods - A Florida Perspective.‖ *Geotechnical Testing Journal*, Vol. 23, No. 1, pp. 55–66.

McVay, M., Klammler, H., Bloomquist, D., Otero, J., and Farone, M. (2010). ―Modification of LRFD Resistance Factors Based on Site Variability.‖

Mertz, D. R. (2007). ―AASHTO-LRFD Background to the Specifications.‖ *Aspire, Precast/Prestressed Concrete Institute.*

Meyerhof, G. (1970). ―Safety Factors in Soil Mechanics.‖ *Canadian Geotechnical Journal*, Vol. 7, No. 4, pp. 349–355.

Nordlund, R. L. (1979). ―Bearing Capacity of Piles in Cohesionless Soils.‖ *Journal of Soil Mechanics and Foundation Engineering*,

Nottingham, L., and Schmertmann, J. (1975). ―An Investigation of Pile Capacity Design Procedures.‖ Final Report D-629 to Florida Department of Transportation, Department of Civil Engineering, University of Florida

Nowak A. S. and Collins K. R. (2000). ―Reliability of Structures.‖ Publisher: McGraw-hill. Nowak, A. S. (1999). ―NCHRP Report 368: Calibration of LRFD Bridge Design Code.

O'Neill, M. W. and Reese, L. C. (1999). ―Drilled Shafts: Construction Procedures and Design Methods.‖ *FHWA Report No. IF-99-025*, Federal Highway Administration, Washington, D.C.

Peck, R. B., W. E. Hanson, and T. H. Thornburn (1974). ―Foundation Engineering.‖ John Wiley & Sons,

Pile Dynamics, Inc. (2000). ―CAPWAP for Windows Manual.‖ Cleveland, Ohio: Pile Dynamics, Inc.

Prakash, S., and Sharma, H. D. (1990). ―Pile Foundations in Engineering Practice.‖ Wiley, New York.

Ramey, G. E., and Hudgins, A. P. (1975). ―Modification of Pile Capacity and Length Prediction Equations Based on Historical Alabama Pile Test Data.‖ Montgomery, AL: State of Alabama Highway Department - Bureau of Research and Development.

Schmertmann, J. H. (1978). ―Guidelines for Cone Penetration Test, Performance and Design.‖ *FHWA Report No. FHWA-TS-78-209*, U.S. DOT, Washington, D.C.

Skempton, A.W. (1951), ―The Bearing Capacity of Clays.‖ *Proc. Building Research Congress*, vol. 1, pp. 180-189.

Terzaghi, K., and Peck, R. B. (1967). ―Soil Mechanics in Engineering Practice.‖ Wiley. Thibodeau, E., and Paikowsky, S. (2005). ―Performance Evaluation of a Large Scale Pile Load Testing Program in Light of Newly Developed LRFD Parameters.‖ *Proceeding: Session of the Geo-Frontiers 2005*

Tomlinson, M. J. (1980/1995). ―Foundation Design and Construction.‖ *6th Edition*. Longman Scientific & Technical, Essex, England.

U.S. Army Corps of Engineers, (1992). ―Pile Layout to Minimize Interference.‖ *Engineer Technical Letter ETL 1110-8-17(FR)*, Department of the Army, US Army Corps of Engineers, Washington, DC

VanderVeen, C. (1953). ―The Bearing Capacity of a Pile.‖ *Proceeding: The 3rd International*

Conference on Soil Mechanics and Foundation Engineering, Vol. 2.

Vesic, A. S. (1977). ―Design of Pile Foundations.‖ *National Cooperative Highway Research Program Synthesis of Highway Practice No. 42*, Transportation Research Board, Washington, D.C.

VITA

1. Corbin, Kentucky
2. Bachelor of Science in Mining Engineering, University of Kentucky
3. Edward Lawson